VYSOKÉ UČENÍ TECHNICKÉ V BRNĚ

BRNO UNIVERSITY OF TECHNOLOGY

FAKULTA CHEMICKÁ
ÚSTAV CHEMIE MATERIÁLŮ

FACULTY OF CHEMISTRY
INSTITUTE OF MATERIALS SCIENCE

CELLULOSE NANOFIBERS AND AEROGEL MATERIALS

DIPLOMOVÁ PRÁCE
MASTER'S THESIS

AUTOR PRÁCE — Bc. MICHAELA SALAJKOVÁ
AUTHOR

BRNO 2009

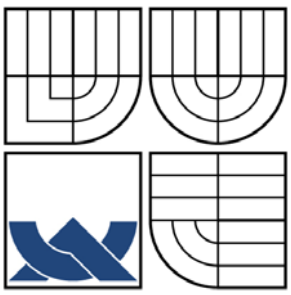

VYSOKÉ UČENÍ TECHNICKÉ V BRNĚ

BRNO UNIVERSITY OF TECHNOLOGY

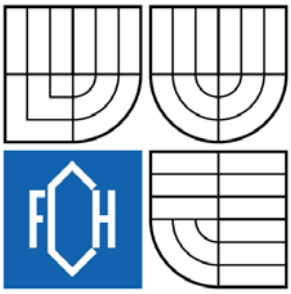

FAKULTA CHEMICKÁ
ÚSTAV CHEMIE MATERIÁLŮ

FACULTY OF CHEMISTRY
INSTITUTE OF MATERIALS SCIENCE

CELLULOSE NANOFIBERS AND AEROGEL MATERIALS

CELULÓZOVÁ NANOVLÁKNA A MATERIÁLY V AEROSOLU

DIPLOMOVÁ PRÁCE
MASTER'S THESIS

AUTOR PRÁCE — Bc. MICHAELA SALAJKOVÁ
AUTHOR

VEDOUCÍ PRÁCE — prof. RNDr. JOSEF JANČÁŘ, CSc.
SUPERVISOR

BRNO 2009

Vysoké učení technické v Brně
Fakulta chemická
Purkyňova 464/118, 61200 Brno 12

Zadání diplomové práce

Číslo diplomové práce:	**FCH-DIP0328/2008**	Akademický rok: **2008/2009**
Ústav:	Ústav chemie materiálů	
Student(ka):	**Bc. Michaela Salajková**	
Studijní program:	Chemie, technologie a vlastnosti materiálů (N2820)	
Studijní obor:	Chemie, technologie a vlastnosti materiálů (2808T016)	
Vedoucí diplomové práce:	**prof. RNDr. Josef Jančář, CSc.**	
Konzultanti diplomové práce:		

Název diplomové práce:

Celulózová nanovlákna a materiály v aerosolu

Zadání diplomové práce:

1) Nanofiber preparation
2) Aerogel preparation
3) Structure characterization
4) Property characterization

Termín odevzdání diplomové práce: 22.5.2009

Diplomová práce se odevzdává ve třech exemplářích na sekretariát ústavu a v elektronické formě vedoucímu diplomové práce. Toto zadání je přílohou diplomové práce.

- -	- -	- -
Bc. Michaela Salajková Student(ka)	prof. RNDr. Josef Jančář, CSc. Vedoucí práce	prof. RNDr. Josef Jančář, CSc. Ředitel ústavu

V Brně, dne 1.10.2008

- -
doc. Ing. Jaromír Havlica, DrSc.
Děkan fakulty

SUMMARY

This thesis deals with preparation and characterization of new microfibrillated cellulose/multi-walled carbon nanotubes (MFC/MWCNTs) composite materials. Three different pre-treatment methods were used in order to disperse MWCNTs in water. The effect of different pre-treatments on the quality of MWCNTs suspension was studied. Composite films containing MFC and MWCNTs were prepared, and their mechanical and electrical properties and morphology were characterized.

MWCNTs suspensions were characterized by UV-VIS spectroscopy, Scanning Electron Microscopy (SEM), and Thermogravimetric analysis (TGA).

Electrical properties of MFC/MWCNTs composite films were measured by Keithly Electrometer/High Resistivity Meter. For characterization of mechanical properties, tensile test was performed using Miniature Materials Tester. The morphology of the composite films was observed using SEM.

Any significant effect of MWCNTs on mechanical properties wasn´t found. Concerning the surface resistivity data, typical percolation behaviour was revealed, indicating conductive composite material was successfully prepared. However, the surface resistivity values differ significantly between the top and bottom sides of the composite films. These results suggested that the preparation process for the composite materials and the compatibility between MFC and MWCNTs need to be improved.

SOUHRN

Tato diplomová práce se zabývá přípravou nových kompozitů na bázi mikrofibrilované celulozy a multi-walls carbon nanotubes (MFC/MWCNTs). Tři různé metody byly použity pro modifikaci MWCNTs. Byl zkoumán vliv použitých modifikací na kvalitu MWCNTs suspense. Dále byly připraveny kompozity obsahující MFC a MWCNTs a vliv MWCNTs na mechanické a elektrické vlastnosti a morfologii byl zkoumán.

MWCNTs suspense byly charakterizovány za použití UV-VIS spektrofotometrie, Rastrovacího elektronového mikroskopu (SEM) a Termogravimetrické analýzy (TGA).

Elektrické vlastnosti byly měřeny pomocí Keithly Electrometer/High Resistivity Meter. Mechanické vlastnosti v tahu byly měřeny za použití Miniature Materials Tester a pro studium morfologie byl použit SEM.

Žádný významný vliv MWCNTs na mechanické vlastnosti nebyl pozorován. Hodnoty získané z měření rezistivity vykazují typický perkolační trend a výrazného snížení rezistivity bylo dosaženo přidáním 1 – 2 wt.% MWCNTs. Nicméně hodnoty se velice liší pro horní a spodní stranu téhož vzorku. Ze získaných výsledků vyplývá, že klíčovým krokem ke zdokonalení vlastností materiálu jsou dobrá suspense MWCNTs a také dosažení vzájemné kompatibility obou složek.

KEYWORDS

Microfibrillated cellulose, Carbon nanotubes, Surface resistivity, Mechanical properties, Scanning electron microscopy

KLÍČOVÁ SLOVA

Mikrofibrilovaná celuloza, Carbon nanotubes, Povrchová rezistivita, Mechanické vlastnosti, Rastrovací elektronový mikroskop

SALAJKOVÁ, M. *Celulózová nanovlákna a materiály v aerosolu.* Brno: Vysoké učení technické v Brně, Fakulta chemická, 2009. 73 s. Vedoucí diplomové práce prof. RNDr. Josef Jančář, CSc.

DECLARATION

I declare that the diploma thesis has been worked out by myself and that all the quotations from the used literary sources are accurate and complete.

PROHLÁŠENÍ

Prohlašuji, že jsem diplomovou práci vypracovala samostatně a že všechny použité literární zdroje jsem správně a úplně citovala.

.....
Signature

Acknowledgements

I would like to thank Prof. Lars Berglund, Asst. Prof. Qi Zhou and Prof. Josef Jančář for creation of the work conditions and supervision and Mikael Segersäll for performing the surface resistivity measurement.
I would also like to thank Ing. Hana Alexová, Mgr. Alena Sýkorová and others who have helped me to make my study stay at KTH possible. Furthermore, financial support from Erasmus Programme and Programme of Student Mobility Support MŠMT is gratefully appreciated.

Poděkování

Ráda bych poděkovala Prof. Larsu Beglundovi, Asst. Prof. Qi Zhou a Prof. Josefu Jančářovi za předání cenných zkušeností a vytvoření podmínek pro realizaci práce a Mikael Segersäll za měření rezistivity.
Dále bych chtěla poděkovat Ing. Haně Alexové, Mgr. Aleně Sýkorové a všem ostatním za trpělivou pomoc při vyřizování studijního pobytu v zahraničí a získání finanční podpory v rámci program Erasmus a Programu podpory mezinárodní mobility studentů veřejných vysokých škol MŠMT.

TABLE OF CONTENTS

1 INTRODUCTION

Concern for the environment, rising oil prices, and basically non-renewable oil resources are main driving forces for research activities that are aimed at replacing petrochemical products with bio-based materials. Targets include bioplastics for packaging, building materials, and a range of other products including fibres. Developing of bio-based alternatives even for a part of the global fibre production may have significant environmental benefits. A further motivation has arisen from consumer demand, with growth of the “eco-friendly” and “organic” markets in textiles (as well as food and other areas), reflecting the increased public interest and awareness of environmental impacts caused by global industrial activities [2].

The synthesis of biological materials in nature occurs by energy efficient processes at moderate temperatures and low pressure, using water as the solvent. The low energy input of these processes is compensated by the precise molecular design of the constituent biopolymers, which drives efficient self-assembly of biomaterials. Owing to their smart design, natural materials outperform most man-made composites. Classical examples of natural high-performance composites in which matrix proteins control the formation of the inorganic component include abalone shells, bone and enamel. Other natural composites with unique properties include cactus spines with high degree of stiffness contributed by an arabinan cellulose composite, and the tunics of sea peaches, composed of cellulose, proteins and mucopolysaccharides. Last, but not least, wood is perhaps one of the most complex natural composite substances and it is widely used as a structural material [5].

There is a growing interest in cellulose I. The attractiveness of this material lies in its abundance, biological origin, hierarchical structure and inherent properties. The smallest discernible building block of cellulose I is fibril with lateral dimension about 5 nm [4] and this fact opens many possibilities in the filed of nanocomposite science. Similar to traditional microcomposites, nanocomposites use a matrix where the nanosized reinforcements are dispersed. The reinforcement is currently considered as a nanoparticle when at least one of its dimensions is less than 100 nm. This particular feature provides nanocomposites unique and outstanding properties never found in conventional composites [3].

In the next part of this study, possible exploitation of another advanced material – carbon nanotubes (CNTs) – was investigated. Since their discovery, CNTs have attracted considerable interest in both academia and industry for their engineering applications, such as electronic devices, biosensors, field emission displays, hydrogen storage, and composites, on account of their extraordinary physical, chemical, and structural properties, such as electrical, mechanical, and thermal characteristics. CNTs generally aggregate in water because they are hydrophobic and form stabilized bundles through van der Waals forces, resulting in the formation of hollow ropes. Therefore, achieving a good dispersion of CNTs is one of the key issues for various applications of CNTs. Recently, CNTs have been used in bio applications, such as cancer therapy [1].

2 OBJECTIVE OF THE WORK

The aim of this thesis was to prepare and characterize nanofibres based composite materials. In the first part of this work, a suitable method enabling dispersion of carbon nanotubes (CNTs) was developed. Quality of the dispersion was evaluated by Scanning Electron Microscopy (SEM). Furthermore, composite materials containing cellulose nanofibres and carbon nanotubes were prepared. Their electrical and mechanical properties and morphology were characterized. The effect of different pre-treatments on CNTs was discussed.

3 THEORY

3.1 Natural fibres

Natural fibres are divided based on their origins: coming from plants, animals or minerals. All plant fibres are composed of cellulose while animal fibres consist of proteins (hair, silk and wool). Plant fibres include bast (or stem or soft sclerenchyma) fibres, leaf or hard fibres, seed, fruit, wood, cereal straw, and other grass fibres. Over the last few years, a number of researchers have been involved in the exploitation of natural fibres as load bearing constituents in composite materials. The use of natural fibres in composite materials has increased due to their low cost and ability to recycle and the fact that they can compete well in terms of strength per weight of material [6].

Natural plant fibres can be considered as naturally occurring composites consisting mainly of cellulose fibrils embedded in lignin matrix. The cellulose fibrils are aligned in the longitudinal direction of the fibre, which render maximum tensile and flexural strengths, in addition to providing rigidity. The reinforcing efficiency of natural fibre is related to the nature of cellulose and its crystallinity. The main components of natural fibres are cellulose (α-cellulose), hemicelluloses (heterogeneous group of branched polysaccharides), lignin (a complex phenolic polymer that fills the spaces in the cell wall between cellulose, hemicellulose and pectin, thereby conferring mechanical strength to the cell walls. Lignin is typically present in the secondary cell walls of trees), pectins (another group of branched polysaccharides cementing together the primary walls of adjacent plant cells) and waxes [6].

3.1.1 Cellulose fibre structure

Cellulose is a straight carbohydrate polymer chain consisting of several 1000 β(1-4)D-glucopyranose units. In cellulosic plant fibres, cellulose is present in amorphous state, but also associates to crystalline domains through intramolecular hydrogen bonding [7]. The most stable conformation about the $\beta(1\rightarrow4)$ linkage involves alternating 180° flips of every second glucose unit, so that the repeating unit of cellulose is rather a cellobiose molecule than a glucose unit. The β-configuration of the glycosidic bond allows the polymer to adopt a fully extended conformation. For example, amylose is built up by $\alpha(1\rightarrow4)$ glycosidic linkages, which are naturally bent, conferring a gradual turn to the polymer chain resulting in a helical conformation [8].

The extended cellulose chains form an array with the flat glucose units fixed edge to edge by hydrogen bonds (Fig. 1). These sheets are further stacked on top of each other and held together by hydrogen bonds and van der Waals interactions. This network of up to 40 cellulose chains makes up the crystalline core of the cellulose fibril. Native cellulose (cellulose I) has two crystalline allomorphs, Iα and Iβ. The main difference between the two crystalline phases is the relative position of the chains with respect to each other. Cellulose in higher plants (woody tissue, cotton etc.) consists mainly of the Iβ phase whereas primitive organisms (bacteria, algae etc.) are enriched in the Iα phase [8].

If cellulose is recrystallized (for example, from base or CS_2) cellulose I gives the thermodynamically more stable cellulose II structure with an antiparallel arrangement of the strands and some inter-sheet hydrogen-bonding. Cellulose III is formed from cellulose mercerized in ammonia and is similar cellulose II but with the chains parallel, as in cellulose Iα and cellulose Iβ [60].

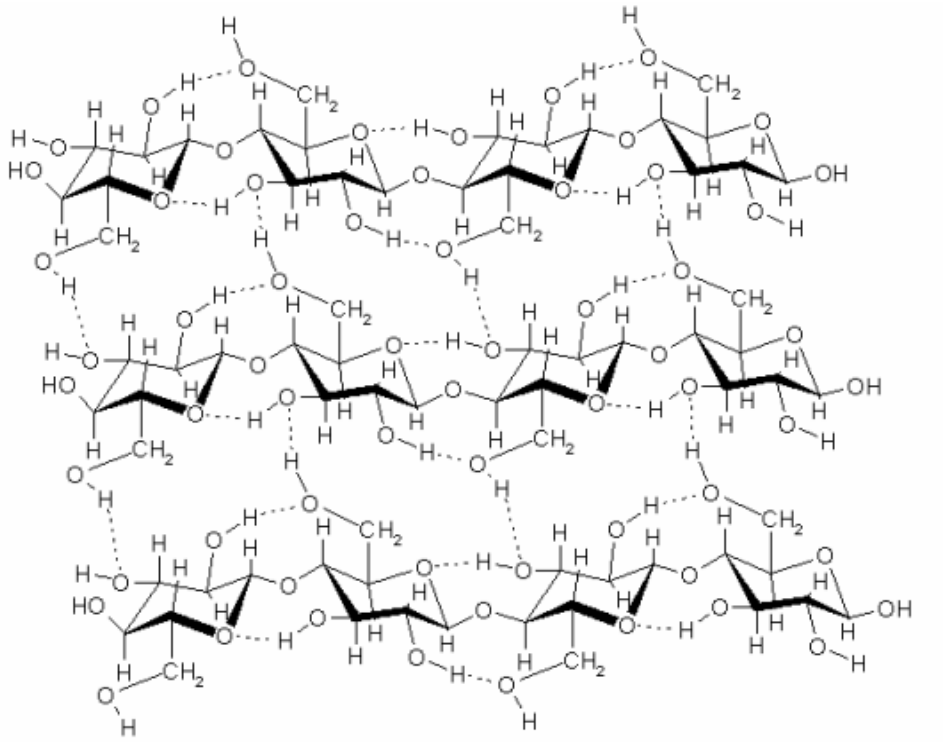

Fig. 1: The structure of a cellulose sheet showing the intra- and inter-chain hydrogen bonds [8].

The crystalline cellulose fibril is further covered by para crystalline cellulose and finally surrounded by hemicelluloses. Hemicelluloses incorporate the amorphous cellulose layer and cross-link the individual fibrils, and form covalent associations with lignin. As mentioned above, together with some proteins, these fibre composites make up the cell wall (Fig. 2 – 3) [8].

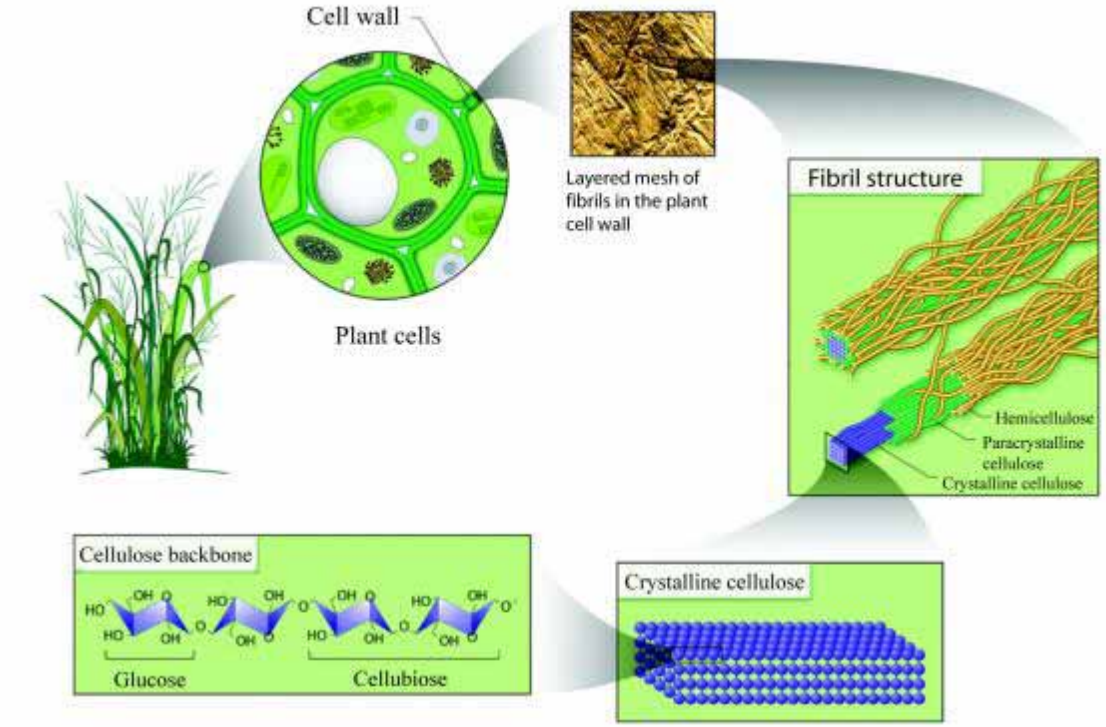

Fig. 2: The cell wall hierarchy, from a single cellulose polymer to the cellulose fibre composite [8].

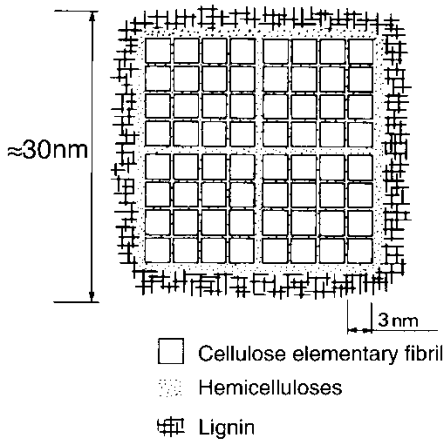

Fig. 3: Model of wood microfibrils, consisting elementary filbrils [9].

3.1.2 Mechanical properties of cellulose

The elastic modulus of the cellulose I crystallite, which is the crystalline cellulose from typical for plant fibres, has been measured to be 128 GPa, and estimates for the strength of the cellulose I crystallite lie in the order of 10 GPa. In spite of the good mechanical properties of cellulose, the strength of cellulosic fibre-reinforced composites remains far below the potential provided by cellulose. Due to the heterogeneous structure and composition of plant fibres, and insufficient fibre-matrix compatibility, typical random-oriented plant fibre-reinforced composites show a tensile strength of 15 – 140 MPa and an elastic modulus of 1 – 13 GPa [7].

3.1.3 Sources of cellulose

Cellulose is produced by many species in nature, both plants and other organisms. The cell walls of plants, algae and oomycetes (e.g. water moulds) are primarily built up by cellulose [8]. Concerning cellulose from higher plants, it may be present in the primary, secondary and tertiary cell wall, although the content is very low in the tertiary wall. In the secondary cell wall of wood tracheids, the microfibrils are predominantly organized in a unidirectional manner. The average microfibril angle is typically 10 – 30° with respect to the axial direction of the tracheid. In the primary cell wall, the cellulose is in the form of a woven mesh of microfibrils [10].

Only one group of animals, the tunicates (sea animal of around 5 – 10 cm in diameter that contains a 1 cm thick cellulose tunic), can synthesise cellulose, while it is digestible by all grass and leave-eating species. Some acetic acid bacteria, for example *Acetobacter xylinum*, are known to synthesise and secrete cellulose into the surrounding media [8, 10].

3.2 Native cellulose (cellulose I)

3.2.1 Microcrystalline cellulose (cellulose nanocrystals, whiskers)

The term “whiskers” is used to designate elongated rod-like nanoparticles (Fig. 5), which have also been referenced in the literature as microfibrils, microcrystals, or microcrystallites, despite their nanoscale dimensions [11].

Stable aqueous suspensions of cellulose nanocrystals can be prepared by acid hydrolysis of the biomass or tunicate. The amorphous regions of cellulose act as structural

defects and are responsible for the transverse cleavage of the microfibrils into short microcrystals under acid hydrolysis. Under controlled conditions, this transformation consists of the disruption of amorphous regions surrounding and embedded within the cellulose microfibrils while leaving the microcrystalline segments intact (Fig. 4). It is ascribed to the faster hydrolysis kinetics of amorphous domains compared to crystalline ones [11]. Degree of polymerisation, DP, depends on the cellulose source and treatment procedure and is about 140 – 400 [12]. The length of the nanocellulose crystals is also dependent on the sample origin but when derived from wood sources typically they are 100 – 300 nm in length and 3 – 10 nm in width and the modulus of cellulose crystal has been reported as 138 – 167 GPa [16].

While cellulose nanocrystals (CNC) obtained by hydrochloric acid hydrolysis exhibit limited dispersibility in water, corresponding treatment with sulphuric acid yields surface esterified nanocrystals with negatively charged sulphate groups providing electrostatic stabilization in aqueous solution. Formation of chiral nematic[1] liquid crystal phases is the result of self-ordering of nanocrystals in aqueous suspension. This phenomenon has made possible new applications based on optical properties of the solidified liquid crystals [15].

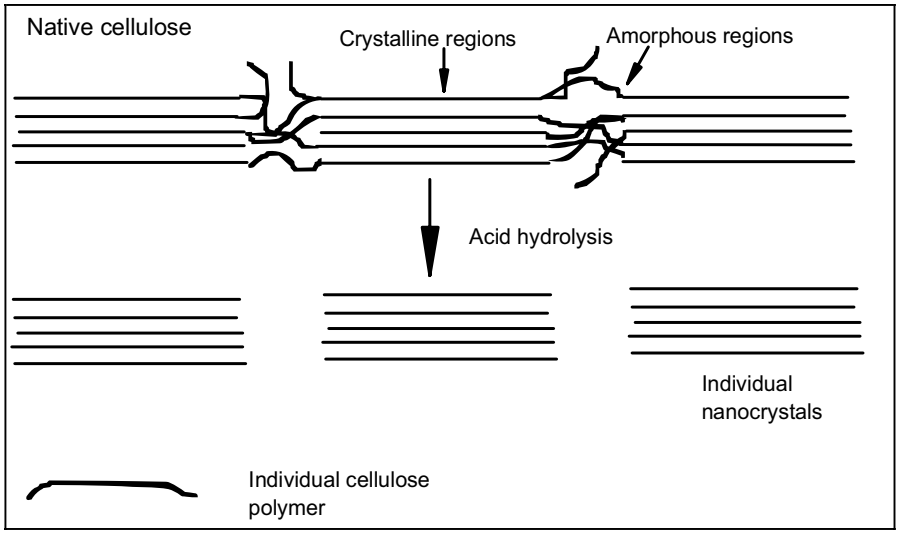

Fig. 4: Schematic illustration of cellulose nanocrystals preparation [13].

[1] This ordering phenomenon corresponds to the helicoidal packing of several nematic planes and has already been observed in other biological systems such as cholesterol [49].

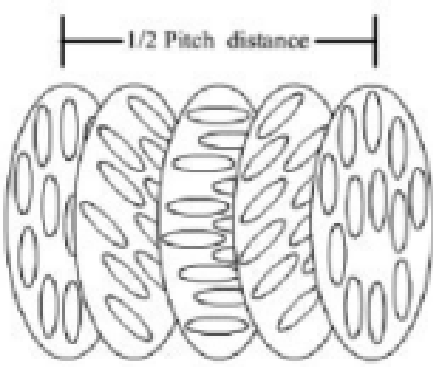

Fig. 5: Cellulose nanocrystals from wood pulp [14].

Because cellulose nanocrystals exhibit very good mechanical properties, many attempts were made to use them as reinforcement in polymer composites. Therefore their compatibility with non-polar polymer matrices has led to increased interest in surface functionalization of CNC. Hasani at al. [15] performed the surface cationization of H_2SO_4 hydrolyzed CNC and investigated some physical properties of cationically-stabilized aqueous CNC suspensions (Fig. 6). As cationization agent, epoxy-propyltrimethylammonium chloride (EPTMAC), previously used in functionalization of for example cotton linters, starch, xylan and chitosan, was used. Surface cationization of CNC with EPTMAC results in aqueous suspensions that are electrostatically stabilized by cationic trimethylammonium chloride groups. Using mild alkaline cationization, crystalline morphology and dimension of cellulose nanocrystals were preserved while resulting in an extensive hydrolysis of the anionic surface sulphate ester groups. The cationization leads to a slight decrease in total (cationic) surface charge density, compared to that of the initial (anionic) charge density of the CNC starting material.

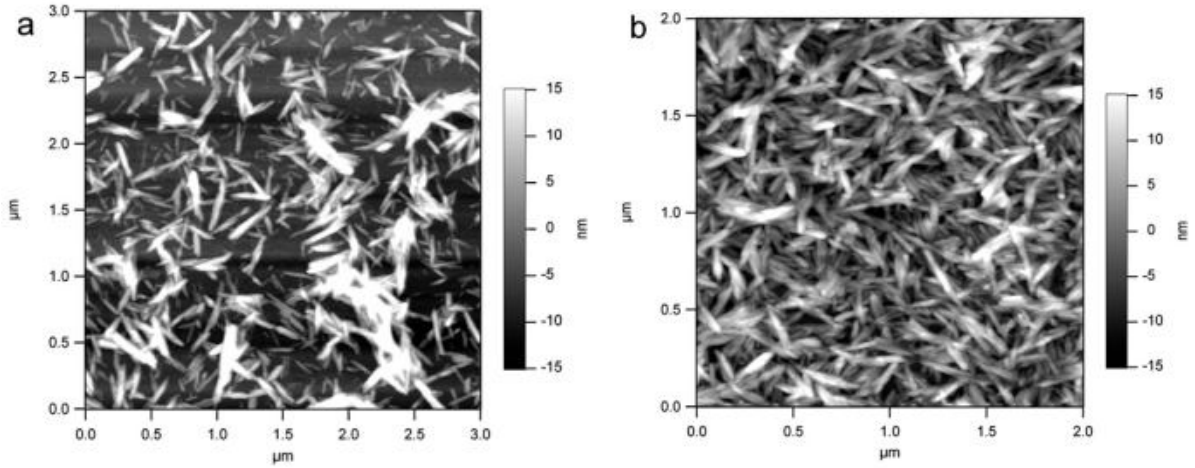

Fig. 6: AFM height images of CNC on mica (a) before and (b) after functionalization with EPTMAC [15].

Goetz at al. [16] reported the preparation and characterization of cellulose whiskers cross-linked with poly(methyl vinyl ether-co-maleic acid) (PMVEMA) and poly(ethylene glycol) (PEG) system. It is the first report on crosslinking of cellulose whiskers and matrix and this crosslinking methodology has been developed for craft cellulosic fibres to enhance the water absorbing properties of treated fibres and they demonstrate that cross-linked cellulose whiskers are capable of forming novel film-like materials that exhibit unique water absorbing properties.

3.2.2 Microfibrillated cellulose (MFC)

Cellulosic pulp fibres can be disintegrated into fine fragments by mechanical refining methods. However, such methods tend either to damage the microfibril structure by reducing molar mass and degree of crystallinity or fail to sufficiently disintegrate the pulp fiber [17].

Another method of MFC preparation was to pass a dilute cellulosic wood pulp fiber/water suspension through a mechanical homogenizer where a large pressure drop facilitates microfibrillation. The MFC typically consist of disintegrated microfibril aggregates with a lateral dimension in the scale of tens of nanometers. In order to facilitate disintegration and lower the energy requirements, one may reduce fibre length by mechanical cutting or the fibre cell wall can be treated and embrittled by acid hydrolysis prior to homogenization. However, acid hydrolysis can significantly lower the molecular weight of cellulose. Another type of pre-treatment is using 2,2,6,6-tetramethylpiperidine-1-oxyl (TEMPO) oxidation step prior to mechanical treatment [17, 18].

The use of enzymatic pre-treatment (Fig. 7) may also reduce processing cost by decreasing the number of passes through the homogenizer, and has advantages from the environmental point of view as compared with chemical methods [17].

MFC nanofibres are expected to show high stiffness [5]. Its polymer molecules crystallize in extended-chain conformation during biosynthesis and form microfibrils with a lateral dimension of around 4 nm [17].

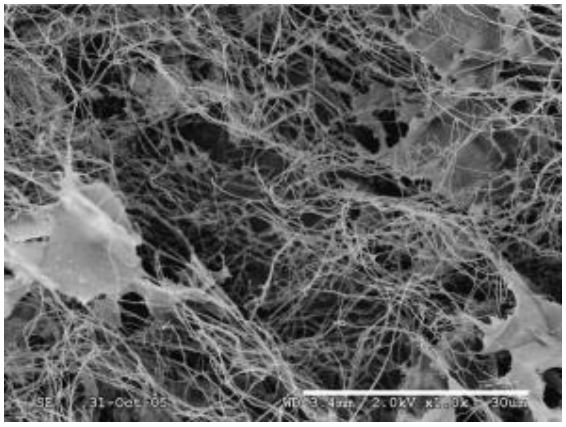

Fig. 7: SEM image of freeze-dried MFC prepared by using enzymatic pretreatment. Scale bar is 30 μm [17].

Affordable laboratory scale production of MFC accelerated extensive research in this area. Several recent publications demonstrate how MFC can be utilized for various purposes, e.g. in nanocomposites, as dispersion stabilizers and as antimicrobial films. However, little has been reported about the use of MFC in paper applications or the properties of pure MFC films [19].

Henriksson at al. [20] prepared and studied cellulose nanopaper structures (Fig. 8). Previously, the porous nature of the nanofibril network was not widely discussed in literature. Nanopaper was prepared from MFC water suspensions. Water was removed using vacuum filtration of diluted nanofibres. After that, the wet films were stacked between filter papers and dried at 55°C for 48 h at about 10 kPa applied pressure. Cellulose nanofibrils of different average molar mass were used. Cellulose nanopaper is a network composed of intertwined nanofibrils, with an aspect ratio exceeding 100 and with random-in-the-plane nanofibril orientation. The tensile strength, toughness, and strain-to-failure do correlate with average molar mass. That means ultimate failure is associated with nanofibril fracture.

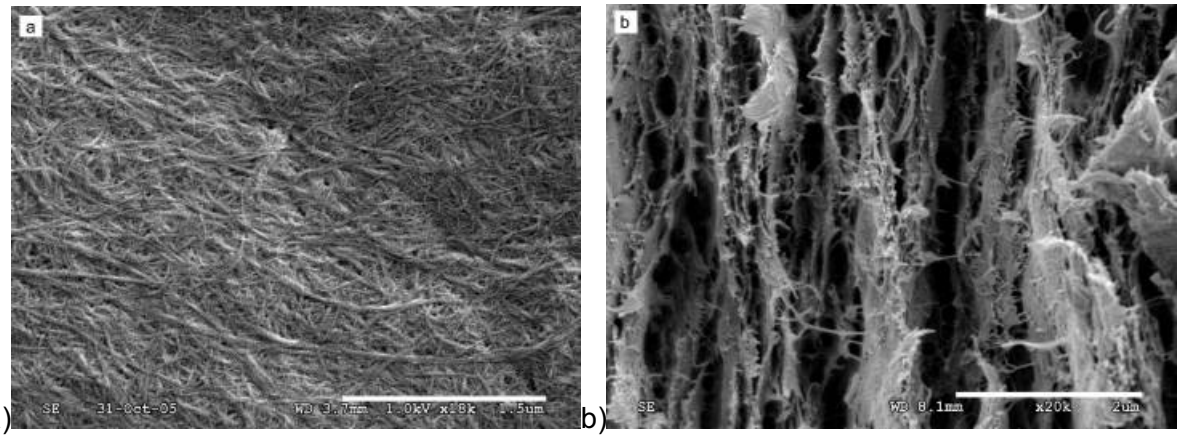

Fig. 8: FE-SEM micrographs of a) a cellulose nanofibril film surface showing a fibrous network (scale bar is 1.5 μm), b) the cross section of a fracture surface of a film showing a layered structure (scale bar is 2 μm) [20].

Syverud at al. [19] focused their work on the strength and barrier properties of MFC films prepared from microfibrils based on wood cellulose fibres. Pure MFC and MFC as a layer on base paper were used in order to increase barrier properties (Fig. 9). The positive results indicate that MFC may contribute to broadening the applicability of cellulose-based packaging.

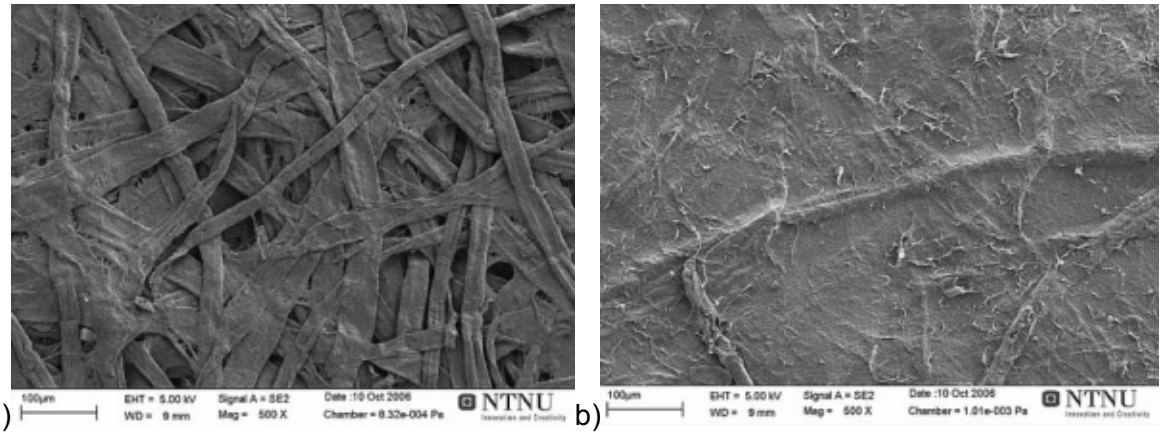

Fig. 9: FE-SEM micrographs of a) base paper and b) base paper coated with 8 g/m^2 MFC [19].

MFC disintegrated from wood pulp can be used in polymer nanocomposites of high mechanical performance [20]. Siqueira at al. [21] evaluated the thermomechanical behaviour of nanocomposite films obtained from PCL (polycaprolactone) and cellulosic nanoparticles from sisal. They focused on the differences induced by the nature of the nanoparticle (whiskers and microfibril) and its surface chemical modification. The chemical grafting was found to improve the dispersion of nanofillers in organic solvents.

Sisal whiskers were found to induce a limited reinforcing effect because of the aggregation of the filler within the nanocomposites film. However, the presence of the filler increases the glass transition, crystallization, and melting temperatures as well as the degree of crystallinity of the PCL matrix. Cellulosic whiskers are probably acting as nucleation sites.

When comparing sisal whiskers and MFC (both chemically modified), it was found that the modulus was higher for MFC-reinforced composites, whereas the elongation at break was lower for a given loading level. The difference was most probably ascribed to the possibility of entanglements of MFC in comparison to rod-like nanoparticles. The

introduction of MFC within the PCL matrix did not induce an increase of the degree of crystallinity of the matrix [21].

Nogi at al. [38] prepared optically transparent nanopaper from cellulose nanofibres (Fig. 10). The dried sheet that was obtained by filtration of well-dispersed nanofibres suspension was not optically transparent but translucent and had a plastic film-like appearance. It was found that surface light scattering caused the lack of transparency. After polishing, material became transparent. Since its invention, paper has played an important role as an information-transfer medium. This study shows that the next step of the paper evolution can be cellulose nanofibre paper having the potential to become an extremely important material supporting future generations of electronic devices [38].

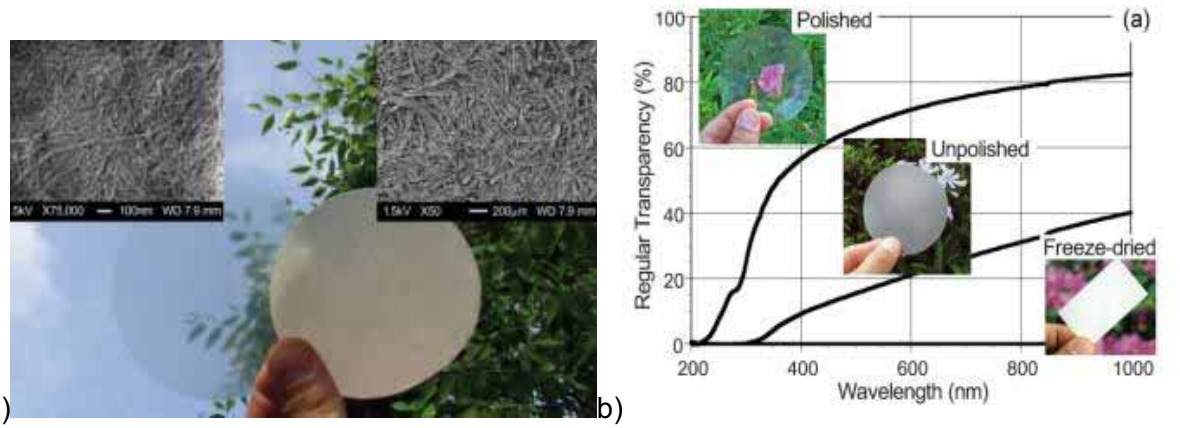

Fig. 10: a) Optically transparent nanofibre paper (left) composed of 15 nm cellulose nanofibres (upper left, scale bar in inset: 100 nm) and conventional cellulose paper (right) composed of 30 mm pulp fibres (upper right, scale bar in inset: 200 nm), b) Light transmittance of the cellulose nanofibre sheets. The thicknesses of the oven-dried nanofibre sheet were 60 μm before and 55 μm after polishing [38].

Svagan at al. [23] prepared nanocomposite foams using MFC in starch matrix by lyophilisation process (Fig. 11). Resulting foams showed microcellular structure with cell dimensions in the range 20 – 70 μm. Compared to the neat amylopectin foam, a significant improvement in modulus and yield strength was observed. The favourable properties of foams prepared by lyophilisation are due to improved mechanical properties of the nanofibril-reinforced cell wall, and the microcellular structure. This is not possible with micrometer-scale cellulose fibres, because of the diameter is too large in comparison to the cell-wall thickness [23].

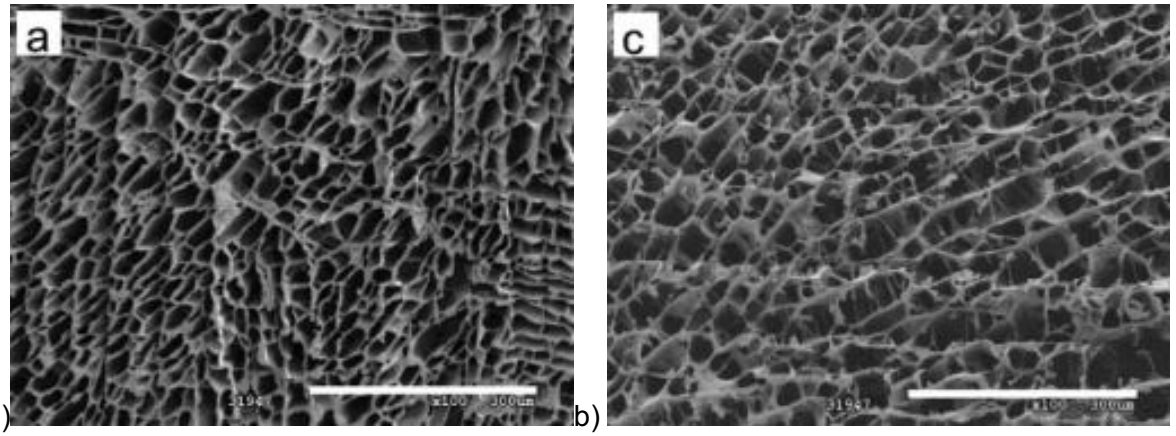

Fig. 11: The cell structures of amylopectin foam with a) 0, b) 40 wt. % MFC. The sections are normal to the cylinder axis of the foam. The scale bars are 300 μm [23].

Pääkkö at al. [24] reported flexible cellulose aerogels formed by long and entangled cellulose I nanofibres without any crosslinkers (Fig. 12). Network renders sufficient strength to oppose the tendency of the collapse during the solvent extraction and renders strength and deformability to the final product. The aqueous MFC gel was converted to a ‘‘sponge-like’’ aerogel in a vacuum oven by freeze-drying without collapse of the gel. An example of how to modify the aerogel network was demonstrated by functionalizing using a conducting polymer to achieve a porous conductive nanocellulose aerogel composite [24].

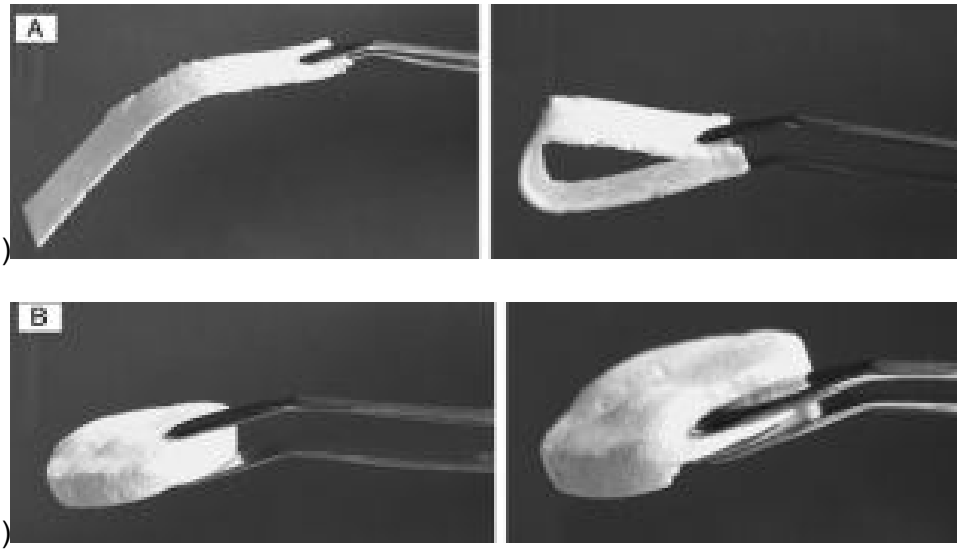

a)

b)

Fig. 12: A demonstration of the suppressed brittleness, increased flexibility and deformability of the aerogels [24].

3.2.3 Bacterial cellulose (BC)

Cellulose is produced by some bacteria e.g. *Acetobacter xylinum*. Bacterial cellulose (BC) is an extracellular product which is excreted into the culture medium. Acetic acid bacteria are not photosynthetic but can convert glucose, sugar, glycerol or other substances to pure cellulose. A typical single cell can convert up to 108 glucose molecules per hour into cellulose. The activities in a single cell are numerous. Each cell acts as a spinneret and produces a bundle of sub-microscopic fibrils fetching polymer aggregates through a row of pores. The bacteria produce a membrane of pure cellulose, which is very strong in its never dried state. It also has an extremely large absorbance of water [10].

It has been suggested that the alteration of chemical or biochemical conditions during the biosynthesis could alter the high order structure of cellulose assemblies. For example, cell division can be depressed by adding antibiotics to the incubation medium resulting in broader microfibrils than those generated under normal conditions. The biosynthesis of BC involves polymerization and crystallization processes and it was assumed that the factors that affect either step will influence the final structure of the BC [25].

The properties of the resulting cellulosic material can be also modulated by using different bacterial strains, by varying the parameters of the cultivation, and by adding chemicals and polymers into the culture medium. Since cellulose is fully biocompatible, interesting potential applications have already emerged in the health-care sector, including wound healing systems and artificial-skin products. Bacterial cellulose can be grown in defined shapes, such as hollow tubes, that can be used to replace blood vessels in surgical operations. Recently, native bacterial cellulose has also been presented as a potential, biocompatible scaffold with good mechanical properties for the engineering of cartilage and blood vessels [5].

Yano at al. [39] used bacterial cellulose nanofibres as reinforcement for optically transparent composite materials (Fig. 13). BC sheet was impregnated under vacuum with transparent thermosetting resin (epoxy, acrylic or phenol-formaldehyde) and fibre content was about 60 – 70 wt.%. Due to the size effect, the nanofibre network caused a very low loss of transparency of the original resin, even at high fibre content. Furthermore, the nanofibre network led to a remarkable reinforcement of the resin, producing composites with significantly higher mechanical strength and low thermal expansion coefficients [39].

a) 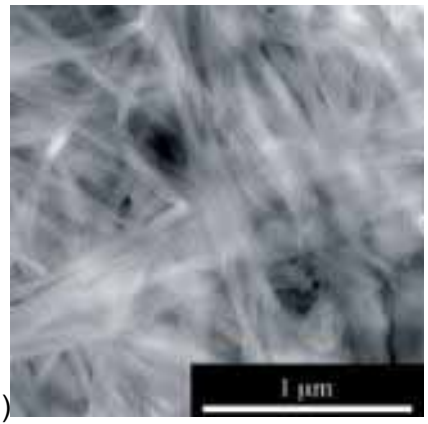

b) 

Fig. 13: a) Tapping mode AFM image of BC/epoxy resin sheet, b) flexibility of 65 µm thick BC/epoxy sheet with 60% BC content [39].

Nogi at al. [40] introduced foldable and ultra-low thermal expansion coefficient (CTE) transparent BC nanocomposites (Fig. 14). Their foldable properties and high thermal stability are achieved by reinforcing a transparent resin that has low Young´s modulus with 5 wt% of low-CTE and high-Young's-modulus cellulose nanofibres, taking advantage of the layered structure of planar BC nanofibre networks. This material has the potential to shift the electronics display industry from the traditional batch process to the much-anticipated more cost-effective continuous roll-to-roll manufacturing process [40].

a) 
b) 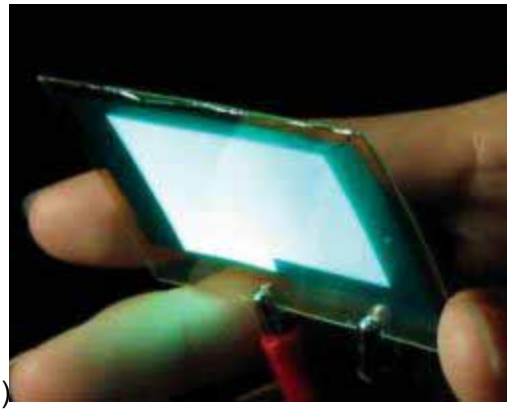

Fig. 14: a) Foldable transparent nanocomposites reinforced with bacterial cellulose nanofibres, b) Luminescence of an organic light-emitting diode deposited onto a transparent BC nanocomposite [40].

3.3 Carbon nanotubes

The unidirectional growth of materials that heads towards formation of nanowires or nanotubes has attracted enormous interest of scientific society in recent years [27]. The history of CNTs dates back to 1976, when carbon filaments of very small diameter (<10 nm) were prepared. However, significance of their synthesis was not fully recognised until the discovery of fullerene chemistry in 1985. This discovery directly stimulated the systematic study of carbon filaments [28]. The fullerene molecule is the fundamental building block of the crystalline phase, and through doping and chemical reactions forms the basis of a large family of materials, many of them having especially interesting properties [29].

Within the different classes of tubes made of organic or inorganic materials carbon nanotubes (CNT) are extremely promising for applications in materials science (nanotechnological applications - fillers in polymer matrices, molecular tanks) and medicinal chemistry (biosensors), because of their interesting electronic, mechanical, and structural properties. As an example of another application can be field-effect transistors, light-emitting diodes, chemical sensors, scanning probe microscopy, flexible, transparent and conducting membrane [27, 30].

3.3.1 Physical structure

CNT consists of graphitic sheets which have been rolled up into a cylindrical shape. The length of CNTs is in the size of micrometers with diameters up to 100 nm. CNTs form bundles that are entangled together in the solid state in the way that gives rise to a highly complex network. Depending on the arrangement of the hexagon rings along the tubular surface, CNTs can be conducting or semiconducting [27].

On the molecular scale, single-walled carbon nanotubes can be viewed either as one-dimensional crystals or as all-carbon semi-flexible polymers. Alternatively, one can think of capped nanotubes as extended fullerenes. For example, one can take a C_{60} molecule and add a belt of carbon to form a C_{70}. By repeating the process, one can make a long tubule of 0.7 nm diameter.

The chemical bond between carbon atoms inside nanotubes is the same as the bond in graphite (sp^2 type with each atom joined to three neighbours) that´s why they exhibit unique strength. Moreover, because of Van der Waals forces, they align themselves into rope and can merge together under high pressure.

Because of their structure, CNTs can be considered as rolled-up graphene sheets (graphene is an individual graphite layer). Fig 16 (a) shows three distinct ways in which a graphene sheet can be rolled into a tube [31, 33].

There are two main types of carbon nanotubes that can have high structural perfection. Single-walled carbon nanotubes (SWCNTs; Fig. 15) consist of a single graphite sheet seamlessly wrapped into a cylindrical tube. Multi-walled carbon nanotubes (MWCNTs; Fig. 15) comprise an array of such nano-tubes that are concentrically nested like rings of a tree trunk. Despite structural similarity to a single sheet of graphite, which is a semiconductor, SWCNTs may be either metallic or semiconducting, depending on the sheet direction about which the graphite sheet is rolled to form a nanotube cylinder. Depending on the appearance of a belt of carbon bonds around the nanotubes diameter, the nanotube is either of the arm-chair, zigzag or chiral variety (Fig. 16) [41].

a) 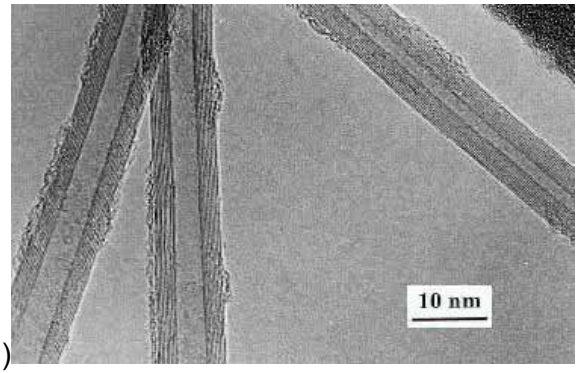

b) 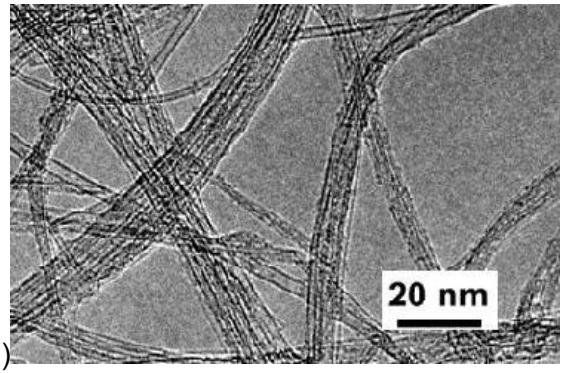

Fig. 15: a) A transmission electron micrograph of multiwalled nanotubes and b) single walled nanotubes [33].

a) 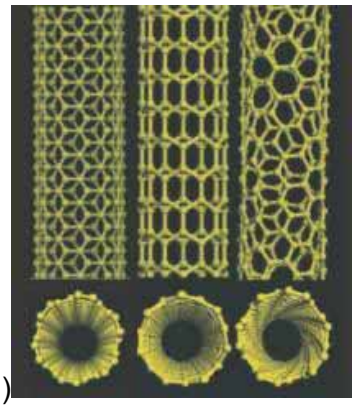
b) 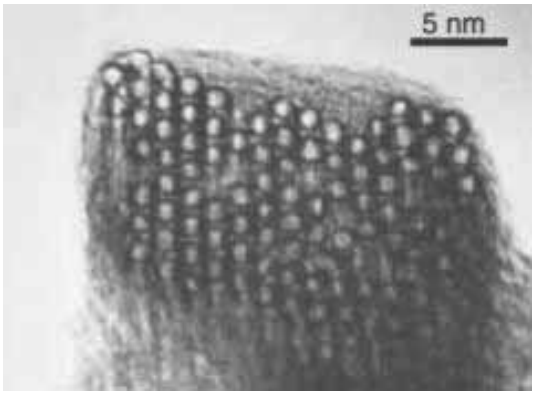

Fig. 16: a) Schematic illustrations of the structures of armchair (left), zigzag (middle), and chiral (rigth) SWCNTs, b) TEM micrograph showing the lateral packing of 1.4-nm-diameter SWCNTs in a bundle [41].

3.3.2 Electrical properties

Rolling up a graphene sheet on a nanometer scale has dramatic consequences on the electrical properties. They can be metallic or semiconducting depending on their structure. Thus, some nanotubes have conductivities higher than that of copper, while others behave more like silicon. There is great interest in the possibility of constructing nanoscale electronic devices from nanotubes, and some progress is being made in this area [33, 36].

3.3.3 Mechanical properties

The small diameter of CNT also has an important effect on the mechanical properties, compared with traditional micron-size graphitic fibres [36]. In terms of tensile strength and elastic modulus, CNT are considered to be the strongest and stiffest materials of earth. This enormous strength is result of covalent bonds between individual carbon atoms. For example, the Young's modulus of the best nanotubes can be as high as 1 000 GPa which is approximately 5x higher than steel. The tensile strength, or breaking strain of nanotubes can be up to 63 GPa, around 50x higher than steel [33].

3.4 Synthesis of carbon nanotubes

As mentioned above, carbon nanotubes are very promising material in various fields, such as composites, energy devices, electronic applications, and medical applications. For novel applications of carbon nanotubes, the control of diameter, chirality, the number of layers and purity is crucial [37]. Many techniques have been developed to synthesize CNT

and possibly control these parameters and quantities: arc discharge, laser ablation, high pressure carbon monoxide (HiPCO), and catalytic chemical vapour deposition (CCVD) [41].

Because of CNTs used in this study were prepared by chemical vapour deposition, this technique is going to be discussed in details.

The initial catalytic chemical vapor deposition (CCVD) method for producing carbon nanotubes was called seeding method. The substrate that contained small evenly dispersed metal catalysts (iron particles) was set into hotspot of the furnace under a constant flow of hydrocarbon (for example benzene) and a mixture of hydrogen and argon. As a result, fibrous materials grew on the surface of the substrate from iron particles. The obtained fibrous carbon material had the carbon nanotubes in the core, and deposited carbons on it [32].

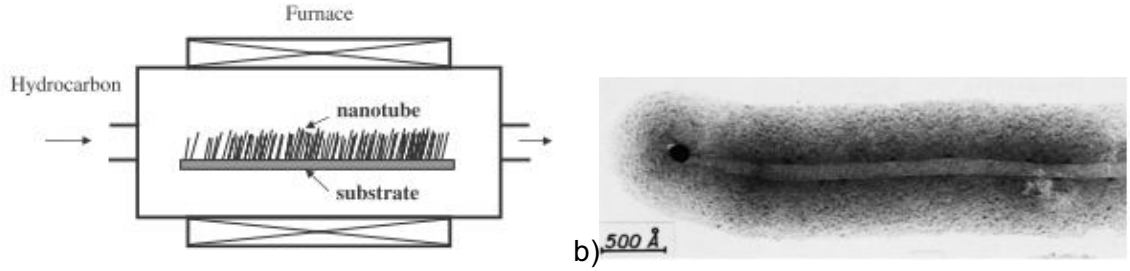

a) b)

Fig. 17: Schematic image of seeding-method-based fibrous carbon production setup, b) Transmission electron microscope image of fibrous carbon grown by seeding method. An iron catalyst particle is observed at the tip of the inner tube [32].

Nevertheless, the described process was non-continuous and therefore it was not suitable for industry. Because of the strong demand for these carbon nanotubes on the market, continuous method called the floating reactant method was developed. In this process, metal catalyst, carbon source and gases are fed from the top end of the vertical furnace (Fig. 18). While the catalyst particles are floating, gradually falling inside the furnace, the tubes growth and carbon deposition processes occur. At the bottom of the furnace, carbon nanotubes are obtained (Fig. 18). This method was very effective for the volume production of CNT, and the quality of the product was high as well. The only disadvantage of this method is the fact, that one can´t get rid of the catalyst while producing carbon nanotubes. As a result, the catalyst must be removed after the synthesis [32].

Once the volume production of CNTs was successfully handled, the needs for various types of CNTs emerged as well. For example, diameter and number of layers of the tube can be controlled by the diameter of the catalyst particle (small diameter of the catalyst results in small diameter of tube) [32].

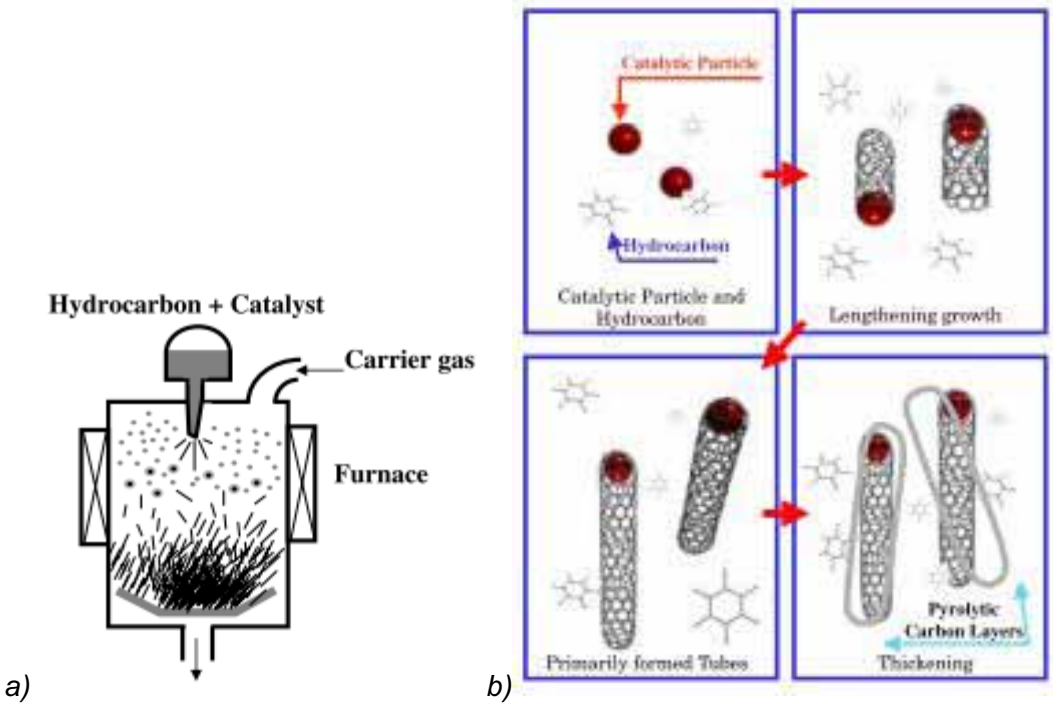

Fig. 18: a) Illustration of floating method setup and b) its growth model. The basic growth mechanism is the same as those of other CCVD methods, since the growth initiates from the catalyst [32].

3.5 Dispersion of carbon nanotubes

The ability to handle carbon nanotubes as individual components and the understanding of their behaviour in various media are essential for characterisation of their intrinsic properties and for further development of their applications [34]. Furthermore, the main bottleneck for the incorporation of CNTs into nanocomposites is that as-produced CNTs are held together in bundles of 50 – 200 individual tubes by very strong van der Waals interactions [35].

Currently two approaches are widely used in nanotube dispersion: the mechanical approach and the chemical approach. The mechanical approach includes ultrasonication and high-shear mixing. These processes are time-consuming and less efficient. Furthermore ultrasonication can result in fragmentation of CNTs, in turn, decreasing their aspect ratio. Besides this, the stability of the dispersion is poor. On the other hand, the chemical approach includes both covalent and noncovalent methods [34, 43].

3.5.1 Noncovalent methods

The non-covalent methods to functionalize CNTs involve using soft matter such as surfactants, oligomers, biomolecules and polymers to ‘‘wrap’’ CNTs, to enhance their solubility (Fig. 19 c) and d)). The advantage of the non-covalent method is that the integrity of CNT structure is not disrupted and the properties of the CNTs are therefore retained. However, the non-covalent interaction between the wrapping molecules and the CNTs is not as strong as the covalent bonds formed in the chemical functionalization processes [51].

Surfactants

Various anionic, cationic, and nonionic surfactants have been used and were proposed to solubilize CNTs through interaction of the organic (alkyl or hydrophobic) groups on the surfactant with the CNT surface and interaction of the ionic portion of the surfactant with the aqueous phase. It was suggested that there exists an optimal surfactant concentration for

dispersion, which results from competition between maximization of surfactant adsorption onto CNT surfaces and a micelle-mediated depletion interaction between adjacent CNT bundles [42].

To date, a wide variety of surfactants have been investigated for dispersion of carbon nanotubes, such as sodium dodecyl benzenesulfonate (SDBS), dodecyltrimethylammonium bromide (DTAB), hexadecyltrimethylammonium bromide (CTAB), octyl phenol ethoxylate (Triton X-100), and sodium dodecyl sulfate (SDS) [43].

Proteins and peptides

Proteins could be conjugated with carbon nanotubes via either spontaneous adsorption onto the nanotube surface or the immobilization more controllably in functionalization reactions. It was demonstrated that common proteins such as lysozyme, histone, hemoglobin, trypsin, glucose oxidase and others were good dispersing agents for SWCNTs and that the dispersing efficiency of these proteins depended on various factors including the primary structure and pH [46].

DNAs/RNAs

Similar to proteins, DNAs and RNAs could be attached to carbon nanotubes noncovalently by adsorption and covalently either directly or through a bifunctional linker. The specific interaction between DNA sequences grafted on the carbon nanotube surface was used in the assembling of nanotubes into architectures necessary for electrical circuits and molecular sensing applications. The functionalization (or wrapping) of carbon nanotubes with DNA not only imparts aqueous solubility but also allows a more precise control of the interfacial properties [46].

3.5.2 Covalent methods

This approach is referred to as covalent functionalization, because functional groups are covalently linked to the CNT surface (Fig. 19 a) and b)), the linkage is permanent and mechanically stable. However, reaction with the graphitic sheets also results in breaking the sp^2 conformation of the carbon atoms. Conjugation of the CNT wall is therefore disrupted, CNTs structures are destroyed (including cutting and opening CNTs) and it has been observed that, compared with the pristine tubes, electrical and mechanical properties of the chemically functionalized CNTs decreased dramatically [45, 51].

The oxidation of CNTs either by wet chemical methods, photo-oxidation, oxygen plasma, or gas phase treatment has gained a lot of attention in an attempt to purify and also enhance the chemical reactivity of the graphitic network. Typically, through the above harsh treatments, the pristine CNTs can be effectively purified and oxygen-containing groups, mainly carboxyl and hydroxyl, have been found to decorate the graphitic surface. The presence of oxygen-containing groups facilitates the exfoliation of CNT bundles, and increases the solubility in polar media [44].

The commonly used oxidants for liquid phase oxidation include HNO_3, H_2O_2 or a mixture of H_2O_2 and HCl, a mixture of H_2SO_4, HNO_3, $KMnO_4$ and NaOH, $KMnO_4$ [45] and a mixture of NH_4OH and H_2O_2 [44].

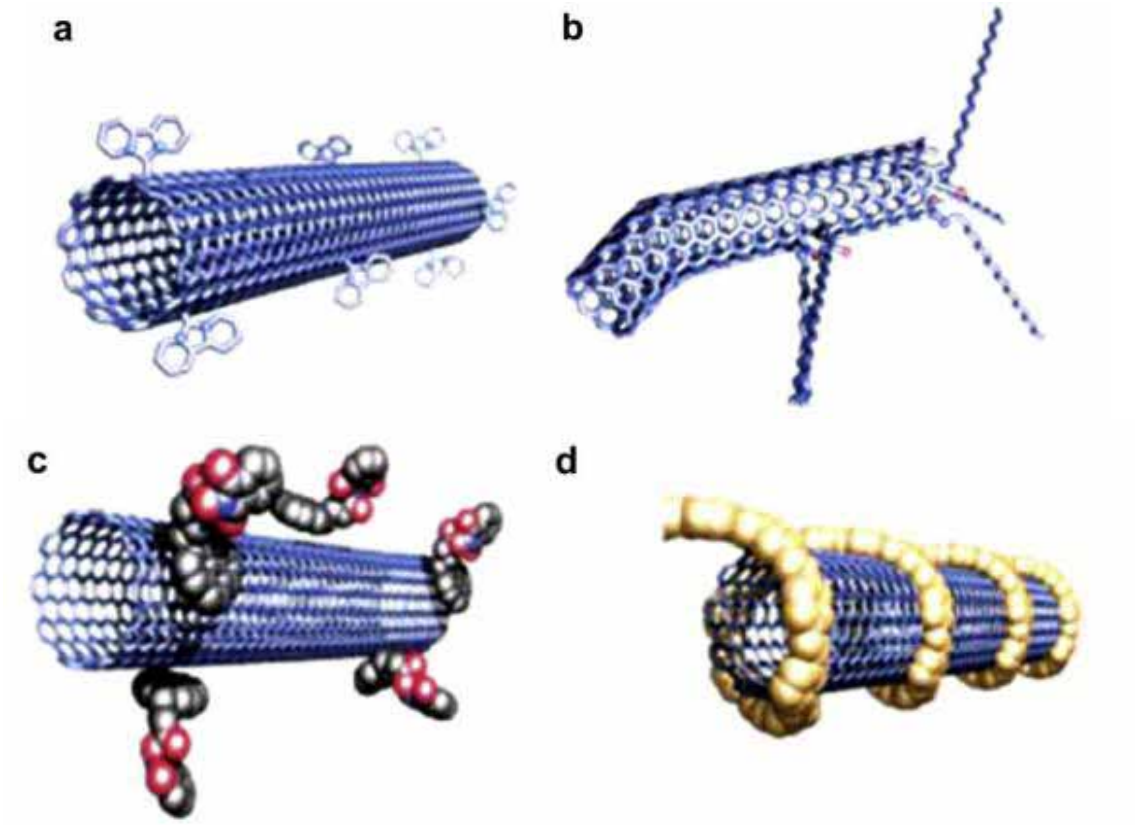

Fig. 19: Schematic representation of functionalized CNTs using different methods. (a) and (b) covalent functionalized CNT, (c) surfactant wrapped CNT, and (d) polymer wrapped CNT [51].

3.6 Carbon nanotubes/cellulose composite

Recently, fabricating applied functional electric devices (nanodevices) that are based on nanotechnology is gaining prominence for novel information-processing devices. Furthermore, fabrication of CNTs sheet and their possible applications (light emitting diodes, high-strength cables, and substrates) has been reported. However, manufacturing difficulties may slow down the commercial utilisation of these sheets in the near future [47].

Jung at al. [26] prepared MWCNT-based electrically conductive transparent papers with bacterial cellulose nanofibrils and an aqueous silk fibroin solution (Fig. 20). It was prepared by adsorbing the MWCNTs onto a bacterial cellulose hydrogel followed by drying the hydrogel at room temperature. The role of the silk was as a coating material to avoid extricating the MWCNTs from the surface of the bacterial cellulose nanofibrils. The electrically conductive transparent papers retained their high transparency even when MWCNTs were incorporated during the preparation process [26].

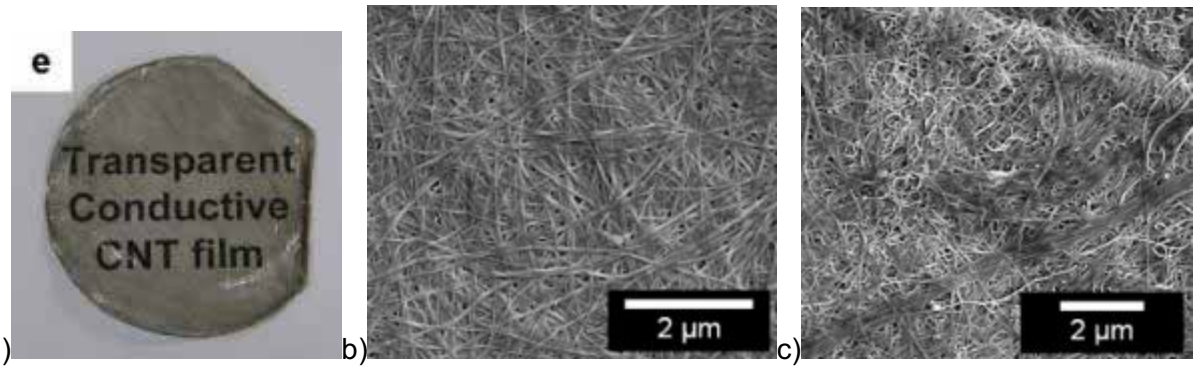

a) b) c)

Fig. 20: a) electrically conductive transparent paper. FESEM images of b) bacterial cellulose membrane and c) CNT-adsorbed bacterial cellulose membrane [26].

Yan Z. at al. [25] studied an effect of acid-treated multi-walled carbon nanotubes (MWCNTs) added into a static culture medium (A. Xylinum) on bacterial cellulose structure (Fig. 21). The acid-treated MWCNTs with -OH groups were dispersed uniformly in the medium. The BC ribbons interwound with the MWCNTs and formed the three-dimensional network [25].

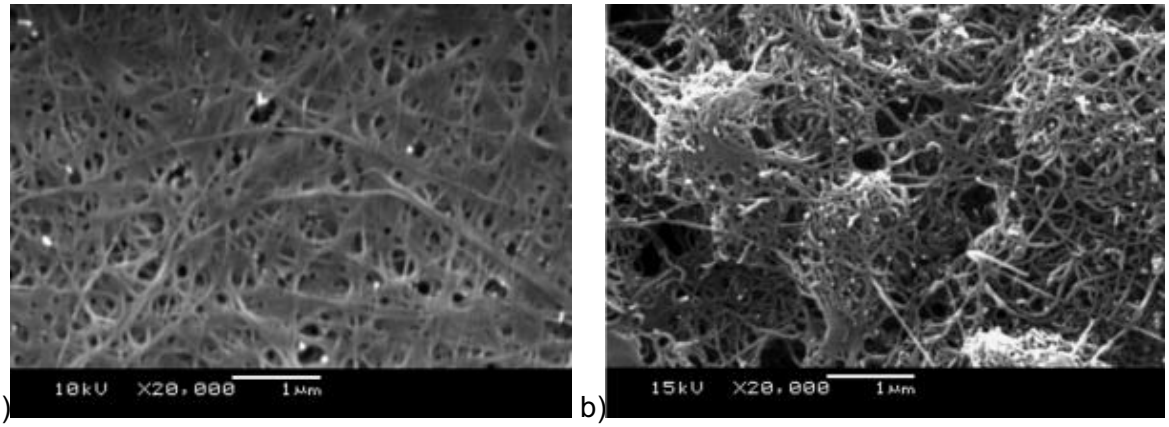

a) b)

Fig. 21: SEM micrographs of a) bacterial celluluose membrane and b) bacterial cellulose interwound with MWCNTs [25].

Oya at al. [47] developed a simple method for making CNT sheets that is based on a traditional method for making Japanese washi paper. Electrically conductive washi that contains SWCNTs (CNT-washi; Fig. 22 – 23) was made by combining a traditional Japanese process and a SWCNT-dispersing process that uses a surfactant in pure water. Controlling the amount of added SWCNTs can easily set the electrical conductivity of the paper. However, the conductivity of paper was not uniform [47].

a) 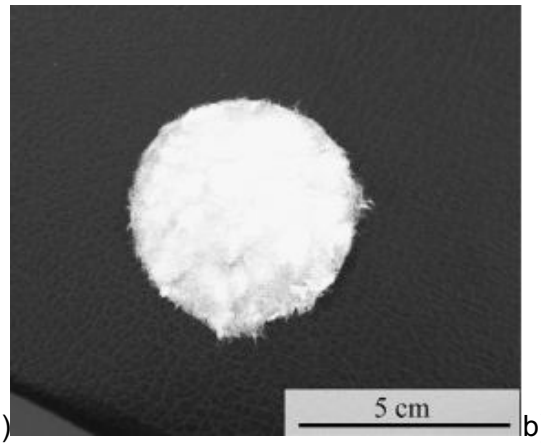

b) 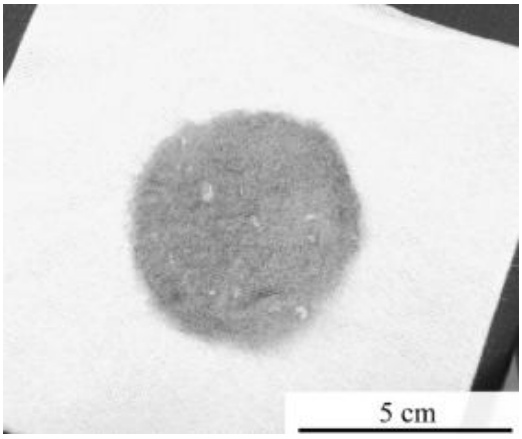

Fig. 22: a) Normal washi and b) CNT-washi [47].

a) 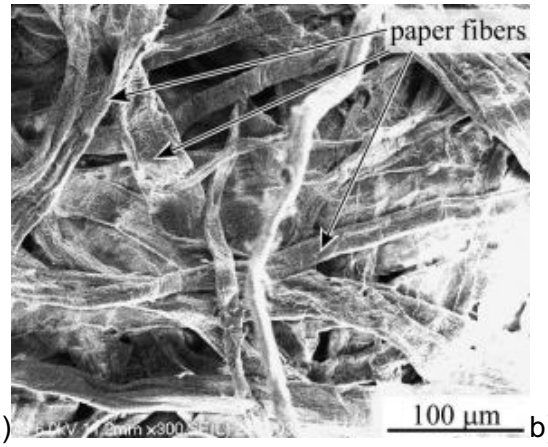

b) 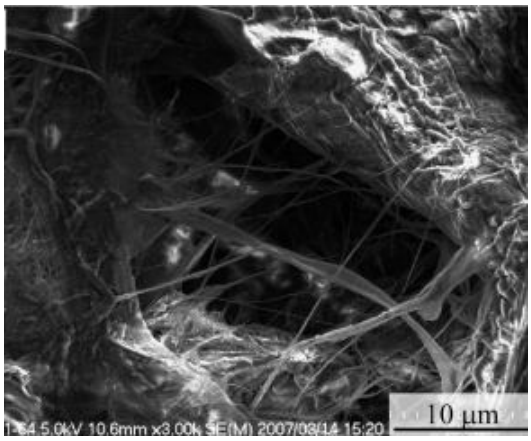

Fig. 23: SEM images of a) normal washi, b) CNT-washi [47].

4 MATERIALS AND METHODS

4.1 Materials

- multi-walled carbon nanotubes (MWCNTs; Thomas Swan, Elicarb®; purity 70 – 90 %)
- sodium dodecyl sulphate (SDS; Biochemical)
- nitric acid (HNO_3; Scharlan; 65 %)
- sulphuric acid (H_2SO_4; Merck; 95 – 97 %)
- ammonium hydroxide (NH_4OH; Prolabo; 25 %)
- hydrogen peroxide (H_2O_2; Sigma-Aldrich; 30 %)
- softwood sulphite pulp (Domjö AB Sweden)
- potassium hydrogen phosphate (K_2HPO_4; Merk)
- potassium dihydrogen phosphate (KH_2PO_4; Merk)
- enzyme (endoglucanase; Novozym 476, A/S, Denmark)
- MiliQ water (18.2 MΩ.cm)

4.2 CNTs suspension

Multi-walled carbon nanotubes (MWCNTs; prepared by chemical vapour deposition, average outer diameter 10 – 12 nm with length in order of tens of microns) were obtained from Thomas Swan, Elicarb® and three different methods (using surfactant, acidic and basic oxidative treatment) were used in order to prepare MWCNTs aqueous suspension. Ultrapure water (resistivity 18.2 MΩ.cm) was used in all experiments.

4.2.1 Surfactant treatment (ST)

Anionic surfactant sodium dodecyl sulphate (SDS) was used. 40 ml of 2% solution of SDS was prepared and 0.2 g of MWCNTs was added (ratio SDS:MWCNTs is 4:1 [48]). Suspension was prepared by high-shear mixing (Ultra Turrax T25 basic, IKA; 13 000 rpm, 1 hour) followed by sonication with rod-type sonicator for 4x2.5 min (Branson Sonifier 250, output 10, 70 % - pulsing 0.7 s on, 0.3 s off) [52].

Then, suspension was centrifuged using 20 500 rpm for 60 min. (Sorvall RC 26 Plus, rotor SS-34, centrifugal force approx. 50 000 g). Supernatant was removed and precipitant was redispersed in 100 ml of water by 4x2.5 min sonication using rod-type sonicator. Suspension was centrifuged again at 4 000 rpm for 30 min (Sorvall Super T21, rotor ST-H750, approx. 3 300 g). Supernatant was collected and kept as stable homogenous MWCNTs suspension (Fig. 25).

5 ml of MWCNTs suspension in round bottom flask was freezed in liquid nitrogen and freeze-dried using freeze-drier (ALPHA 2-4 LD Plus, Christ). Freeze dried suspension was used for thermogravimetric analysis to determine the ratio between SDS and MWCNTs and to determine the concentration of MWCNTs in the suspension.

4.2.2 Acidic treatment (AT)

The treatment was done according to Yan Z. at al [25]: 100 mg of MWCNTs was dispersed in 100 ml of mixture of HNO_3 (65%) and H_2SO_4 (95 – 97%) in ratio 1:3. Mixture was stirred with magnetic stirrer and refluxed at 80°C for 10 hours. After that, it was diluted into approx. 1 000 ml of water, filtrated on PTFE membrane (Advantech, pore size 100 nm) and washed with water until pH = 4. Wet cake of MWCNTs was redispersed in approx. 35 ml water and sonicated for 2 min. using rod type sonicator, (output 10, 70 %) and stable homogenous suspension was obtained.

20 ml of MWCNTs suspension was evaporated using Rotavapor (Büchi Rotavapor R-200) in order to increase the concentration of MWCNTs. Concentrated suspension (volume approx. 5 ml) in round bottom flask was freeze-dried. Resulting dry MWCNTs suspension was weighed and from obtained value, concentration was determined.

Adjusting condition of acidic treatment

200 mg of MWCNTs was dispersed in 100 ml of mixture of HNO_3 (65%) and H_2SO_4 (95 - 97%) in ratio 1:3. Mixture was stirred with magnetic stirrer and refluxed at 80°C for 4 hours. Samples of MWCNTs were taken during the reaction after 1, 2, 3 and 4 hours. 25 ml of reaction mixture was diluted into approx. 200 ml of water, filtrated using nylon-66 membrane (Aldrich, pore size 200 nm) and washed with water. MWCNTs were washed from the membrane, diluted with water to obtain approx. 40 ml of suspension and sonicated for 2 min. using rod type sonicator (output 10, duty cycle 70 %). All suspensions were stable in water (Fig. 25). Concentration of suspension was determined by UV-VIS spectrophotometer (UV-Visible Spectrophotometer Cary 50 Bio, Varian). Extinction coefficient was taken from previous experiment where concentration was determined from the dry content and calibration curve was plotted.

4.2.3 Basic oxidative treatment (BT)

300 mg of MWCNTs was dispersed in 25 ml of mixture of NH_4OH (25%) and H_2O_2 (30%) in ratio 1:1 [44]. Mixture was stirred with magnetic stirrer and refluxed at 80°C for 5 hours. Mixture was cooled to ambient temperature and allowed to settle down for approx. 20 min. Upper clear liquid was removed and MWCNTs were washed with water on membrane with pores size 200 nm. After that, the wet cake was washed from the membrane, diluted to resulting volume of approx. 50 ml of water and sonicated with rod-type sonicator for 2 min. (output 10, 70 %).

Because of stable suspension was not obtained; it was centrifuge for 10 min at 4 300 rpm (approx. 3 800 g) and supernatant (clear water) was removed. Precipitant was redispersed in 60 ml of 2% SDS solution (SDS:MWCNTs = 4:1 [48]) by high-shear mixing (Ultra Turrax, 13 000 rpm) for 1 hour followed by sonication with rod-type sonicator for 4x2.5 min (output 10, 70 %) [52]. After that, stable suspension was centrifuged at 4 000 rpm for 30 min (approx. 3 300 g) in order to remove agglomerates of MWCNTs. Supernatant was collected and used for further experiments as a stable MWCNTs suspension (Fig. 25).

6 ml of MWCNTs suspension in round bottom flask was freezed in liquid nitrogen and freeze-dried. Freeze-dried MWCNTs was used for thermogravimetric analysis.

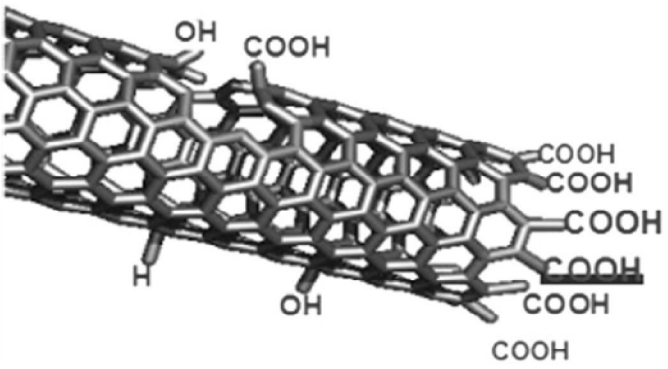

Fig. 24: Schematic representation of the attack to the MWCNTs during the oxidation process [67].

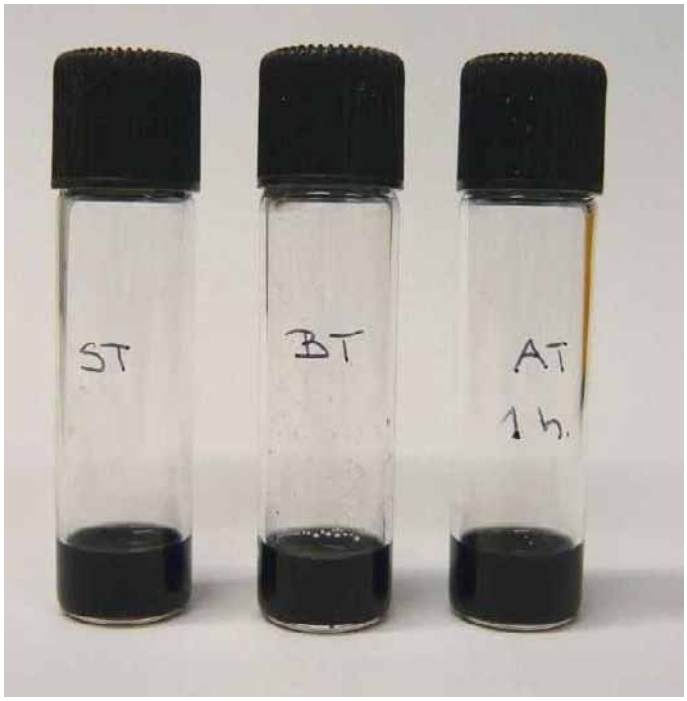

Fig. 25: MWCNTs suspensions prepared by different treatments (ST = using surfactant, BT = basic oxidative treatment and AT 1 hour = acid treatment for 1 hour).

4.3 Suspension characterisation

4.3.1 Thermogravimetric analysis (TGA)

Thermogravimetric Analysis (TGA) measures the weight change and rate of change in the weight of a material as a function of temperature or time in a controlled atmosphere. Measurements are used primarily to determine the composition of materials and to predict their thermal stability at temperatures up to 1000°C. The technique (Fig. 26) can characterize materials that exhibit weight loss or gain due to decomposition, oxidation, or dehydration. Using TGA method, one can determine thermal and oxidative stability of materials, composition of multi-component systems and lifetime of a sample, decomposition kinetic, effect of reactive or corrosive atmosphere and moisture and volatiles content of material [58].

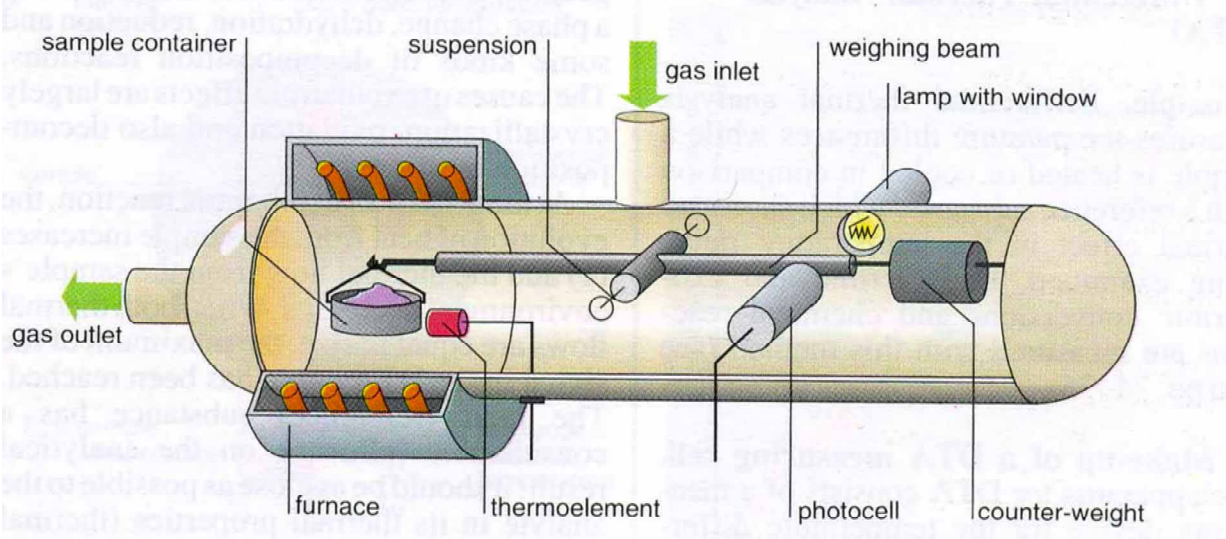

Fig. 26: Simplified diagram of setting for TGA [61].

TGA (TGA/SDTA 851e Mettler Toledo; Fig. 27) was performed in order to determine the net amount of MWCNTs in freeze-dried suspension and was done for ST and BT suspension. As a control, pure SDS and MWCNTs were used. TGA was performed in temperature range from 25°C to 1 000°C (heating rate 10°/min.) in alumina cup under nitrogen atmosphere (flow 50 ml/min). From obtained results, concentration of MWCNTs in suspensions was calculated.

Fig. 27: TGA Mettler Toledo.

4.3.2 UV-VIS spectroscopy

Bundled carbon nanotubes are not active in the UV–VIS region and only individual carbon nanotubes absorb in this region. Therefore, dispersion of carbon nanotubes can be characterized using UV–VIS absorption spectroscopy (Fig. 28). Concentration of MWCNTs dissolved or dispersed into the solution can then be determined using the specific extinction coefficient of carbon nanotubes [43].

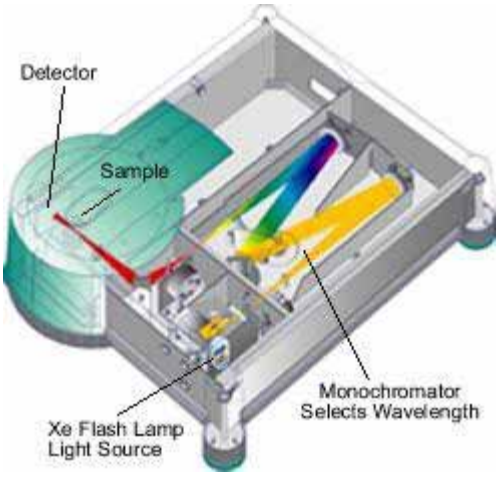

Fig. 28: Schematic illustration of UV-VIS spectrophotometer [61].

MWCNTs suspensions were diluted in order to get concentration series and absorbance at 500 nm [43] in case of ST and BT suspension and absorbance at 530 nm [34] for AT suspensions were measured using UV-VIS spectrophotometer. The cuvette length was 1 cm. Calibration curves were plotted and extinction coefficients were calculated for faster determination of MWCNTs concentration.

4.3.3 Field-Emission Scanning Electron Microscopy (SEM) analysis

The scanning electron microscope (SEM) is very powerful technique for surface characterization of heterogeneous organic and inorganic materials on nanometer (nm) to micrometer (μm) scale. SEM is capable of obtaining three-dimensional-like images of the surfaces of the very wide range of materials [56, 63].

A major reason for the SEM's usefulness is the high resolution on the order of 1 – 5 nm. Another important feature of the SEM is the large depth of field, which is, in part, responsible for the three-dimensional appearance of the specimen image [63].

The basic components of the SEM are the lens system, the electron gun, the electron collector, the visual and photorecording cathode rays tubes (CRTs) and the associated electronics (Fig. 29 left) [63]. It uses a focused beam of high-energy electrons to generate a variety of signals at the surface of solid specimens. The signals that derive from electron-sample interactions reveal information about the sample including external morphology, chemical composition, and crystalline structure and orientation of materials making up the sample [54].

Accelerated electrons aimed at a material surface result in a number of interactions with the atoms of the target sample. Accelerated electrons can either pass through the sample without interaction, or undergo elastic (or inelastic) scattering. Elastic and inelastic scattering result in a number of signals that are used for imaging, quantitative and semi-quantitative information of the target sample and generation of an X-ray source. Typical signals used for imaging include secondary electrons (SE; reveal surface topography), backscattered electrons (BSE; reveal chemical composition), cathodoluminescence (CL), auger electrons and characteristic X-rays (Fig. 29 right) [55].

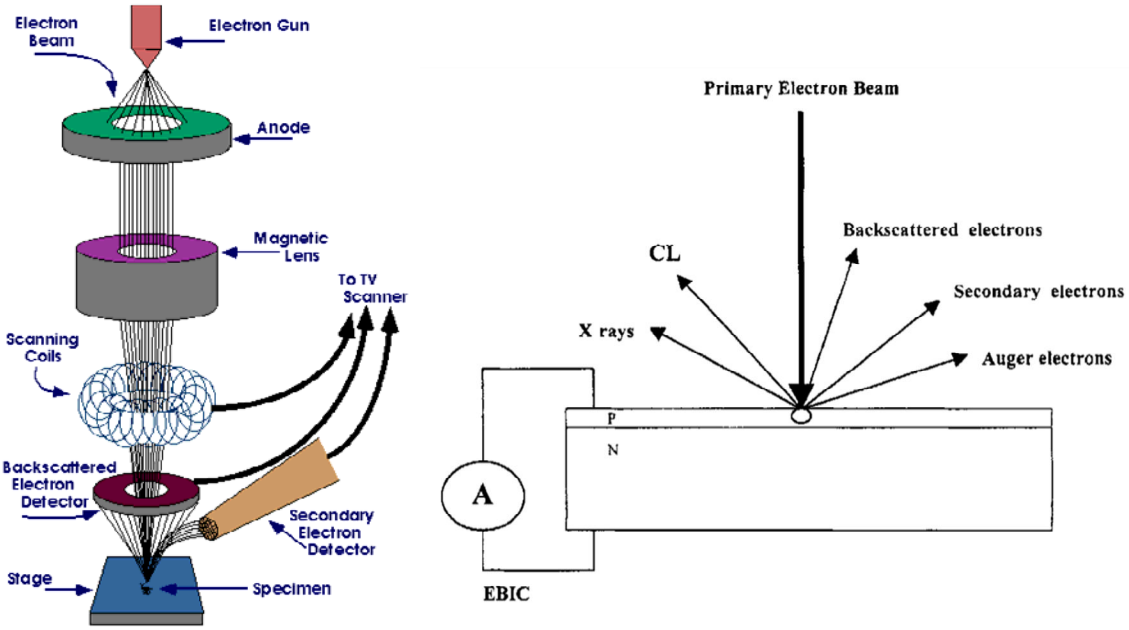

Fig. 29: Basic principal of SEM (left [56]) and signals available in a SEM due to electron beam interaction (right [57]).

SEM analysis was performed in order to investigate the quality of the suspension (Hitachi S-4300; Fig. 31). Small samples (layer of MWCNTs deposited on wet MFC films and dried) were cut and placed in desicator overnight. The samples were mounted onto a metal sample holder using colloidal graphite (Ted Pella Inc.; Fig. 30) and were used without coating. Low accelerating voltage (0.7 kV) and short working distance (2 – 3 mm) were used. Secondary electron detector was used. For each sample, pictures of the same area were taken under two different magnifications.

a)  b) 

Fig. 30: SEM sample holder with samples attached using colloidal graphite: a) top view and b) side view.

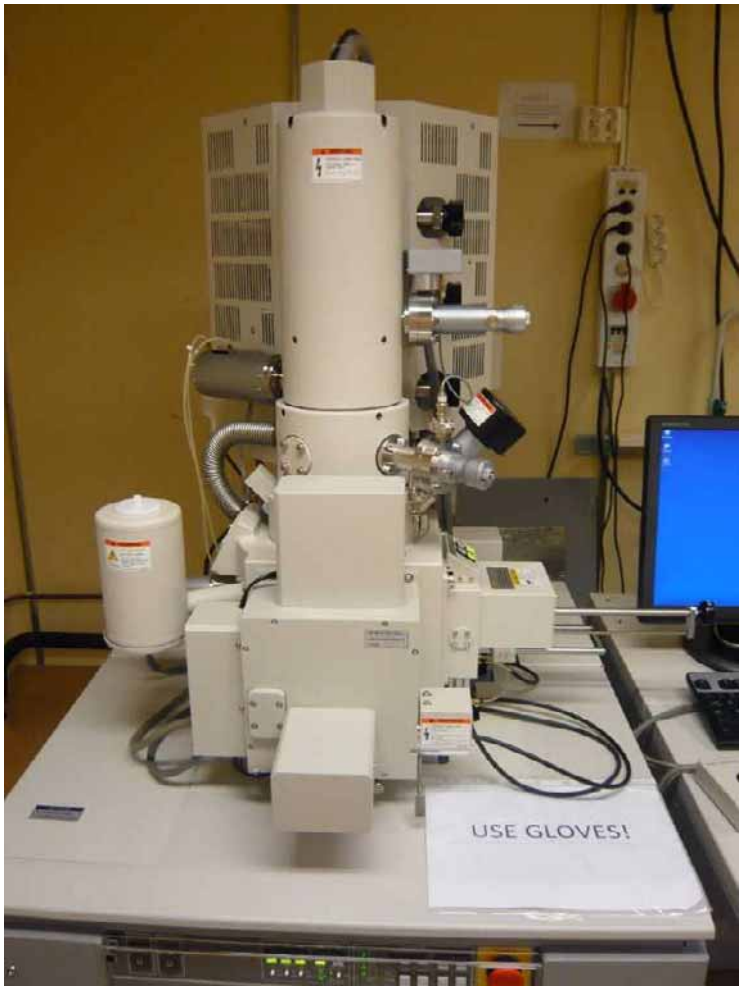

Fig. 31: Field-emission scanning electron microscope (Hitachi S-4300).

4.4 Microfibrillated cellulose (MFC) preparation

Microfibrillated cellulose (MFC) was prepared from softwood sulphite pulp using enzymatic treatment according to Henriksson [6]. Prior enzymatic treatment, fibres were mechanically treated by refining (PTI disintegrator, Tico 732 Hengstler; 30 000 revolutions) and beating (PFI-mil 2 000 revolutions) in order to make cellulose more accessible to enzymes. After that, enzymatic treatment was performed: 4% pulp was dispersed in buffer solution (pH = 7) containing 9 mmol of K_2HPO_4 and 11 mmol of KH_2PO_4 and 0.25% (related to the weight of the pulp) of enzyme (endoglucanase) was added. This enzyme is supposed to degrade cellulose in disordered regions. The wood pulp fibres were incubated for 2 hours at 50°C and washed with deinoized water on Büchner funnel. After that, 1 l of boiling water was added and fibres were incubated again at 90°C for 30 min to stop the enzyme activity and washed. Fibres were beaten again (4 000 revolutions).

2% fibre suspension in water was subjected to the shear forces using Microfluidizer M-110EH (Microfluidics Inc., USA). During the process, the suspension viscosity increased with increasing number of passes through the homogenizer [6]. Resulting 2% suspension of MFC was kept at 4°C (Fig. 32).

Fig. 32: MFC suspension (2 %).

4.5 Composite film preparation and characterization

For composite film preparation, following composition was used (Tab. 1). Two different sizes of films were made: diameter 35 mm (for tensile test, TGA and SEM) and 75 mm (for resistivity measurement) and thickness was 30 – 40 μm.

Tab. 1: Composition used for films preparation.

Dry content of MFC (%)	1.93	
Weight of dry MFC/film (g)	small	large
	0.05	0.20
Weight of wet MFC/film (g)	2.59	10.36
Concentration of MW susp.	ST	0.10%
	BT	0.14%
	AT	0.10%

wt. % of MWCNTs	weight of MWCNTs (mg)		volume of MWCNTs susp. (ml)					
	Small	large	ST		BT		AT	
			small	Large	small	large	small	large
0.00	0.00	0.00	0.00	0.00	0.00	0.00	0.00	0.00
0.10	0.05	0.20	0.05	0.20	0.04	0.15	0.05	0.20
0.50	0.25	1.00	0.25	0.98	0.18	0.73	0.25	1.00
1.00	0.50	2.00	0.49	1.96	0.36	1.45	0.50	2.00
2.00	1.00	4.00	0.98	3.92	0.73	2.91	1.00	4.00
5.00	2.50	10.00	2.45	9.80	1.82	7.27	2.50	10.00*

*was not prepared because of the amount of AT suspension was not enough and because of limited time, additional amount couldn´t be made

MWCNTs suspension was added to MFC nanofibres, total volume was adjusted to approx. 26 ml (0.2 wt.% of MFC) and mixed using high shear mixing (13 000 rpm) for 3x1.5 min, followed by stirring with magnetic stirrer for 1 day. After that, water was removed using vacuum filtration (Fig. 33) resulting in a wet film. Obtained film (top side of the film was marked) was stuck in between of two metallic grids, placed in between of two sheets of filter paper and dried at 93ºC and vacuum for 10 min in sheet former (Rapid Kothen RK3A-KWT PTI; Fig. 34). Control sample (100 % MFC film) was prepared using the same procedure. Photographs of composite films are shown on the Fig. 35 – 37.

Fig. 33: Filtration setup used for composite film preparation.

Fig. 34: Sheet former Rapid Kothen.

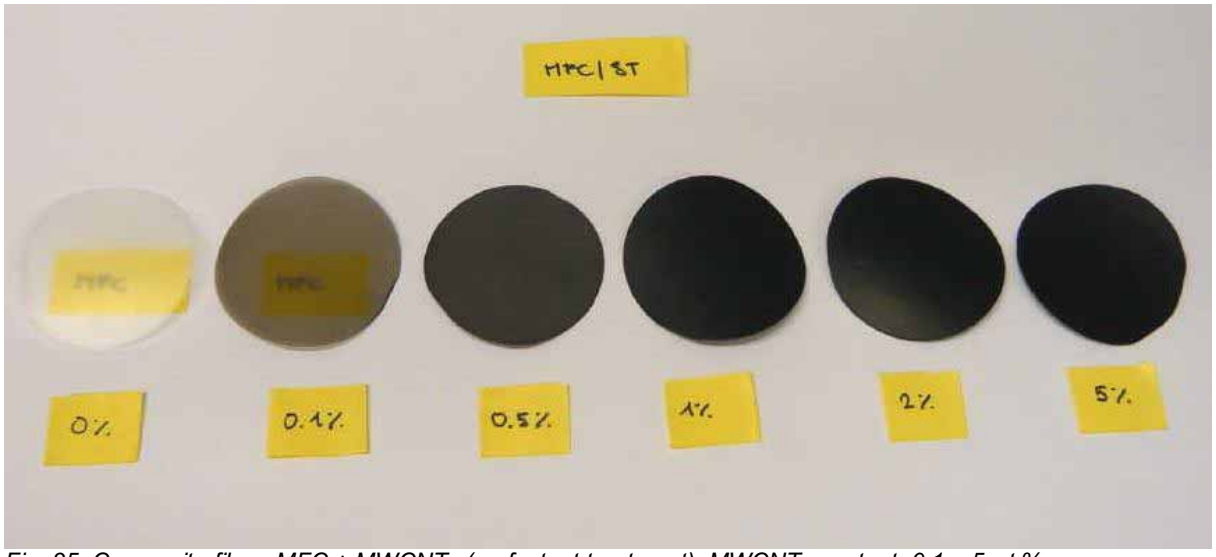

Fig. 35: Composite films: MFC + MWCNTs (surfactant treatment). MWCNTs content: 0.1 – 5 wt.%.

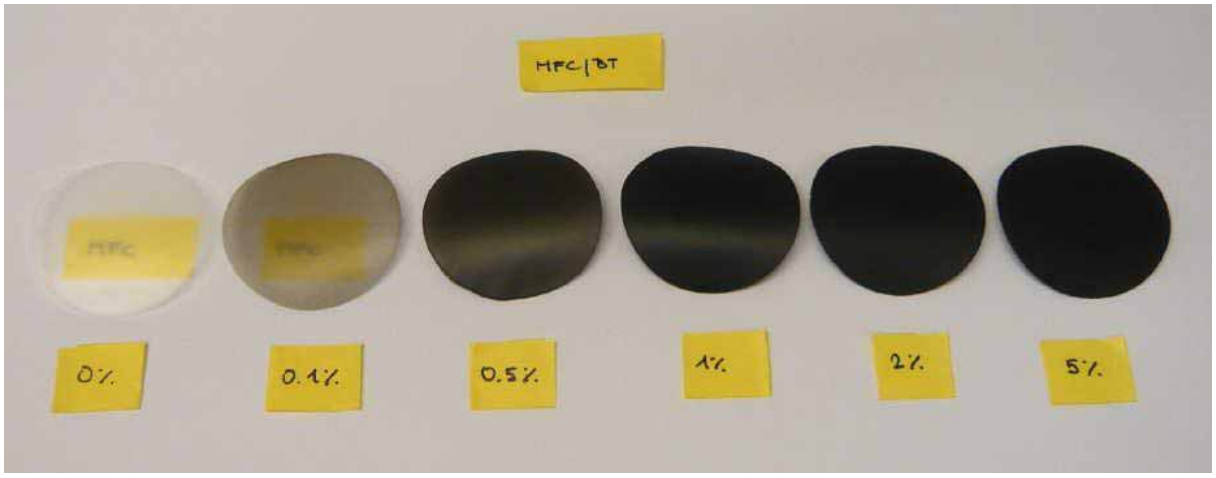

Fig. 36: Composite films: MFC + MWCNTs (basic oxidative treatment). MWCNTs content: 0.1 – 5 wt.%.

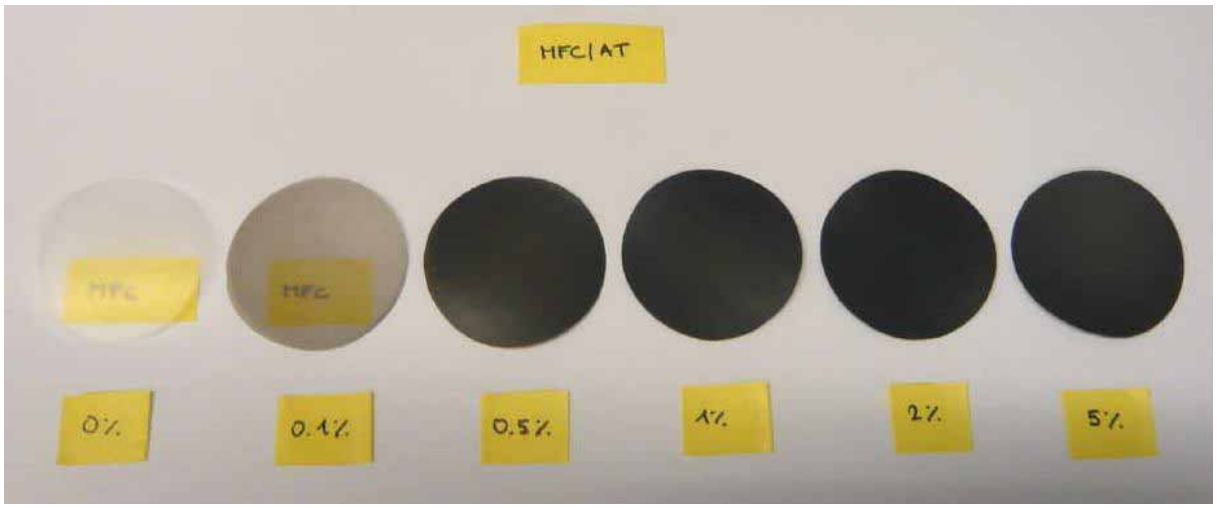

Fig. 37: Composite films: MFC + MWCNTs (acid treatment for 1 hour). MWCNTs content: 0.1 – 5 wt.%.

4.5.1 TGA analysis

Thermogravimetric analysis was done in order to obtain exact MWCNTs content in the composite films. TGA was performed in temperature range from 25°C to 1 000°C (heating rate 10°/min.) in alumina cup under nitrogen atmosphere (flow 50 ml/min).

4.5.2 Surface resistivity measurement

Two methods are usually used for determination of resistivity/conductivity values. The first one is based on the electrical properties of the test specimen surface, while the second one is based on the bulk electrical characteristics of the test material. Surface experiments are used more frequently for evaluation of electrical properties of polymer materials [59].

Surface resistivity is defined as the electrical resistance of the surface of a material. It is measured from electrode to electrode along the surface of the sample. Since surface length is fixed, the measurement is independent of the physical dimensions (i.e., thickness and diameter) of the sample [65].

Surface resistivity (ρ_S) was measured on both sides of the samples using Keithly 6517B Electrometer/High Resistivity Meter together with a Keithly 8009 Resistivity Test Fixture (Fig. 38). The measurement was performed in University of Perugia (Terni, Italy).

Surface resistivity was measured by applying a voltage potential across the surface of the sample, measuring the resultant current and then performing the following calculation [65]:

$$\rho_S = \frac{53.4V}{I}\,\text{ohms} \tag{1}$$

Where: ρ_S is the surface resistivity of the sample.
V is the applied voltage from the Electrometer.
I is the current reading from the Electometer [65].

Derivation of resistivity equation

The ASTM standard states that surface resistivity shall be calculated as follows:

$$\rho_S = \frac{\mathrm{P}}{\mathrm{g}}\mathrm{R} \tag{2}$$

Where: R is the surface resistance in ohms.
g is the distance between the guarded electrode and the ring electrode (0.125 inches).
P is the effective perimeter of the guarded electrode for the particular electrode arrangement employed.

For the Model 8009, that was used for the measurement and has circular electrodes, P is calculated as follows:

$$\mathrm{P} = \mathrm{D}_0\pi \tag{3}$$

Where D_0 is the effective diameter of the guarded electrode: 2.125 inches. Thus,

$$\mathrm{P} = 2.125\pi \tag{4}$$

By substituting the values for g and P into eq. (2), it becomes:

$$\rho_S = \frac{2.125\pi}{0.125}\mathrm{R} = 53.4\mathrm{R} \tag{5}$$

Surface resistance (R) is derived by dividing the applied test voltage (V) by the subsequent measured current (I). By substituting R with V/I, eq. (1) is obtained [65].

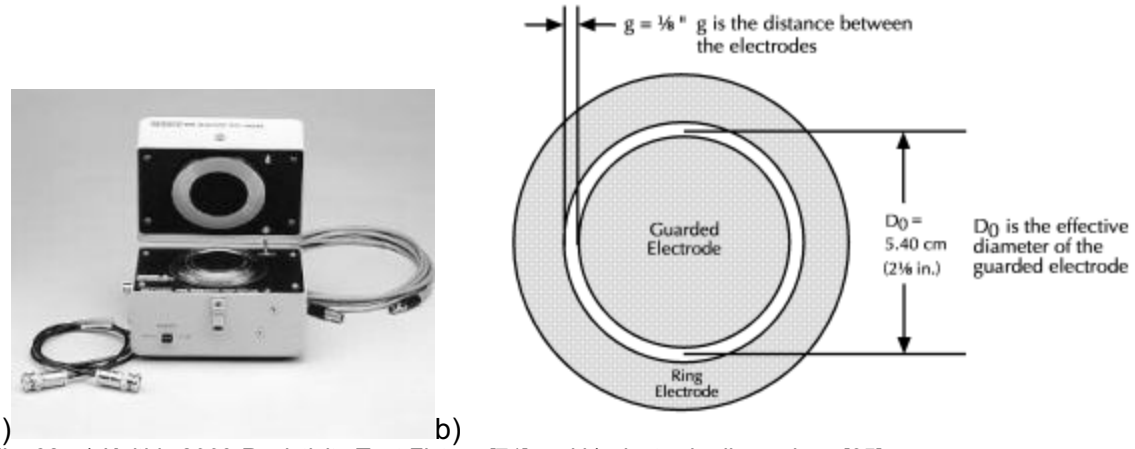

a) b)

Fig. 38: a) Keithly 8009 Resistivity Test Fixture [71] and b) electrode dimensions [65].

4.5.3 Tensile test

A tensile test is probably the most fundamental type of mechanical test that can be performed on material. Tensile tests are simple, relatively inexpensive, and fully standardized. In the initial part of the tensile test, the relationship between the applied force (or load) and the elongation of the specimen is linear. In this linear region, the ratio of stress (σ) to strain (ε) is a constant (Fig. 39 a):

$$\frac{\sigma}{\varepsilon} = E \qquad (6)$$

and E is the slope of the line in this region (it is called the Young´s Modulus). The Equation (6) is known as Hooke´s law.

The Young's modulus is a measure of the stiffness of the material, but it only applies in the linear region of the curve. If a specimen is loaded within this linear region, the material will return to its original state after removing the load. At the point that the curve is no longer linear and deviates from the straight-line relationship, Hooke's Law no longer applies and permanent deformation occurs in the specimen. This point is called the elastic or proportional limit. From this point on, the material reacts plastically to any further increase in load or stress. It will not return to its original, unstressed condition if the load was removed.

A value called yield strength of a material is defined as the stress applied to the material at which plastic deformation starts to occur while the material is loaded. The maximum load the specimen sustains during the test is called ultimate tensile strength (UTS). The UTS may or may not equate to the strength at break depending on the material [65].

Tensile test was performed using Miniature Materials Tester MiniMat2000 with loading cell 200 N. Rectangular samples with dimensions 5x30 mm were tested. The gap between the clamps was 10 mm and loading rate was 1 mm/min and test was performed until the sample broke. Stress-strain curves were recorded by computer and used for further analysis. Young´s modulus, tensile strength and strain-to-failure were calculated using Matlab.

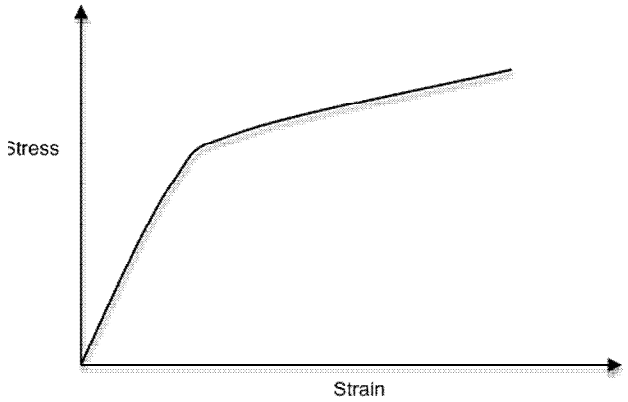

a)

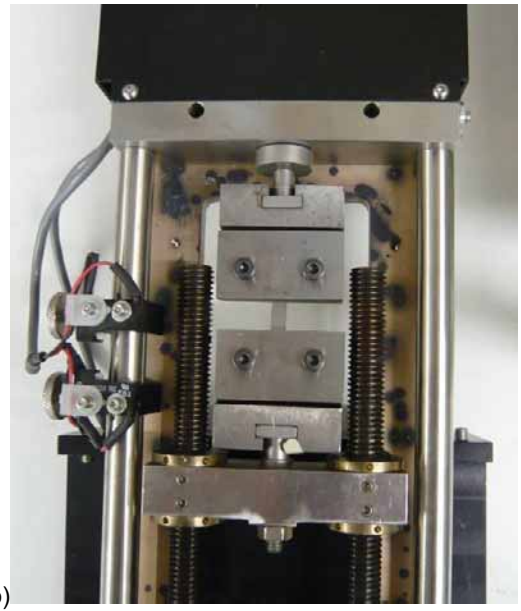

b)

Fig. 39: Typical stress strain curve of MFC film, accordng to [20], b) sample clamped in steel clamps during tensile test.

4.5.4 SEM analysis

In order to investigate the surface of composite films, SEM analysis was done. Small samples (5x5 mm) were cut and placed in desiccator overnight. The samples were mounted onto a metal sample holder using colloidal graphite and coated with carbon (Carbon coater Cressington 108 carbon/A; 3 s) and with gold/palladium (Sputter coater Cressington 208 HR; 4 nm). Low accelerating voltage (0.7 – 1 kV), short working distance (2 – 3 mm) and secondary electron detector were used. Each sample was investigated both from its top side and bottom side and pictures of the same area were taken under different magnifications.

5 RESULTS AND DISCUSSION

5.1 CNTs suspension

MWCNTs suspension was prepared using three different pre-treatments: non-covalent modification using surfactant (ST) and two covalent modifications using acidic treatment (AT) and basic oxidative treatment (BT). All CNTs suspensions appeared black and homogenous, without visible agglomerates.

5.1.1 Dry content determination

Dry content was determined by freeze-drying of MWCNTs suspensions and resulting values are summarized in Tab. 2. Value obtained for AT suspension is actually MWCNTs concentration in the suspension, because no surfactant was used. However, for ST and BT suspension, obtained values refer to dry content of both MWCNTs and surfactant. Therefore thermogravimetric analysis had to be done in order to get exact MWCNTs concentration.

Tab. 2: Dry content values determined by freeze-drying.

Suspension Type	Dry content (mg/ml)
ST	4.422*
BT	17.183*
AT 10 hours	0.100#

*dry content of MWCNTs and surfactant
#dry content was measured only for suspension treated for 10 hours. Remaining concentrations (treatment for 1 – 4 hours) were determined by UV.

5.1.2 Thermogravimetric analysis (TGA)

Thermogravimetric analysis was performed for ST and BT suspensions. From obtained curves (Fig. 40), MWCNTs concentrations in the suspensions were calculated.

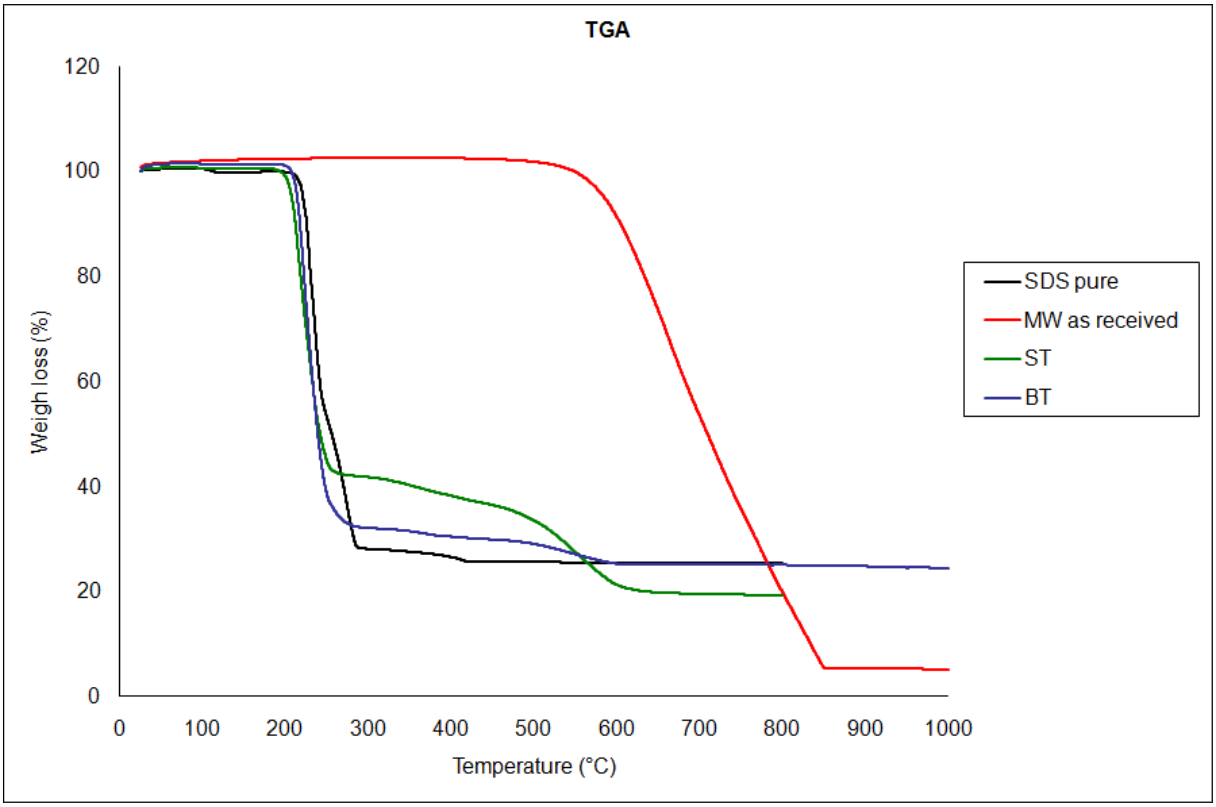

Fig. 40: TGA profiles for pure SDS, as received MWCNTs, ST and BT suspensions.

On the Fig. 40, the red curve corresponds to as received MWCNTs, The weight loss starts to be significant at around 550˚C and gradually decreases up to 850˚C. It is well known that different structural forms of carbon can exhibit different oxidation behaviour depending on the available reaction sites. For example, disordered or amorphous carbon tends to be oxidised at around 500˚C, because of its lower activation energy for oxidation or due to the presence of a large number of active sites. On the other hand a well graphitized structures start to oxidise at a relatively higher temperature between 600˚C and 700˚C, depending on the type of CNTs [44]. The onset temperature is also influenced by bundle diameter, the number of walls and the crystallinity of CNTs. Material that remains at 900˚C is metal oxides [53].

The black curve corresponds to the pure SDS and the weigh loss can be observed between 220˚C and 420˚C. Therefore for the curves corresponding to ST and BT suspension, the weigh loss occurring between these temperatures is attributed to the loss of SDS and the second weigh loss is related to MWCNTs.

The obtained values are shown in Table 3.

Tab. 3: MWCNTs content and concentration in ST and BT suspensions determined by TGA and dry content.

Suspension Type	MWCNTs content (%)	MWCNTs concentration (mg/ml)
ST	23	1.020
BT	8	1.375

For AT suspension, dry content was determined only after 10 hours of the treatment and concentrations of remaining suspensions were determined by UV-VIS reading using calibration curve.

5.1.3 UV-VIS spectroscopy

Absorbance was measured at 500 nm in case of ST and BT suspension and at 530 nm for AT suspensions. Because concentrations of suspensions (ST, BT and AT 10 hours) are known from dry content measurement and TGA, calibration curves were plotted (Fig. 41 – 43) for fast determination of suspension concentration.

All the results are straight lines. Therefore Lambert-Beer law (Equation 7) can be used to determine extinction coefficient of MWCNTs.

$$A = \varepsilon l c \tag{7}$$

where *A* is absorbance, ε extinction coefficient, *l* the path length and *c* the concentration [42].

Using calibration curve AT 10 hours, concentration of suspensions treated for 1 – 4 hours were calculated. Concentrations of all suspensions are listed in Table 4.

Tab. 4: Summary of concentration values of MWCNTs suspensions.

Suspension Type	Concentration (mg/ml)
ST	1.020
BT	1.375
AT 1 hour	1.000
AT 2 hours	0.593
AT 3 hours	0.550
AT 4 hours	0.415
AT 10 hours	0.100

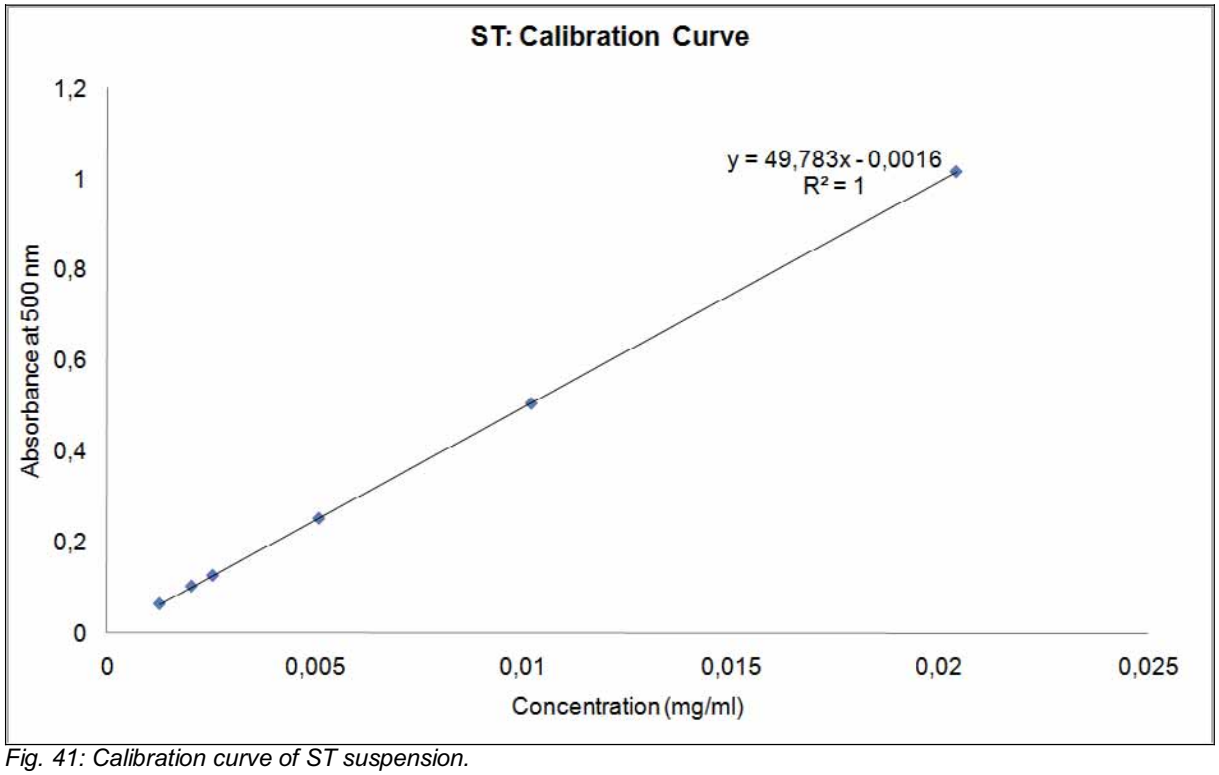

Fig. 41: Calibration curve of ST suspension.

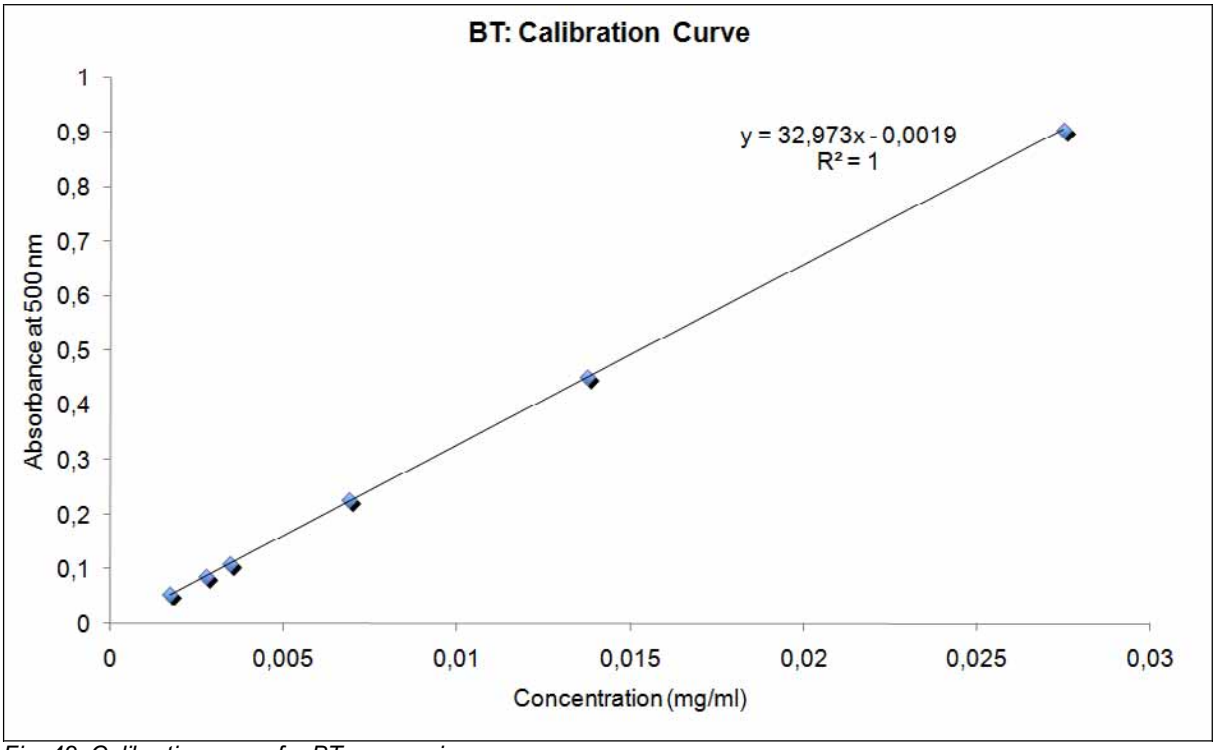

Fig. 42: Calibration curve for BT suspension.

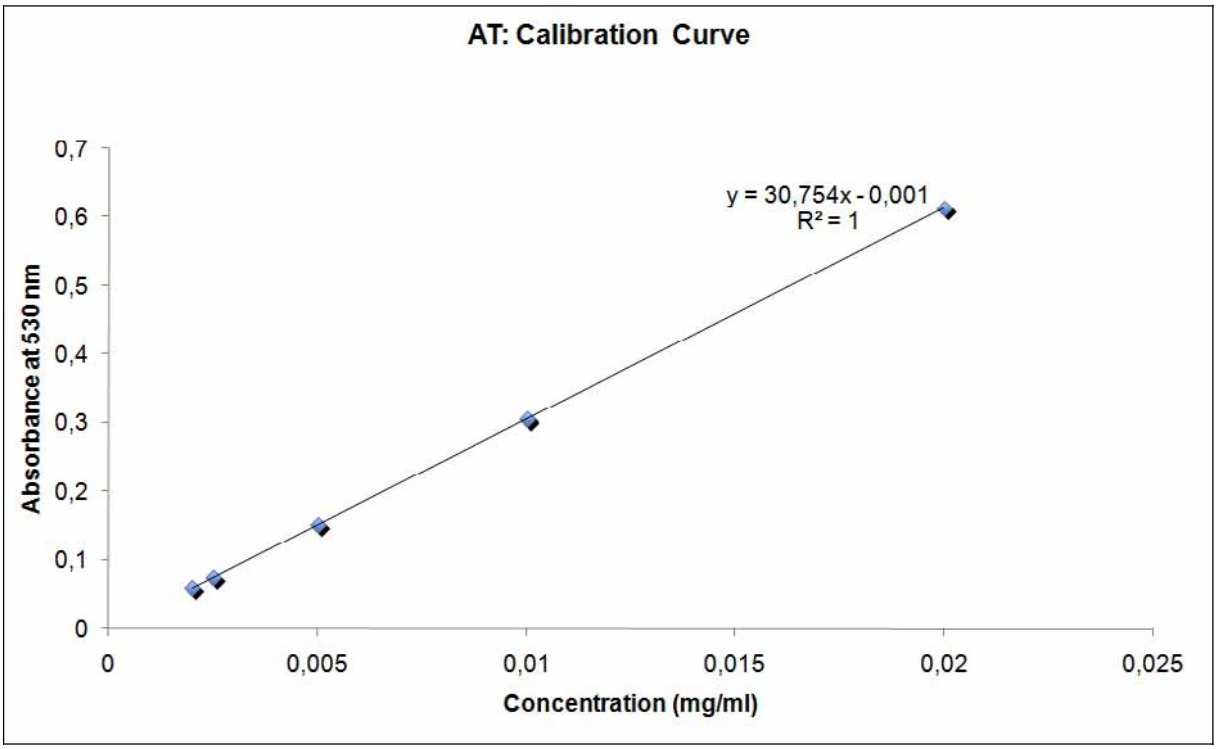

Fig. 43: Calibration curve for AT 10 hours suspension.

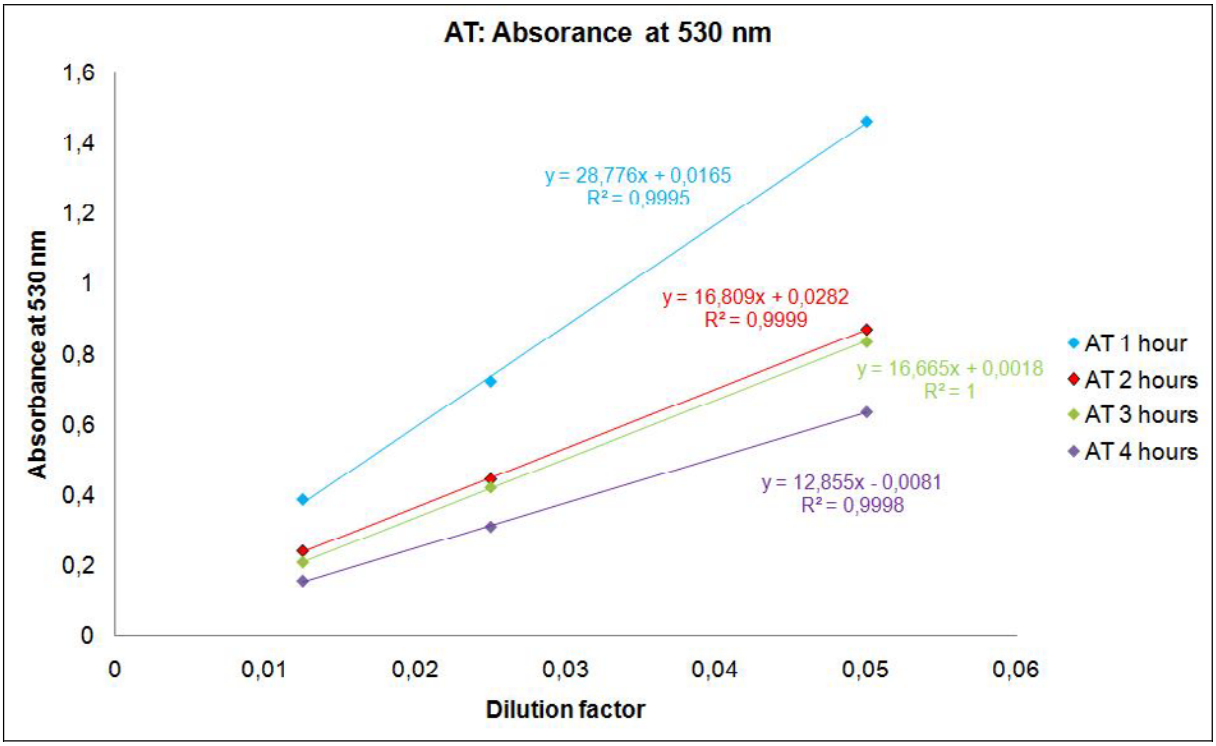

Fig. 44: Absorbance at 530 nm for MWCNTs treated with acid mixture fro 1 – 4 hours. Using calibration curve from Fig. 43, concentrations were calculated.

5.1.4 Field-Emission Scanning Electron Microscopy (SEM) analysis

SEM analysis was done in order to study MWCNTs suspension morphology and the effect of different treatments on the amount of impurities, diameter and length of MWCNTs. For observation, low acceleration voltage (0.7 kV) and short working distance (the distance from the centre of the lens to the specimen plane; 2 – 3 mm) was used. At such a low voltage, the beam interaction with the specimen is confined to regions very close to the surface. This provides an image, which is rich in surface details. When low acceleration voltage is used, image resolution can be increased by lowering the working distance [64].

On the pictures (Fig. 45 – 46), there are SEM micrographs of as received MWCNTs dispersed using surfactant SDS (ST suspension). On the picture Fig. 45, there is micrograph of MWCNTs layer under the lowest magnification. Layer of MWCNTs seems to be homogenous but a bit rough. The layer roughness can be attributed to impurities or bundles and agglomerates of CNTs. From Fig. 45, impurities are not so obvious. However, on the picture Fig. 46, there is micrograph taken under higher magnification (25 000x). One can see particles among the MWCNTs. These particles are believed to be catalyst residues (metal particles – mostly iron, cobalt, nickel [69]).

Because of large amount of impurities, one should consider method of purification of MWCNTs.

Purification methods of CNTs can be basically classified into three categories, namely chemical, physical, and a combination of both. The chemical method purifies CNTs based on the idea of selective oxidation (carbonaceous impurities are oxidized at a faster rate than CNTs) and the dissolution of metallic impurities by acids. This method can effectively remove amorphous carbon and metal particles except for those encaged in polyhedral graphitic particles. However, the chemical methods always influence the structure of CNTs due to the oxidation involved. The physical method separates CNTs from impurities based on the differences in their physical size, aspect ratio, gravity, and magnetic properties, etc. In

general, the physical method is used to remove graphitic sheets, carbon nanospheres (CNSs), aggregates or separate CNTs with different diameter/length ratios. In principle, this method does not require oxidation, and therefore prevents CNTs from severe damage. However, the physical method is always complicated, time-consuming and less effective. The third kind of purification combines the merits of physical and chemical purification [45].

As en example of chemical method commonly used in literature can be refluxing in 3 M HNO_3 for 16 or 24 hours [74, 75] or by sequential reflux processes using 3 M HNO_3 followed by 5 M HCl [76].

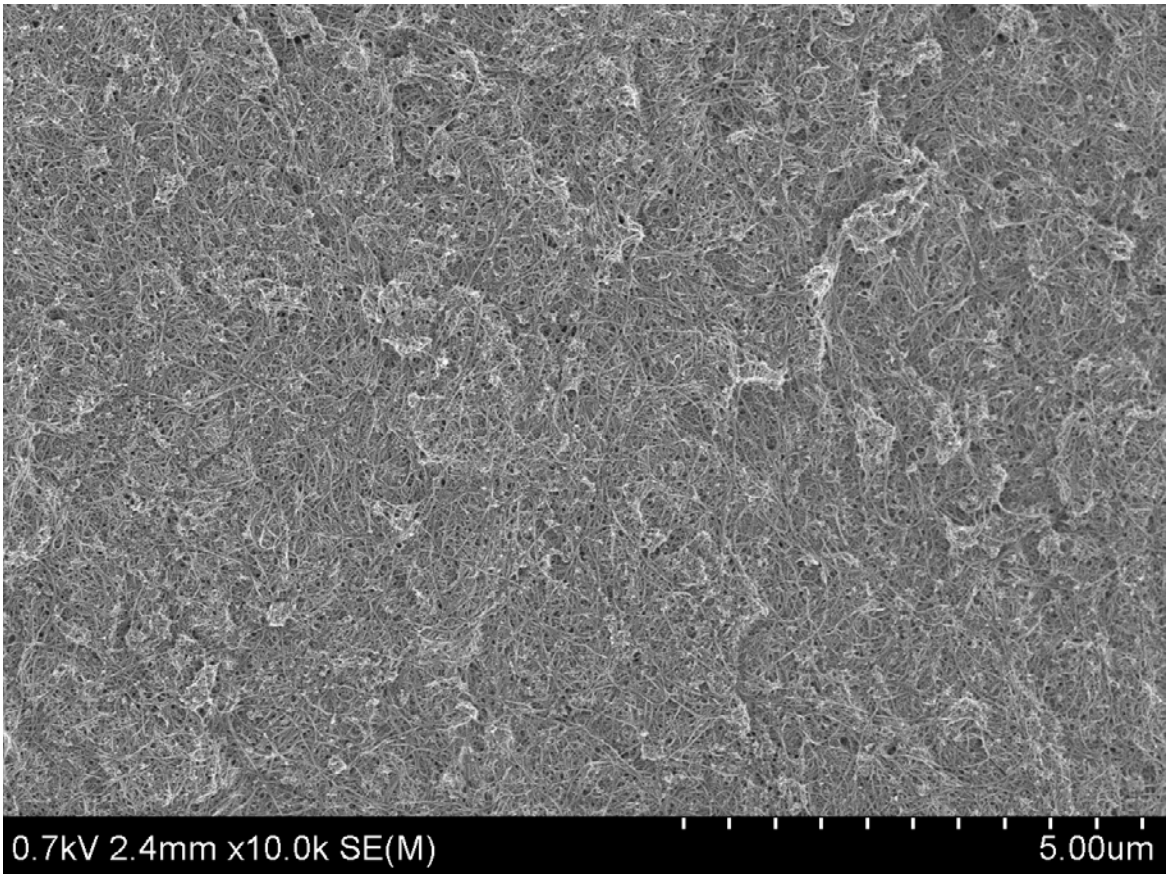

Fig. 45: SEM micrographs of ST MWCNTs layer. Magnification is 10 000x.

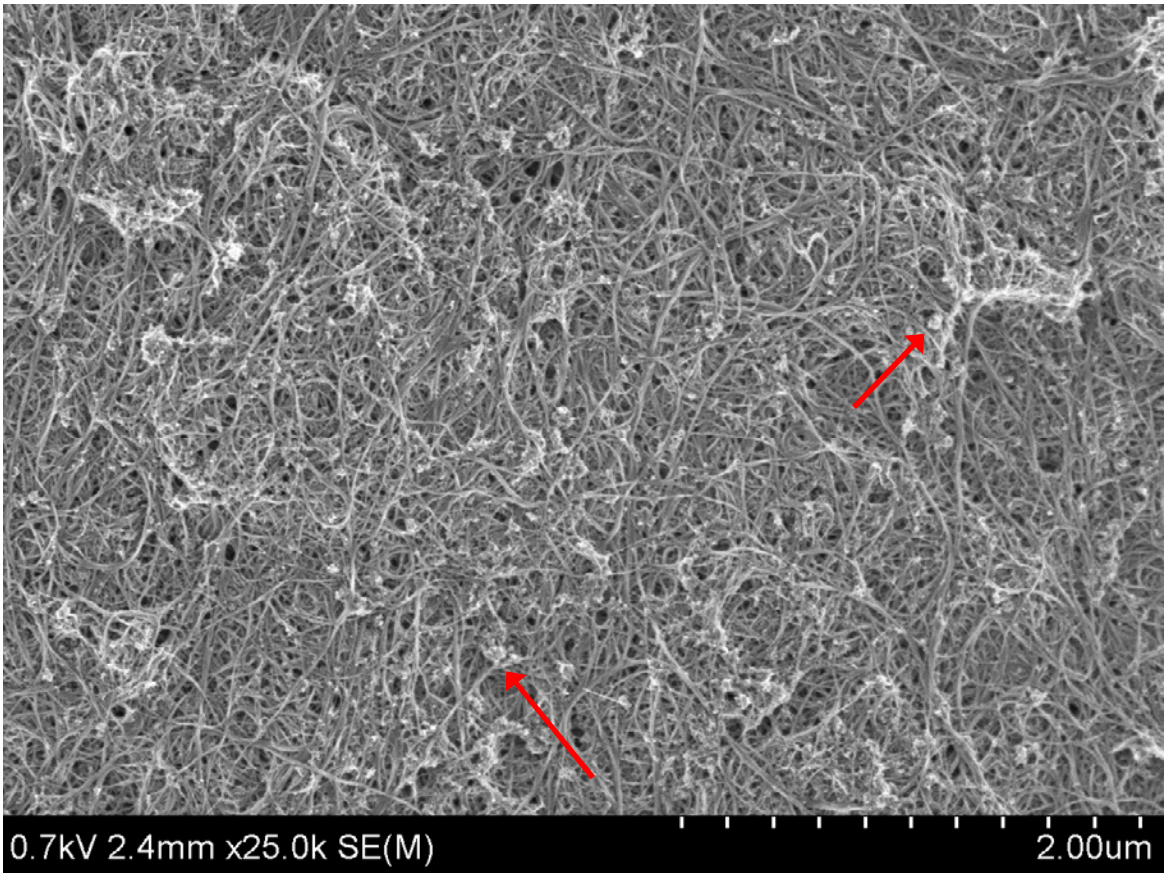

Fig. 46: SEM micrographs of ST MWCNTs layer. Magnification is 25 000x.

On the pictures (Fig. 47 – 48) there are SEM micrographs of MWCNTs treated with NH_4OH/H_2O_2 mixture (BT suspension). It is obvious from Fig. 47, that MWCNTs layer is homogenous throughout the sample and more even than ST suspension layer (Fig. 45). From the picture taken under higher magnification (Fig. 48), one can see network of MWCNTs without agglomerates, bundles and impurities. Thus, using this treatment, impurities were successfully removed. Although basic oxidative treatment is supposed to be mild and non-destructive for CNTs and at the same time producing material of high purity [44], MWCNTs seem to be slightly shortened, but quality of dispersion is better than previous ST suspension.

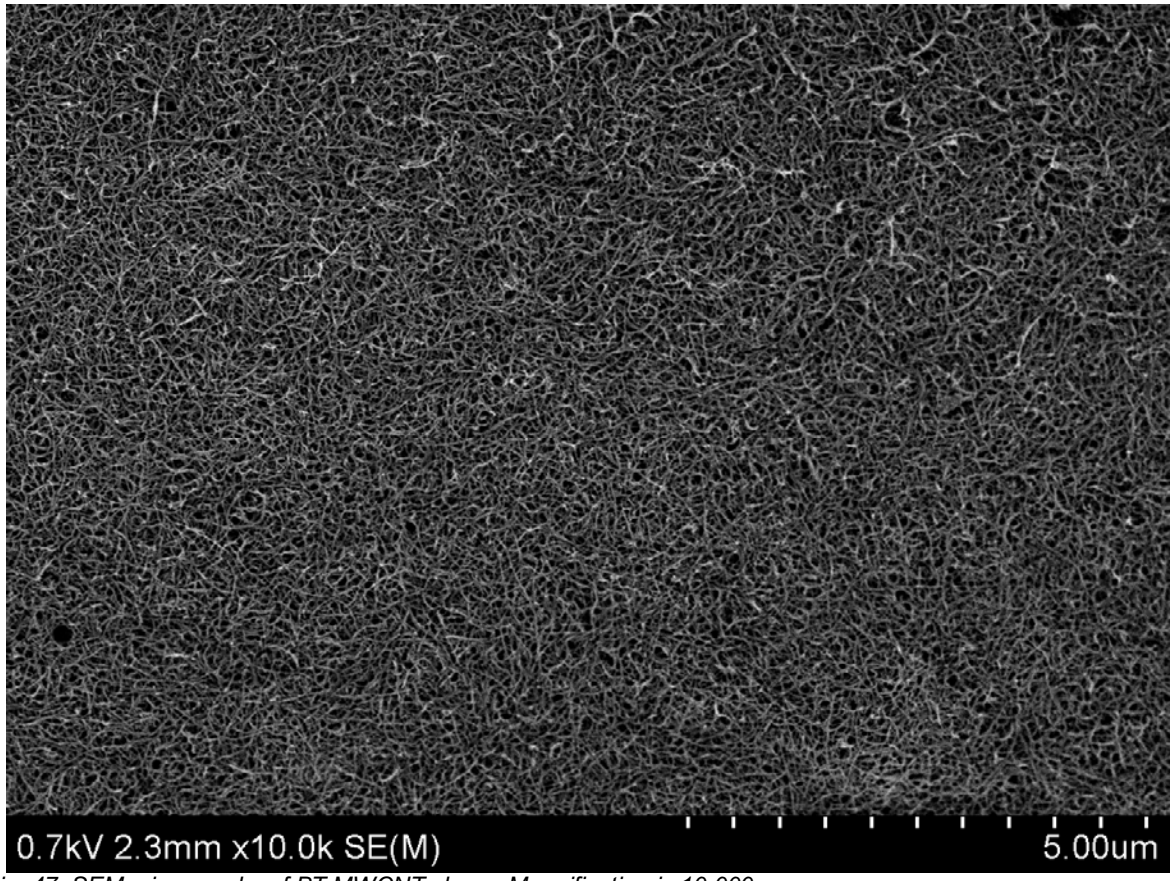

Fig. 47: SEM micrographs of BT MWCNTs layer. Magnification is 10 000x.

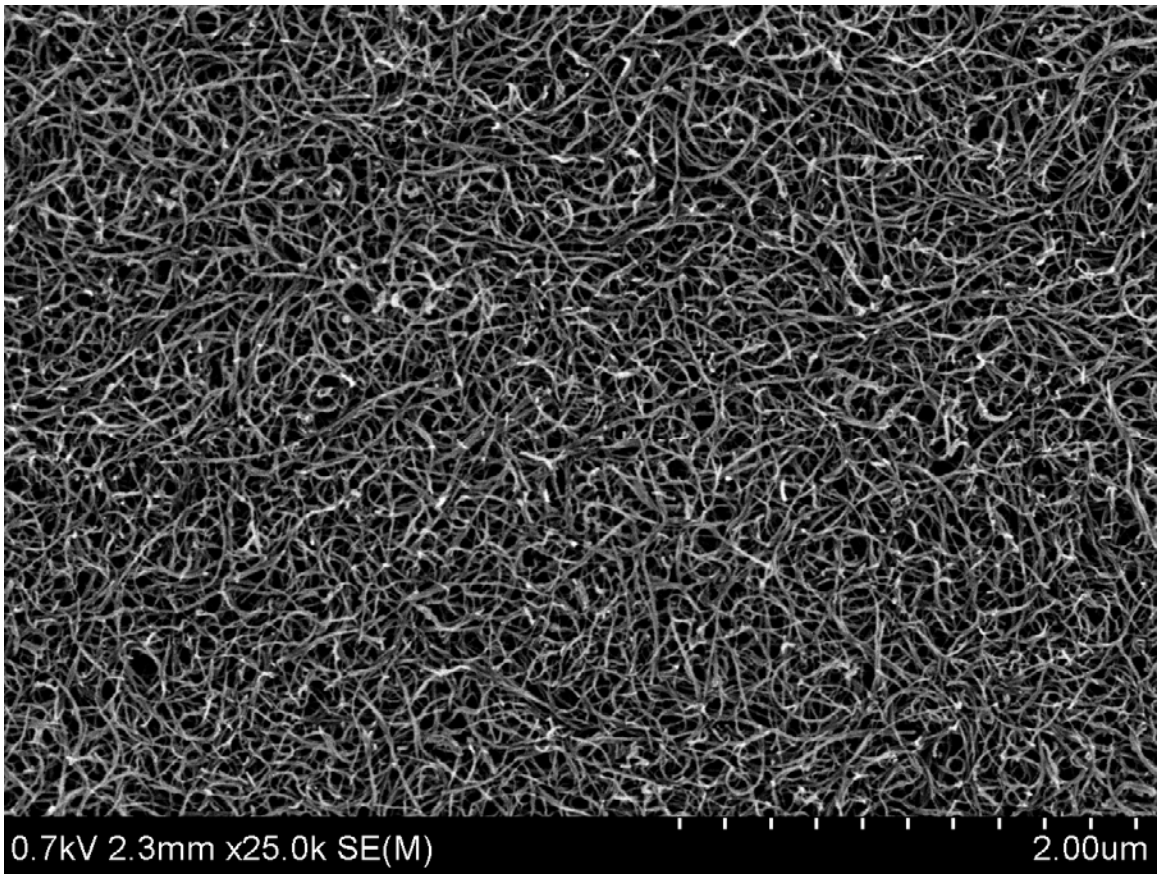

Fig. 48: SEM micrographs of BT MWCNTs layer. Magnification is 25 000x.

On the pictures (Fig. 49 – 54), MWCNTs treated with HNO_3/H_2SO_4 are shown. First, according to [25], treatment was done for 10 hours. Yield of the reaction was very low (approx. 3 %) and as obvious from Fig. 54, MWCNTs were significantly shortened and destroyed. Layer was not homogenous and even. That is why conditions of the treatment had to be adjusted and treatment was done for 1 – 4 hours in order to investigate the rate of the reaction.

It is known that HNO_3/H_2SO_4 treatment can lead to the opening of the nanotube caps as well as the formation of holes in the sidewalls. Chemical modification is thus limited mostly to the opening of the nanotubes caps and to the formation of functional groups at defect sites along the sidewalls. There are various oxygen containing groups (mainly carboxyl groups) present [67].

It was found that only after 1 hour of reaction, stable water suspension was obtained. Corresponding SEM micrographs of these MWCNTs samples are on the pictures (Fig. 49 – 50). Layer appears homogenous (Fig 49), even and without impurities and bundles (Fig. 50). However, MWCNTs are slightly shortened. Increasing time of the reaction (2, 3 and 4 hours, Fig. 51 – 53) caused MWCNTs shortening, the layer is less homogenous and the amount of amorphous carbon increased with the increasing time of the reaction (Fig. 51 – 54). That's why for further experiments, MWCNTs treated with acid mixture for 1 hour (AT 1 hour) were chosen.

In order to quantitatively determine the concentration of carboxylic groups on the surface of treated MWCNTs, titration can be done [44] or Raman spectroscopy can be used [68]. This can be objective of further study.

SEM analysis can be improved by using evaporating of droplet MWCNTs suspension on silicon wafer. For further analysis, transmission electron microscopy (TEM) can be done. Using TEM, individual walls of MWCNTs can be observed.

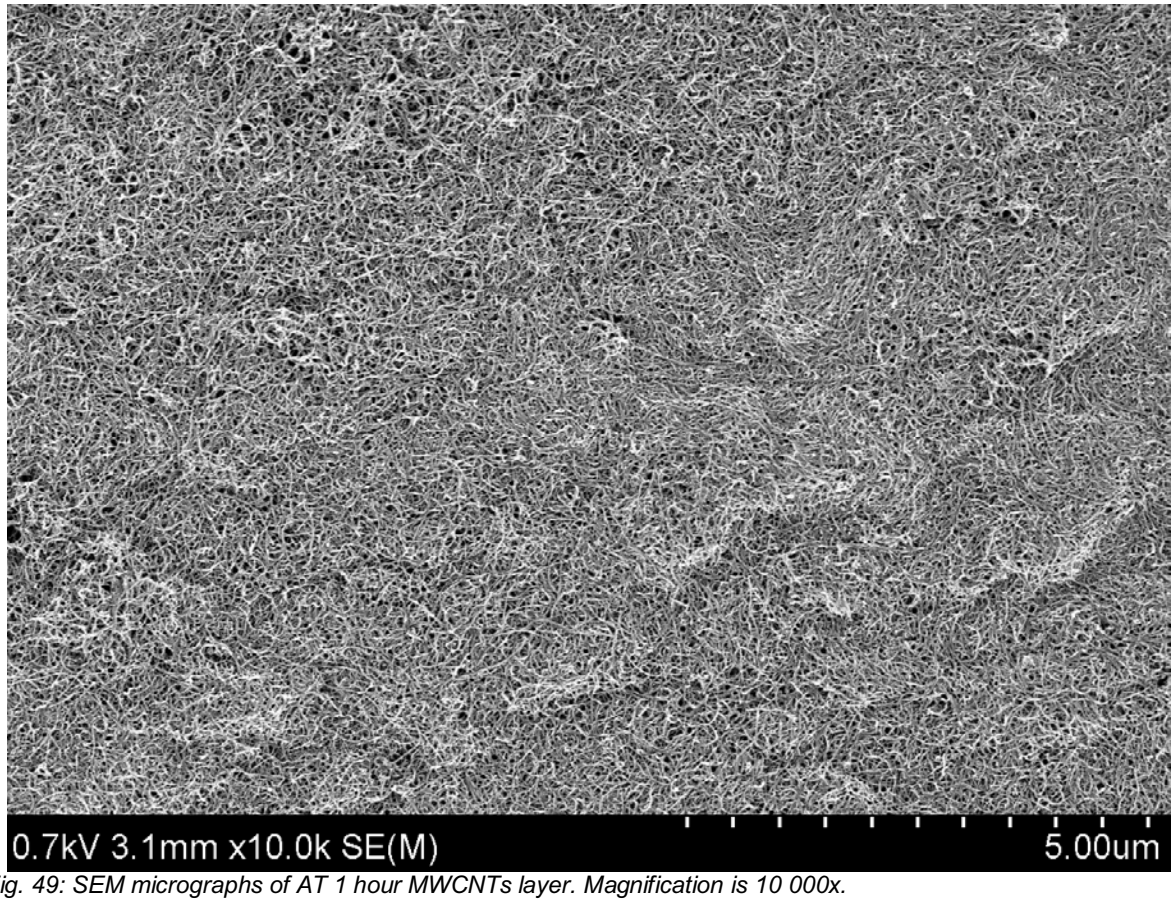

Fig. 49: SEM micrographs of AT 1 hour MWCNTs layer. Magnification is 10 000x.

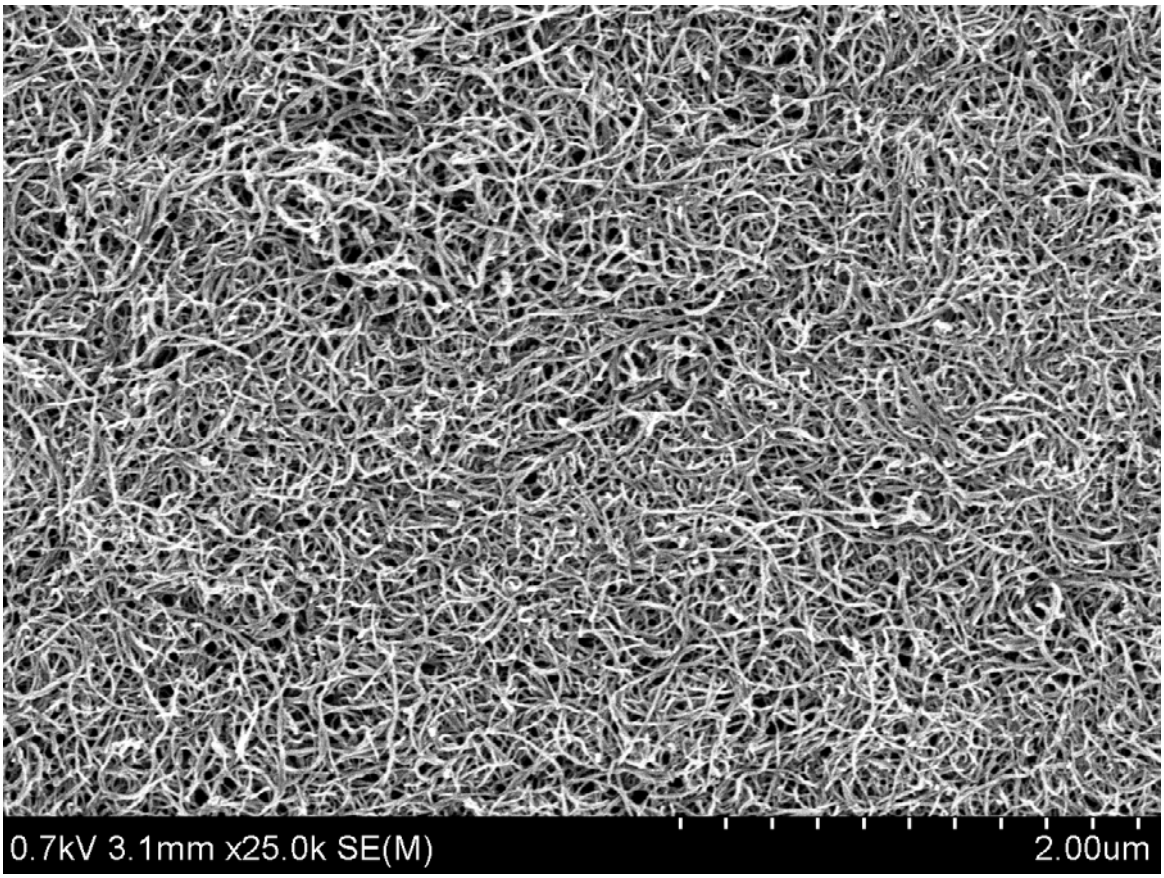

Fig. 50: SEM micrographs of AT 1 hour MWCNTs layer. Magnification is 25 000x.

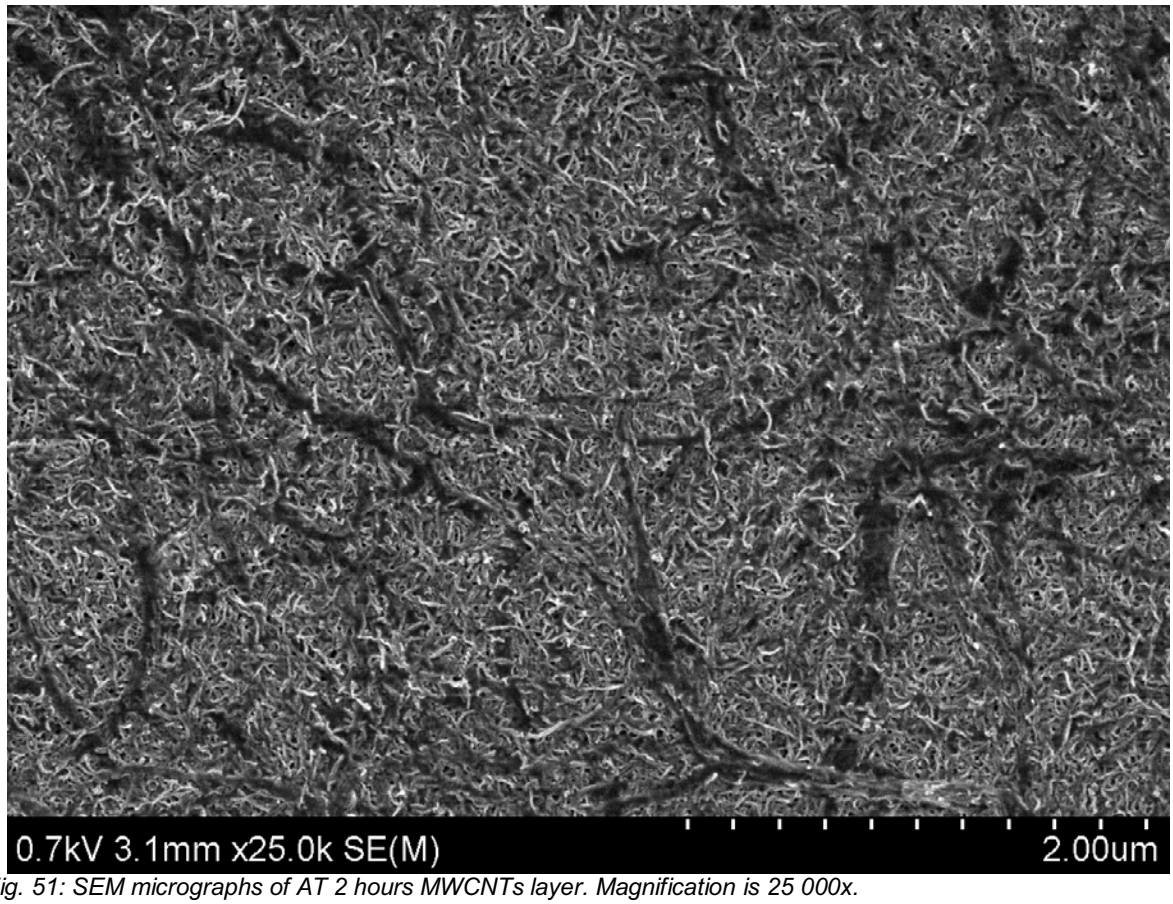

Fig. 51: SEM micrographs of AT 2 hours MWCNTs layer. Magnification is 25 000x.

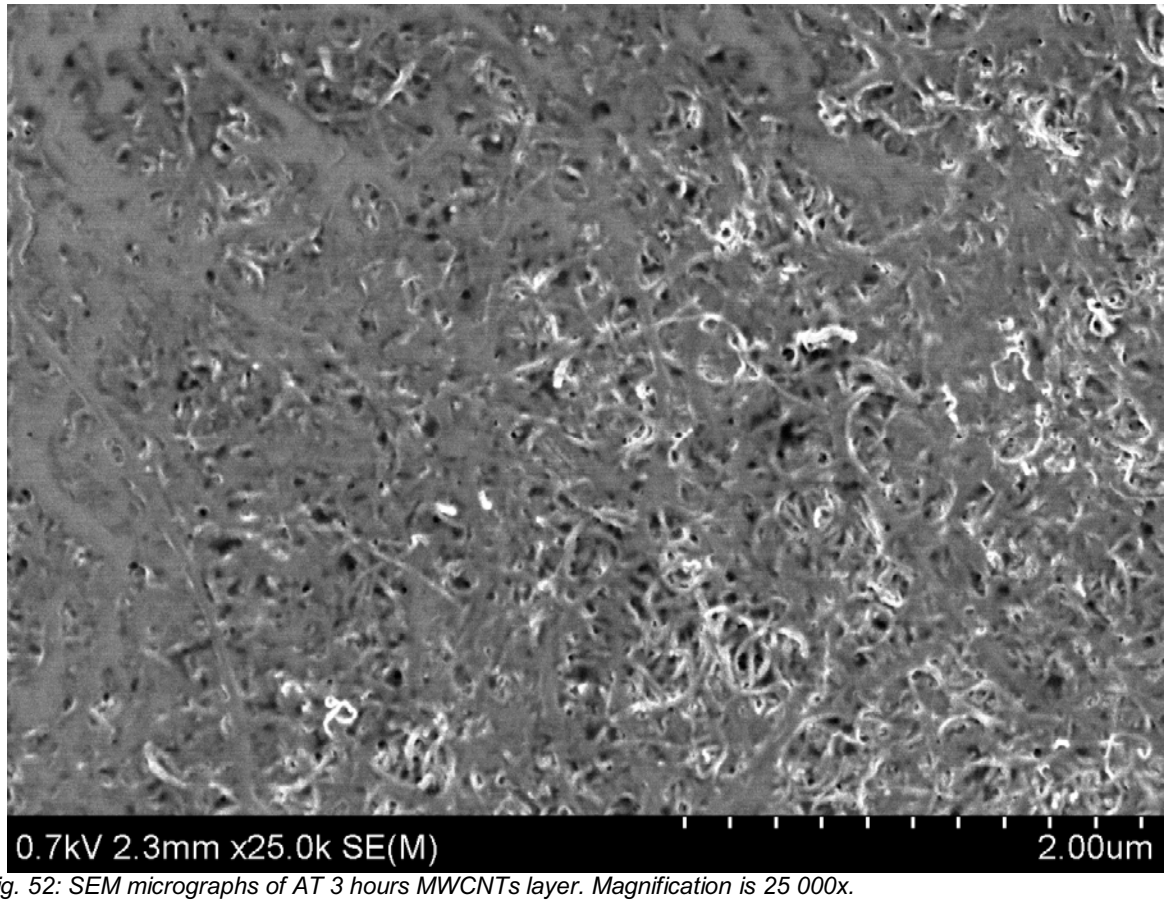

Fig. 52: SEM micrographs of AT 3 hours MWCNTs layer. Magnification is 25 000x.

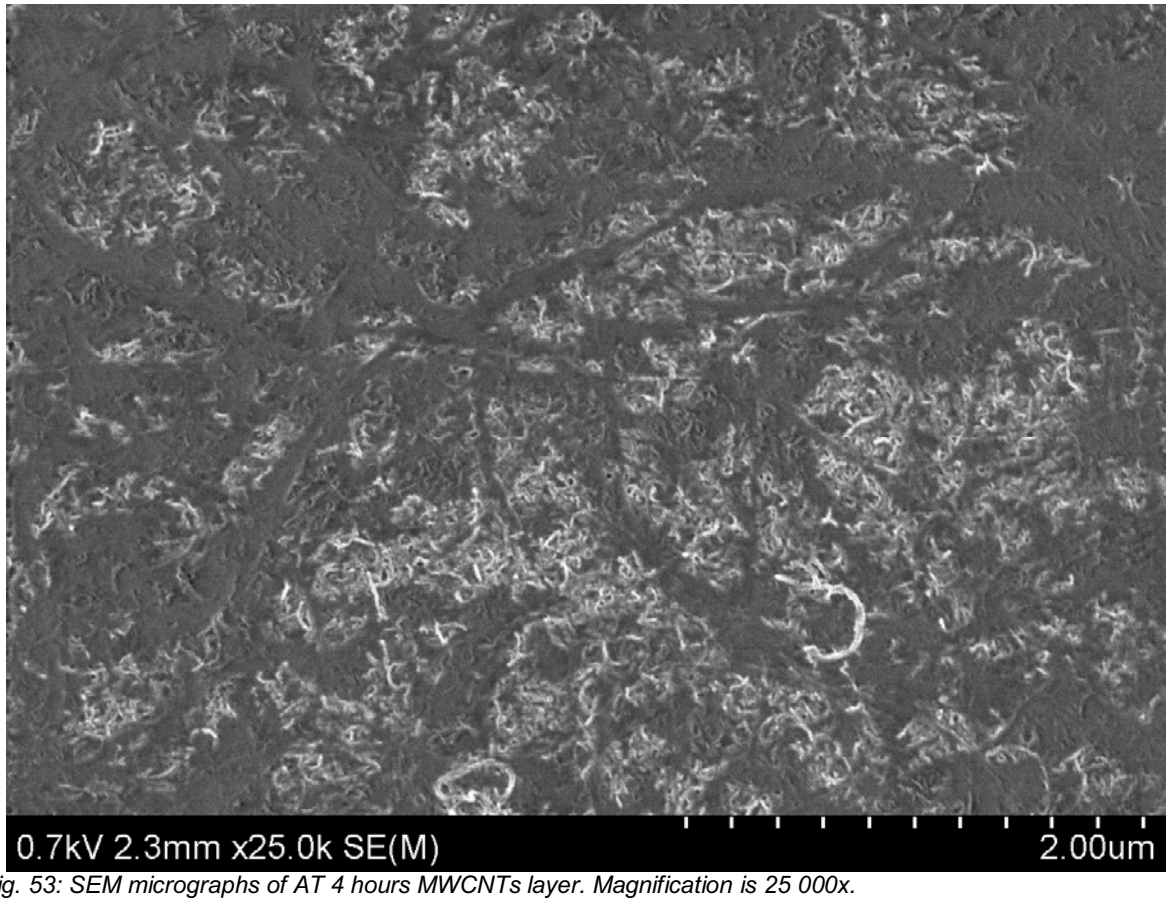

Fig. 53: SEM micrographs of AT 4 hours MWCNTs layer. Magnification is 25 000x.

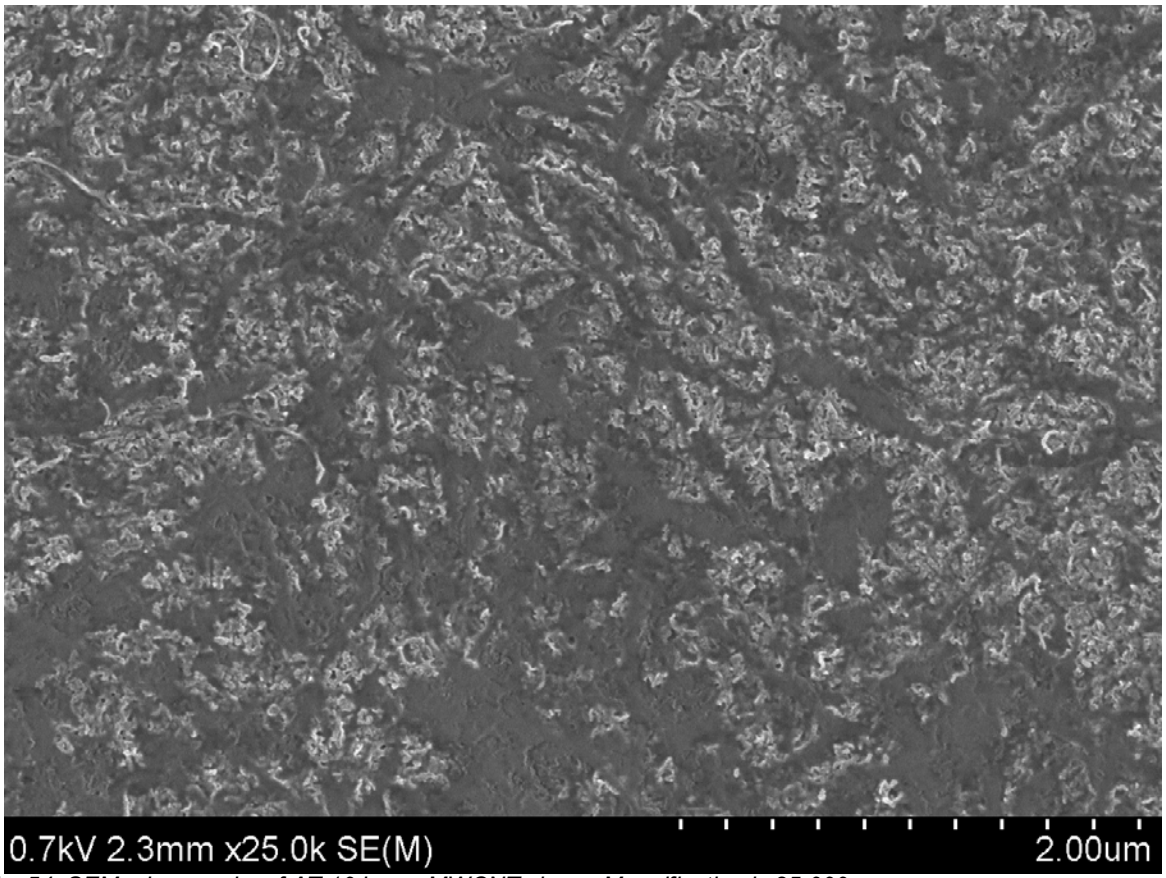

Fig. 54: SEM micrographs of AT 10 hours MWCNTs layer. Magnification is 25 000x.

5.2 Composite film characterization

Composite films containing MFC and MWCNTs were prepared. The MWCNTs content varied from 0.1 – 5 wt.% and as a control 100 % MFC film was prepared. Effect of different MWCNTs treatment on the structure and properties of the composite films was studied.

5.2.1 TGA analysis

On the Fig. 55 – 57, data from thermogravimetric analysis for different MWCNTs treatment and different content of MWCNTs in MFC matrix are shown. Pure MFC film was used as a control sample.

First, in low temperature range (up to about 120°C), there is small weight loss, that is attributed to the evaporation of adsorbed water. After that, two steps of MFC degradation can be observed in the range of 360 – 600°C. The first process corresponds to the primary pyrolysis of cellulose, and the second process relate to the slow charring process of the solid residue [73].

At temperature around 360°C, there is significant difference in the weigh loss of the samples with different MWCNTs content (for acid and surfactant treatment; Fig. 55 and 57) – the higher amount of MWCNTs, the smaller weigh loss at this temperature. MWCNTs are probably quite uniformly dispersed through the area of the sample.

On the other hand for base treated MWCNTs (Fig. 56), this trend is not so obvious. It is believed to be because of non-homogenous dispersion of MWCNTs in MFC matrix. However, this hypothesis needs to be further investigated by SEM.

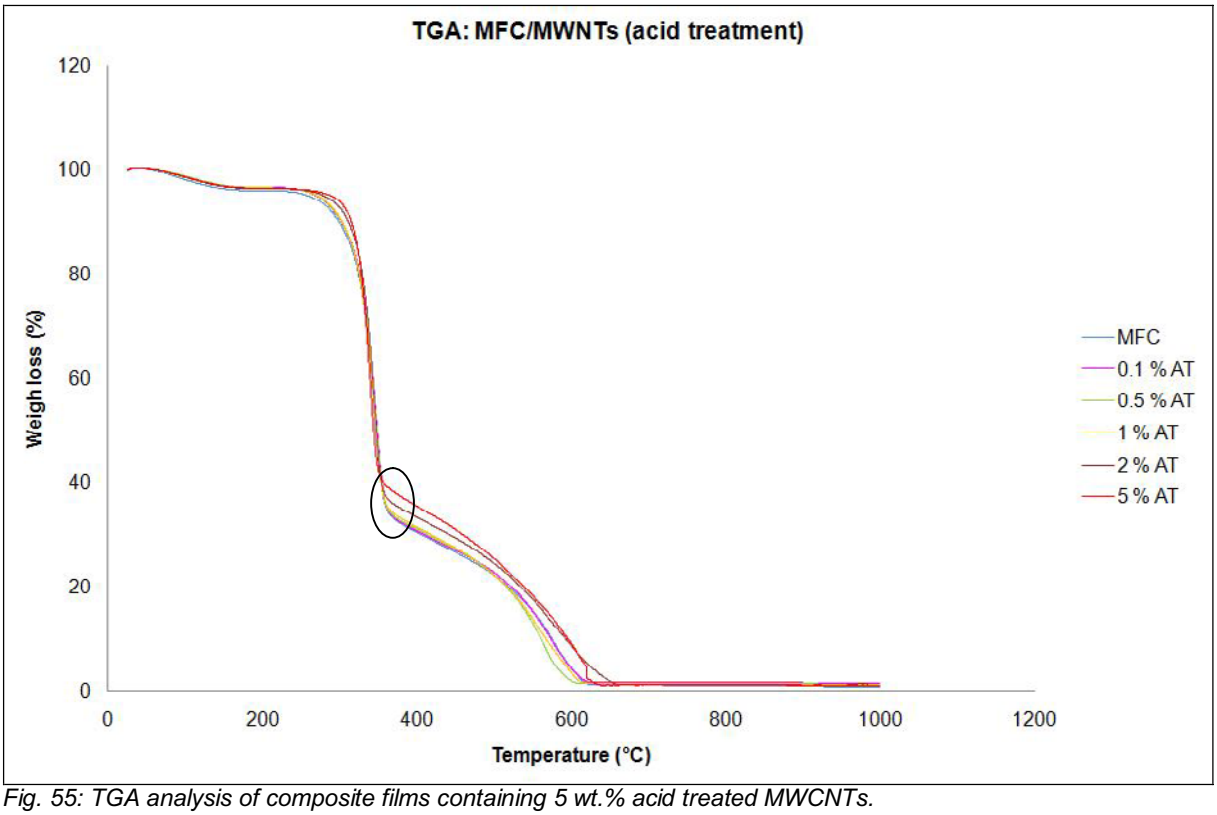

Fig. 55: TGA analysis of composite films containing 5 wt.% acid treated MWCNTs.

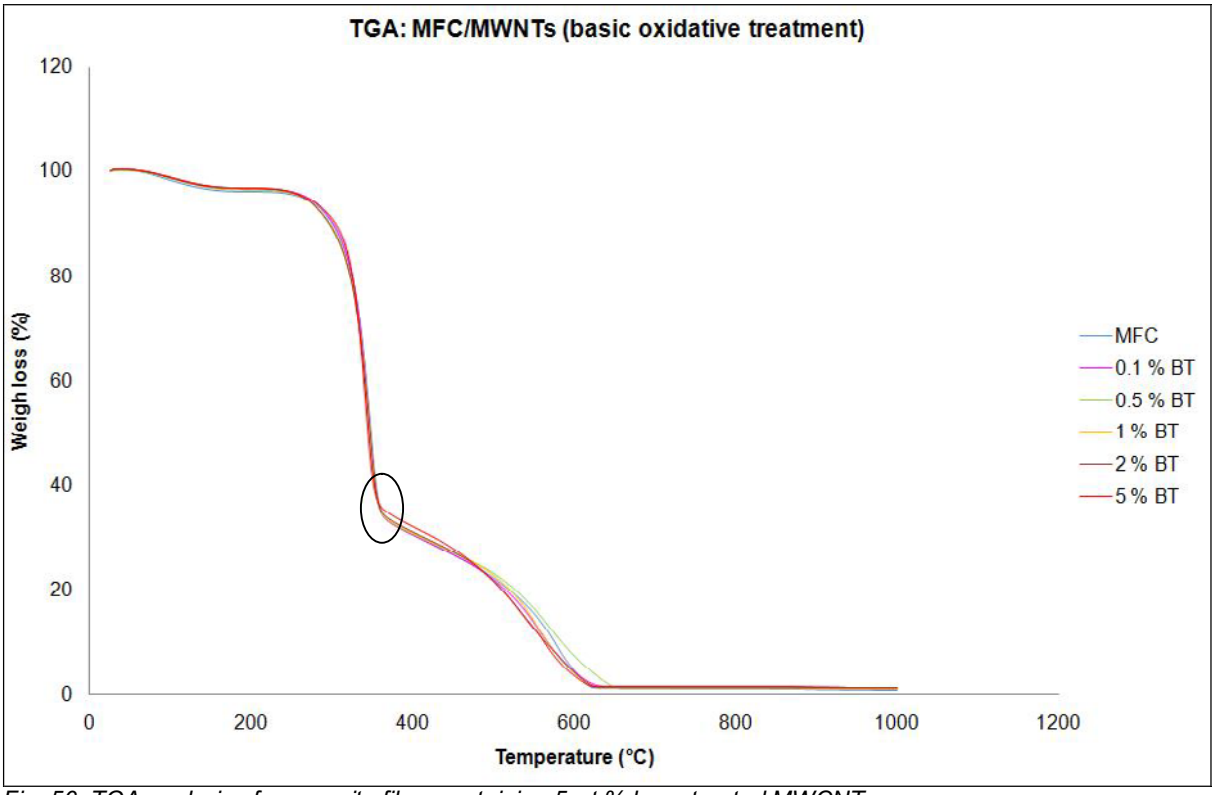

Fig. 56: TGA analysis of composite films containing 5 wt.% base treated MWCNTs.

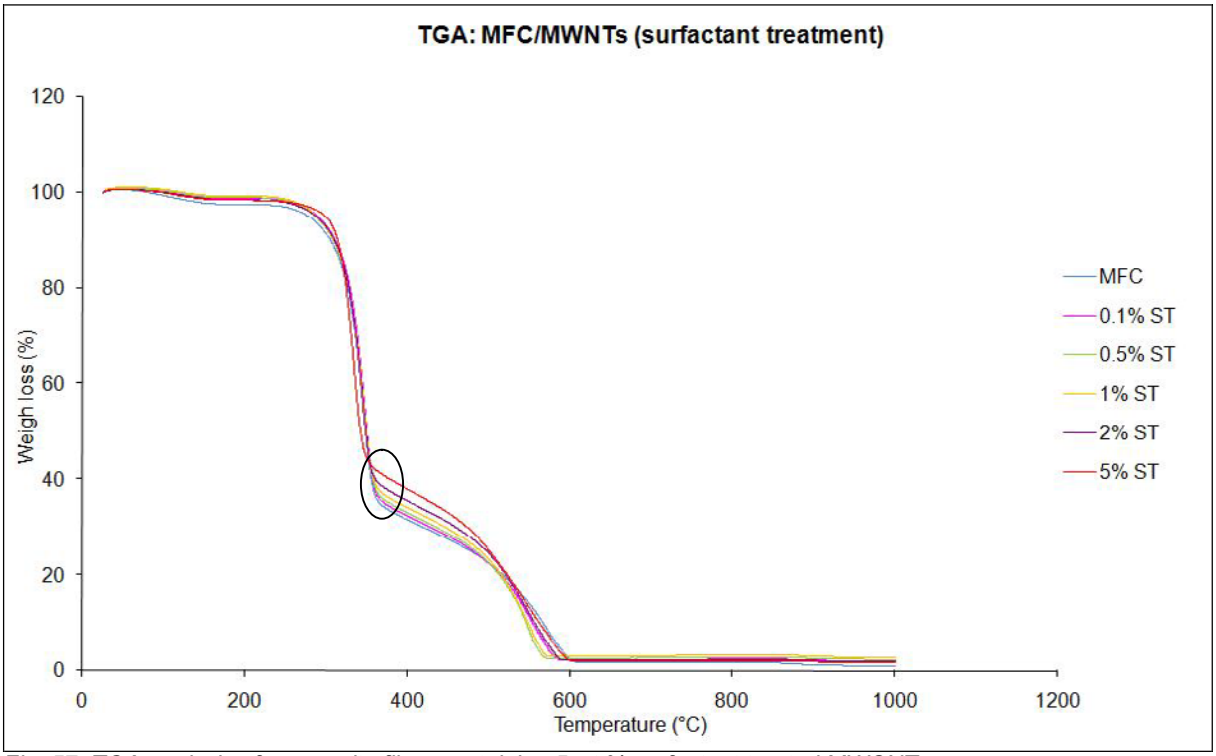

Fig. 57: TGA analysis of composite films containing 5 wt.% surfactant treated MWCNTs.

5.2.2 Surface resistivity measurement

Surface resistivity data are summarized in Tab. 5 and comparison with published data [47] was done.

On the Fig. 58, there is dependence of surface resistivity on the content of MWCNTs in MFC matrix for top and bottom sides of the samples.

For obtaining conductive CNTs-polymer composites, the highly electrical conductive CNTs filler is dispersed into the polymer matrix. Hence, a three-dimensional conductive network of the CNTs in the polymer matrix is obtained. The so-called percolation theory is generally used to describe the insulator-to-conductor transition in composites made of conductive filler in an insulating matrix. The electrical conductivity of a composite is strongly dependent on the filler loading. At low filler concentrations, the conductivity remains very close to the conductivity of the pure, electrically insulating matrix since the fillers are dispersed individually or in small clusters in the matrix. When a critical filler volume fraction, the percolation threshold, is reached, the conductivity drastically increases by many orders of magnitude with very little increase in the filler loading. It coincides with the formation of a conductive, three-dimensional network of the filler in the continuous phase. Finally, the conductivity levels off at a certain value, the maximum conductivity of the composite [77].

Obtained curves exhibit typical percolation behaviour. Beyond certain MWCNTs content, no further improvement is observed. For different treatments, concentration needed for percolation threshold differs. However, for all three groups of samples, there is significant difference in surface resistivity between top and bottom side (Fig. 58). The values are always higher in case of top side of the samples. It is believed that this fact is caused by uneven distribution of MWCNTs in the samples. For pure MFC film, there is no difference in surface resistivity for the top and bottom side.

Top sides of the samples

For composite films containing acid treated MWCNTs, almost no significant decrease in surface resistivity is observed when 0.1 – 2 wt.% of MWCNTs is added.

In case of MWCNTs treated with basic oxidative treatment, slight increase followed by decrease is observed, although the resistivity hasn´t reached constant value even when 2 – 5 wt.% of MWCNTs was added.

For films prepared with MWCNTs treated with surfactant, significant decrease in surface resistivity occurs when 1 – 2 wt.% MWCNTs was added to MFC.

Bottom sides of the samples

As mentioned above, the surface resistivity values obtained from bottom sides of the samples were lower as well as MWCNTs concentrations where percolation threshold is observed are lower. In case of films with acid treated MWCNTs, surface resistivity is decreasing when 1 – 2 wt.% of MWCNTs is added. The surface resistivity value for the bottom side of the sample containing of 2 wt.% AT MWCNTs is almost 7 orders of magnitude lower than the top side of the same sample.

Concerning composite films containing MWCNTs treated with basic oxidative treatment, significant decrease in the surface resistivity occurs when 1 wt.% of MWCNTs is added and this value is about 7 orders of magnitude lower than the surface resistivity of the top side of the same sample.

The highest decrease in surface resistivity is observed in case of films containing MWCNTs treated with surfactant. Only by adding of 0.5 wt.% of MWCNTs, the surface resistivity decreases almost by 9 orders of magnitude in comparison to the pure MFC film.

Obtained results suggested that the best incorporation of MWCNTs into MFC network occurs for MWCNTs dispersed using surfactant. For this group of samples, the difference between top and bottom side is less obvious.

For MWCNTs treated with basic oxidative treatment, the difference between the top and bottom side of the samples are very large, that means that the distribution of MWCNTs in the sample is not even. Although MWCNTs treated with basic oxidative treatment were dispersed using surfactant as well, the concentration of surfactant was higher than in case of ST suspension, because the molecules that are not adsorbed on the CNTs were not removed. The different surfactant concentration might effect the stability of cellulose-MWCNTs system.

For acid treated MWCNTs, higher amount of MWCNTs has to be added in order to achieve electrical conductivity. It is known that covalent modification of CNTs might result in decrease in electrical and other properties [45, 51].

Oya at al. [47] made electrically conductive washi paper that contains SWCNTs (Tab. 6). The obtained surface resistivity value was of $2.74 \cdot 10^3$ Ω/sq by adding of 2.33 wt.% of SWCNTs, that is one order of magnitude lower than measured value. The percolation behaviour with increasing amount of CNTs up to certain value is in agreement with measured data of MFC/MWCNTs.

Fugetsu at al. [72] reported on the mass production of CNT-based sheets having uniform electrical conductivities by using a common papermaking process. By adding 8.32 wt.% of MWCNTs, surface resistivity value 21 Ω/sq was obtained.

Tab. 5: Surface resistivity data for composite containing surfactant treated MWCNTs.

Surface resistivity [Ω/sq]						
	top side			bottom side		
MCF	$9.67 \cdot 10^{13}$			$6.72 \cdot 10^{13}$		
	AT	BT	ST	AT	BT	ST
0.1%	$4.55 \cdot 10^{13}$	$6.42 \cdot 10^{13}$	$9.06 \cdot 10^{13}$	$4.94 \cdot 10^{13}$	$5.41 \cdot 10^{13}$	$5.40 \cdot 10^{13}$
0.5%	$1.64 \cdot 10^{14}$	$1.50 \cdot 10^{14}$	$1.93 \cdot 10^{14}$	$1.39 \cdot 10^{14}$	$7.00 \cdot 10^{13}$	$6.61 \cdot 10^{04}$
1%	$9.72 \cdot 10^{13}$	$1.19 \cdot 10^{15}$	$1.60 \cdot 10^{10}$	$1.40 \cdot 10^{12}$	$1.29 \cdot 10^{06}$	$2.92 \cdot 10^{04}$
2%	$2.26 \cdot 10^{13}$	$5.82 \cdot 10^{13}$	$3.26 \cdot 10^{05}$	$1.43 \cdot 10^{06}$	$1.02 \cdot 10^{06}$	$2.95 \cdot 10^{04}$
5%	---	$1.09 \cdot 10^{10}$	$4.09 \cdot 10^{04}$	---	$5.45 \cdot 10^{04}$	$3.62 \cdot 10^{04}$

Tab. 6: Surface resistivity data for Washi paper [47].

Washi paper [47]					
SWCNTs content (wt. %)	0	0.33	1.00	1.66	2.66
Surface resistivity (Ω/sq)	$1.00 \cdot 10^{11}$	$1.00 \cdot 10^{11}$	$2.07 \cdot 10^{6}$	$1.01 \cdot 10^{4}$	$2.74 \cdot 10^{3}$

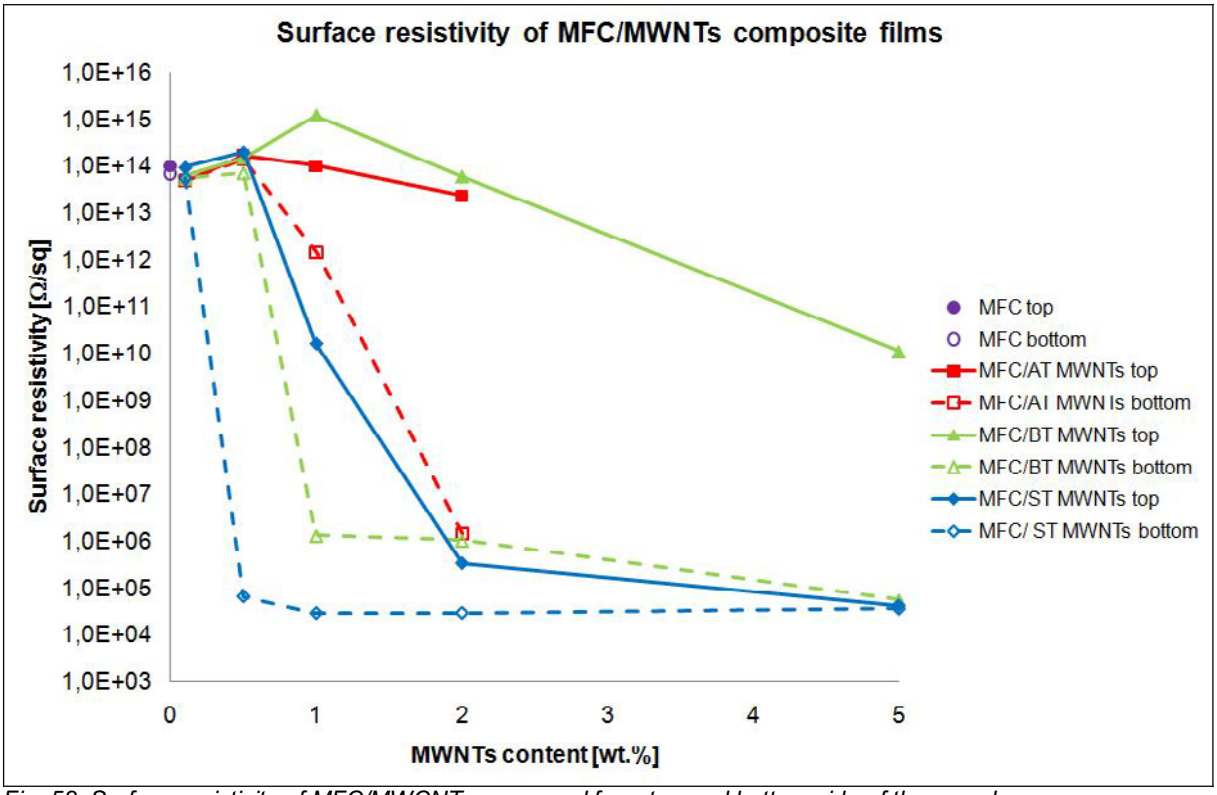

Fig. 58: Surface resistivity of MFC/MWCNTs measured from top and bottom side of the samples.

Electrical properties of a material depend on the separation between the collection of energy states that are filled by electrons (Fig. 59 red) and the additional “conduction” states that are empty and available for electrons to hop into (Fig. 59 light blue). Metals conduct electricity easily because there are so many electrons with easy access to adjacent conduction states. In semiconductors, electrons need an energy boost from light or an electrical field to jump the gap to the first available conduction state. The form of carbon known as graphite is a semimetal that just barely conducts, because without these external boosts, only a few electrons can access the narrow path to a conduction state [70].

In a graphite sheet, one particular electron state (which physicists call the Fermi point) gives graphite almost all of its conductivity. Only one third of all carbon nanotubes combine the right diameter and degree of twist to be truly metallic nanowires. The remaining two thirds of nanotubes are semiconductors [70].

Thick multiwalled nanotubes may have even more complex behaviour, because each layer in the tube has a slightly different geometry [70].

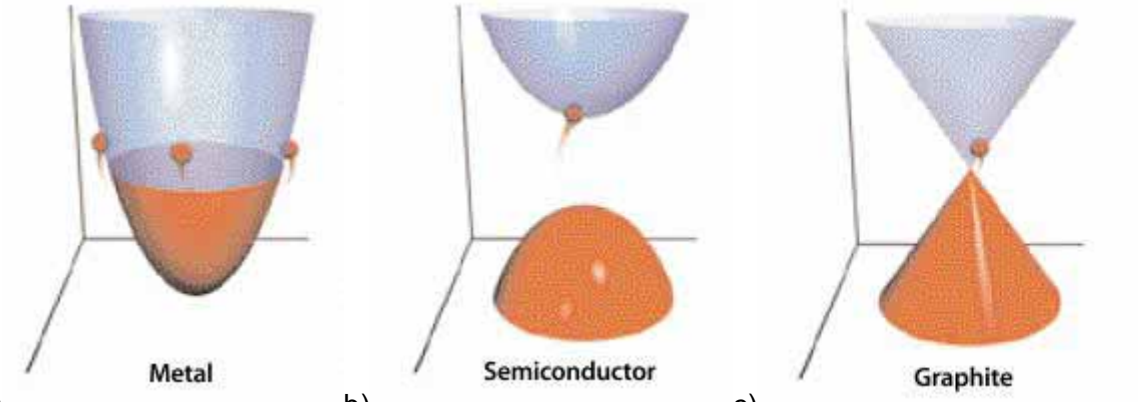

a) b) c)

Fig. 59: Electrical properties of a) Meta,. b) Semiconductor, c) Graphite [70].

5.2.3 Tensile test

The average values of the mechanical properties are summarized in Tab. 7 – 9. The values in parentheses are the sample standard deviations.

In the Fig. 60 – 62 there are typical stress-strain curves for composite films containing MFC and varying content of MWCNTs treated in three different ways: using acid mixture (AT), basic oxidative treatment (BT) and using surfactant (ST). The stress-strain behaviour in uniaxial tension is fairly linear up to about 0.5 – 1.0 %. At a stress about 100 MPa (yield stress), the curves are bended and followed by a linear strain-hardening region. This region called the plastic region [20].

Tab. 7: Young´s moduli of composite films with MFC matrix and varying MWCNTs content and free different MWCNTs treatments.

	Young´s modulus (GPa)		
MFC	9.6 (0.9)		
	AT	BT	ST
0.1%	7.7 (1.1)	11.6 (0.9)	9.7 (0.8)
0.5 %	8.2 (0.7)	11.0 (0.5)	7.3 (0.4)
1 %	10.2 (0.8)	9.2 (0.9)	9.3 (1.0)
2 %	10.2 (0.5)	10.5 (1.2)	7.8 (1.1)
5 %	11.4 (0.7)	9.0 (1.3)	8.3 (1.2)

Tab. 8: Tensile strength of composite films with MFC matrix and varying MWCNTs content and free different MWCNTs treatments.

	Tensile strength (MPa)		
MFC	279.6 (24.2)		
	AT	BT	ST
0.1 %	257.4 (23.3)	288.0 (40.0)	256.0 (40.4)
0.5 %	288.6 (15.8)	245.3 (16.2)	253.9 (18.4)
1 %	286.0 (10.4)	224.2 (9.6)	239.2 (22.9)
2 %	249.9 (35.3)	220 (19.1)	239.2 (23.4)
5 %	254.2 (27.7)	192.5 (15.7)	230.5 (21.4)

Tab. 9: Strain-to-failure of composite films with MFC matrix and varying MWCNTs content and free different MWCNTs treatments.

	Strain-to-failure (%)		
MFC	11.9 (1.5)		
	AT	BT	ST
0.1%	14.9 (2.8)	11.8 (2.1)	10.8 (1.8)
0.5%	15.8 (1.3)	10.6 (3.0)	15.1 (2.5)
1%	12.3 (1.3)	11.4 (2.5)	12.6 (1.8)
2%	11.2 (0.8)	10.1 (2.8)	12.3 (1.6)
5%	10.2 (2.2)	7.5 (1.1)	12.6 (1.1)

The results in Tab. 7 – 9 show that there is no significant effect of MWCNTs on mechanical properties of MFC films. Data for MFC films are in agreement with previously published data by Henriksson [20]. Small difference might be caused by different drying process (Henriksson dried the films at 55 °C for 48 h at about 10 kPa applied pressure [20]) and also by molecular weight of cellulose. For more accurate comparison, molecular weight distribution needs to be determined, for example using size exclusion chromatography. Further investigation and characterization of MFC can be done.

For different MWCNTs treatment, different effect on mechanical properties is observed.

By adding of small amounts (0.1 – 1 %) of acid treated MWCNTs, decrease in Young´s modulus and tensile strength is observed. On the other hand, strain-to-break is slightly improved (Fig. 60).

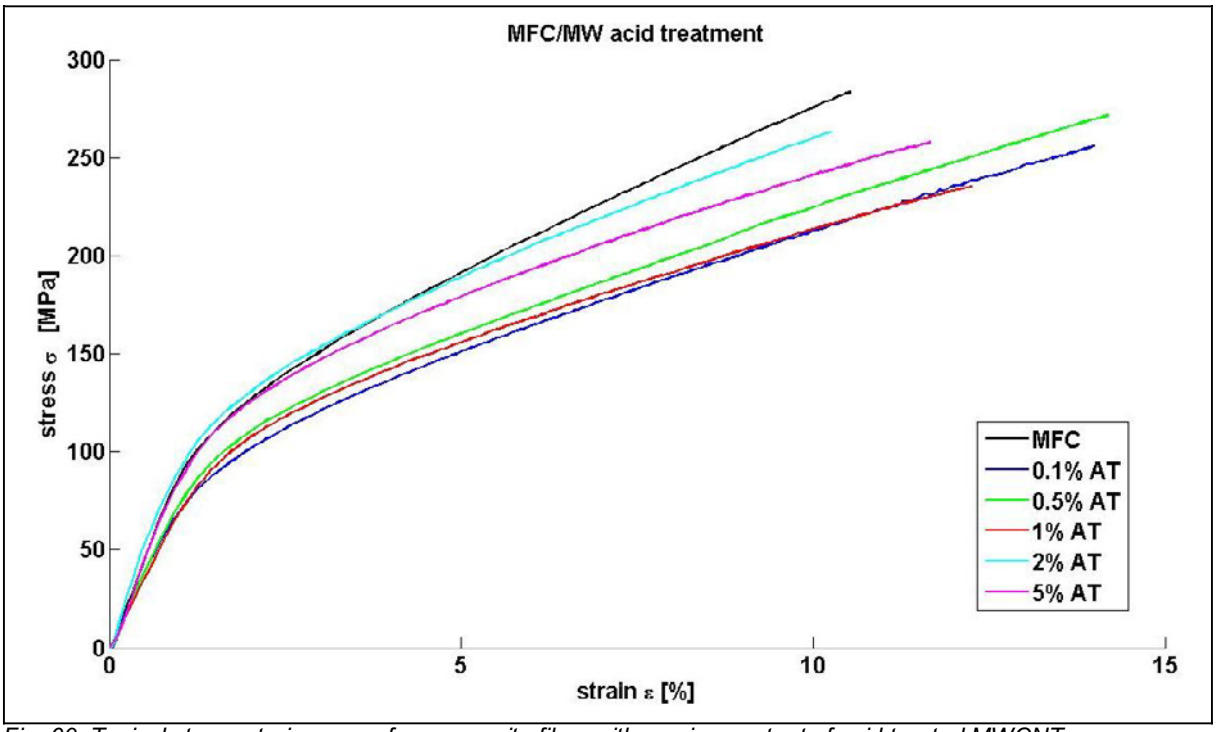

Fig. 60: Typical stress-strain curves for composite films with varying content of acid treated MWCNTs.

Opposite behaviour to acid treated MWCNTs can be observed in case of MWCNTs treated by basic oxidative treatment (Fig. 61). By adding 0.1 of MWCNTs, slight increase in

mechanical properties was achieved. When 0.5 wt.% MWCNTs was added, Young´s modulus and tensile strength haven´t changed and small decrease in strain-to-failure can be seen. However, by adding 1 – 5 wt.% of MWCNTs, mechanical properties further decreased.

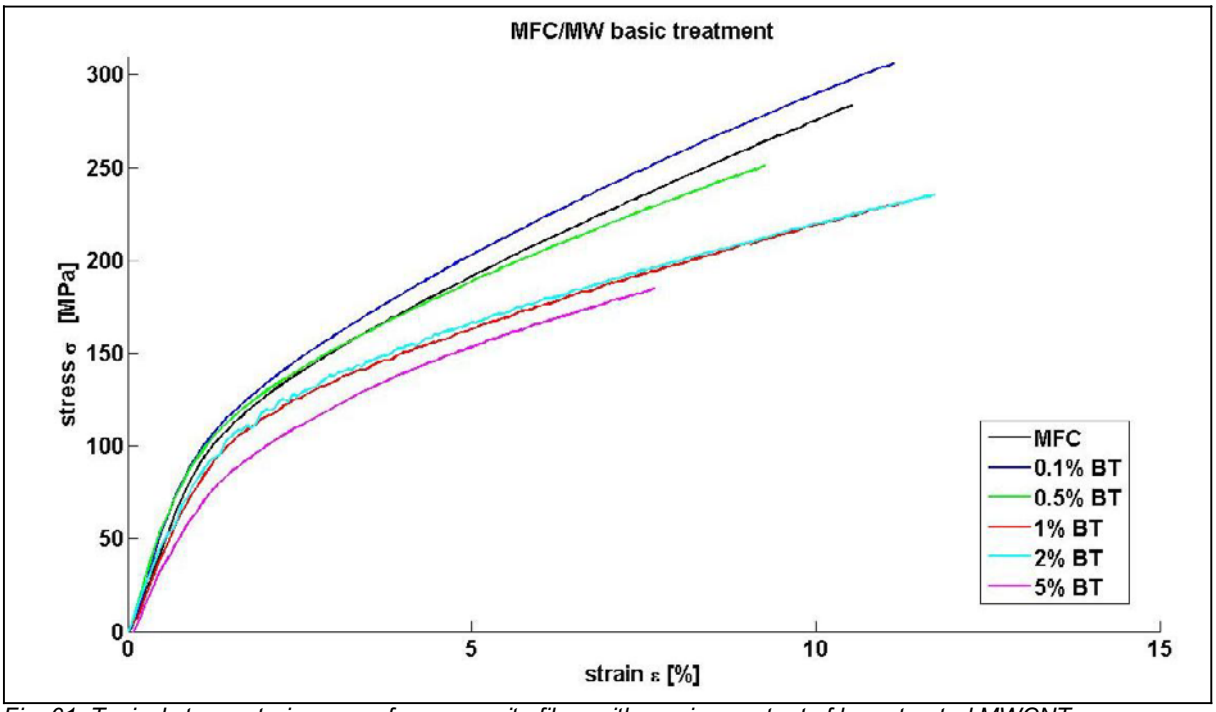

Fig. 61: Typical stress-strain curves for composite films with varying content of base treated MWCNTs.

Mechanical properties of composite films containing surfactant treated MWCNTs are more similar to previous group. However, no increase was observed. By adding 0.1 wt.% of MWCNTs. mechanical properties haven´t changed. Nevertheless, when more MWCNTs was added (0.5 – 5 wt.%), Young´s modulus and tensile strength decreases.

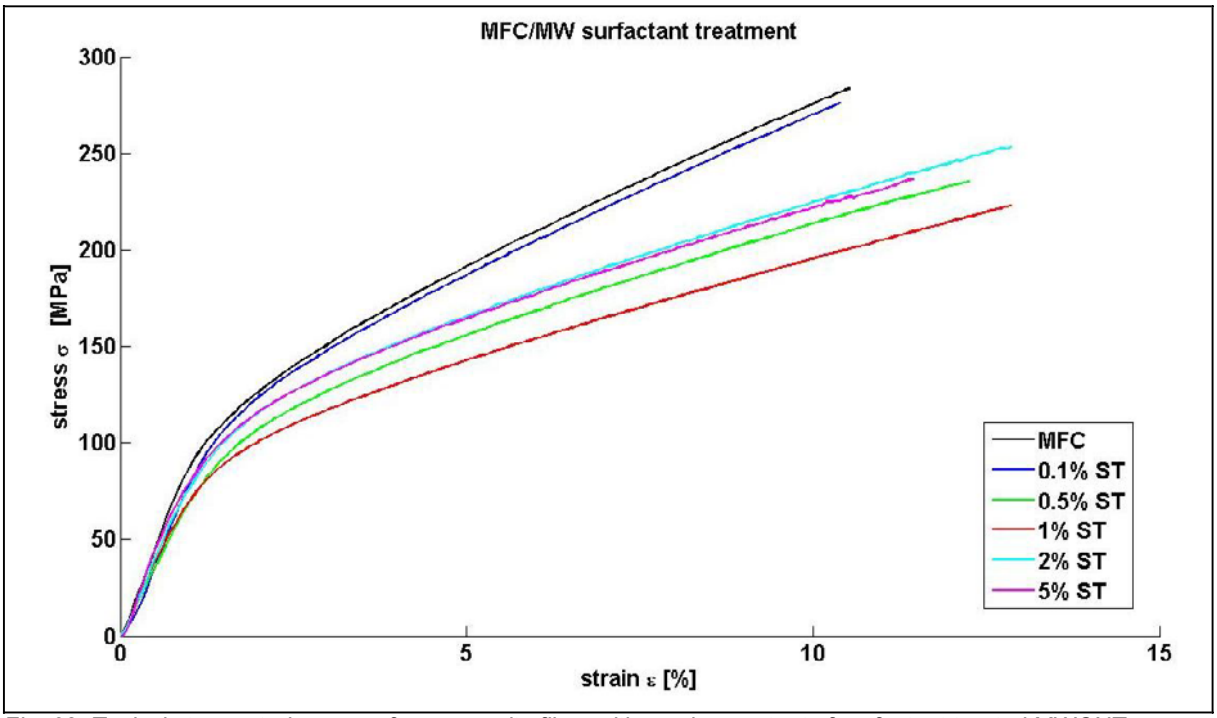

Fig. 62: Typical stress-strain curves for composite films with varying content of surfactant treated MWCNTs.

For better understanding of mechanical behaviour of composite films, microstructure of the material was investigated.

5.2.4 Field-Emission Scanning Electron Microscopy (SEM) analysis

In order to observe surface of composite films, SEM analysis was done. Each sample was observed from both sides.

On the Figures 63 and 64, there are SEM micrographs of pure MFC film from top (Fig 63) and bottom (Fig. 64) side under magnification of 25 000. MFC film consists of network of cellulose nanofibres that are entangled with respect to each other. The orientation seems to be mostly random-in-the-plane and the structure is in agreement with previously published data [20]. There is no significant difference in the nanofibrils network on the top and bottom side.

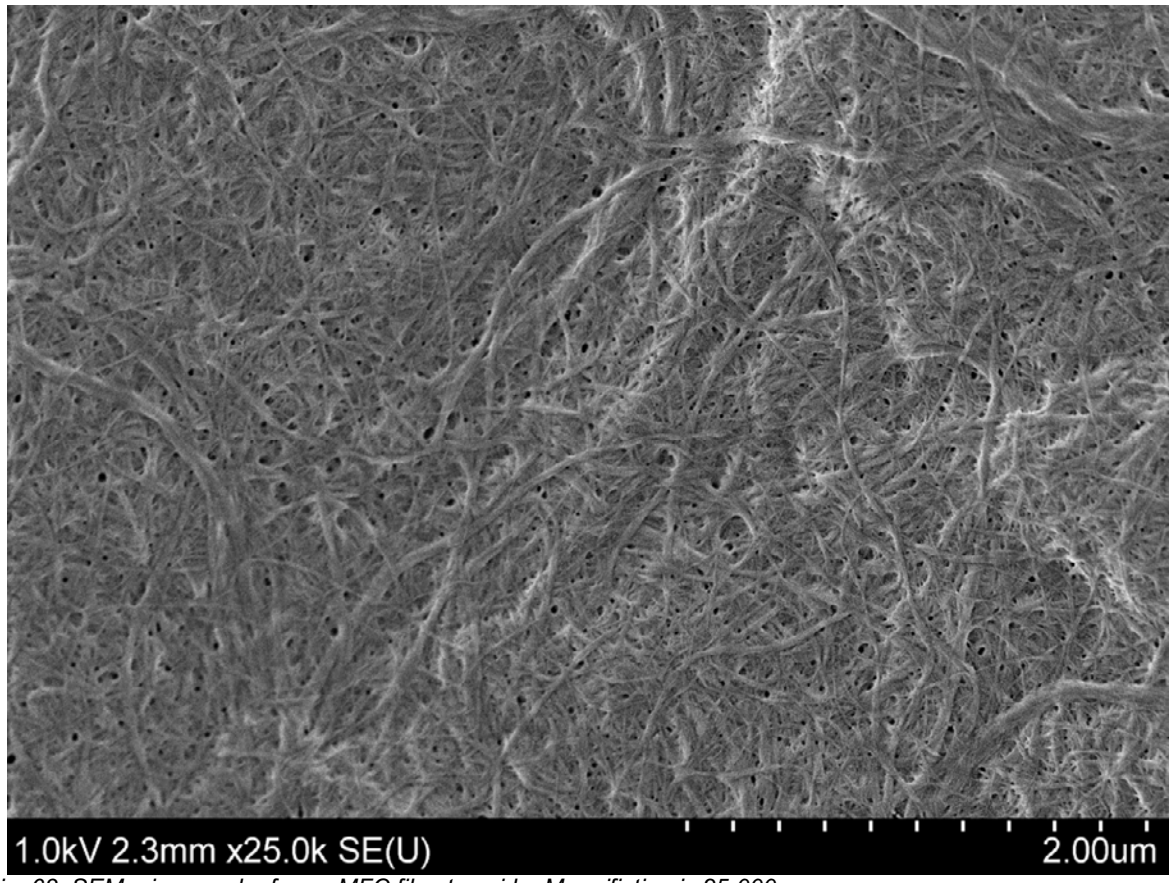

Fig. 63: SEM micrograph of pure MFC film, top side. Magnifiction is 25 000x.

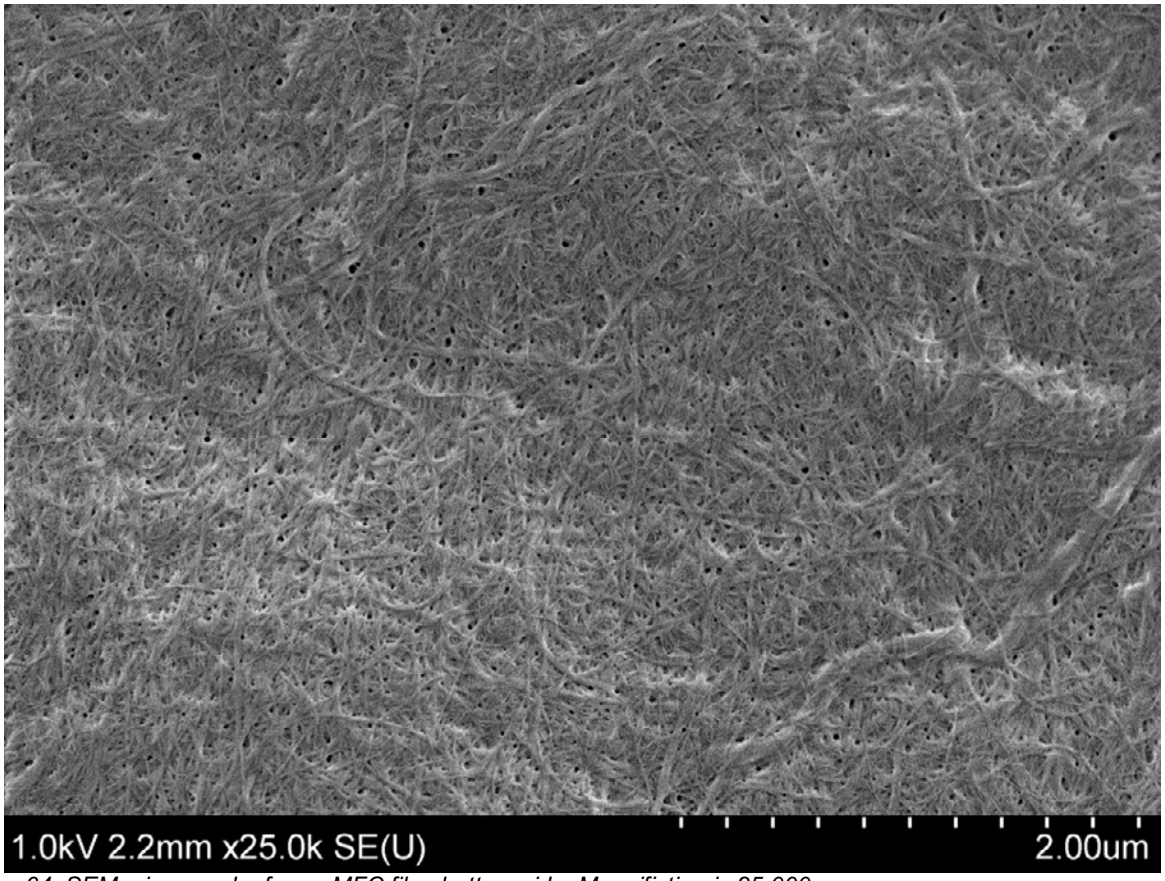

Fig. 64: SEM micrograph of pure MFC film, bottom side. Magnifiction is 25 000x.

Pictures under the same magnification were taken from both sides for the rest of the samples. On the Fig. 65, there is SEM micrograph of the top side of the composite film containing 5 wt.% of acid treated MWCNTs and on the Fig. 66, there is shown picture of the same sample from bottom side.

From the top side (Fig. 65), one can see network of MFC nanofibres, only very small amount of MWCNTs was found on this side of the sample. On the other hand, on the bottom side of the sample (Fig. 66), there is network of MWCNTs incorporated into MFC network. MWCNTs network seems to be homogenous with respect to the area of the sample and this is in agreement with TGA data (Fig. 55). This is also in agreement with the data for surface resistivity (Fig. 58 and Tab. 5), where significant difference in the top and bottom sides of the samples was observed.

However, MWCNTs are not homogenous through the thickness of the sample; therefore no improvement in mechanical properties is observed.

Separation of MWCNTs and MFC might happen during vacuum filtration that is used during the film preparation as the water is removing from the system. Cellulose nanofibres form stable network via hydrogen bonds and MWCNTs might be pushed away because of higher affinity of cellulose to cellulose than cellulose to MWCNTs.

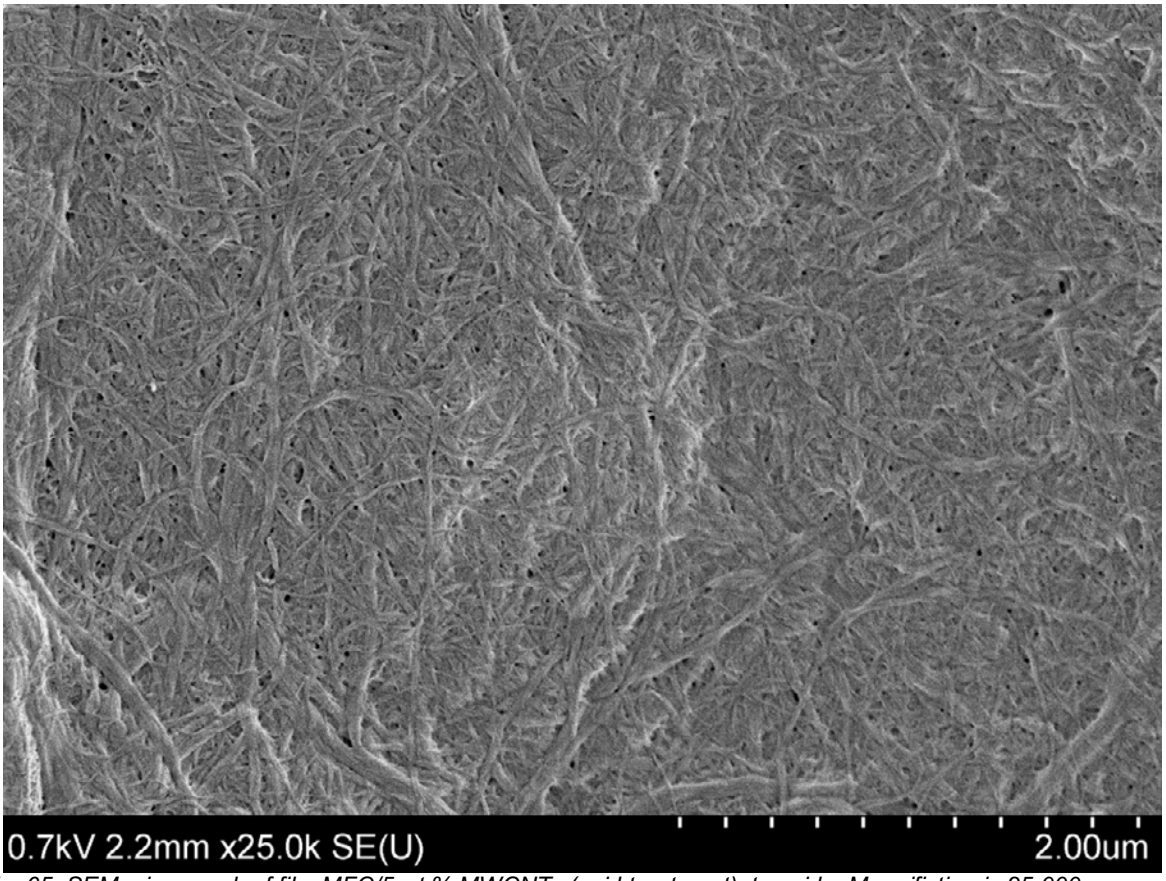

Fig. 65: SEM micrograph of film MFC/5 wt.% MWCNTs (acid treatment). top side. Magnifiction is 25 000x.

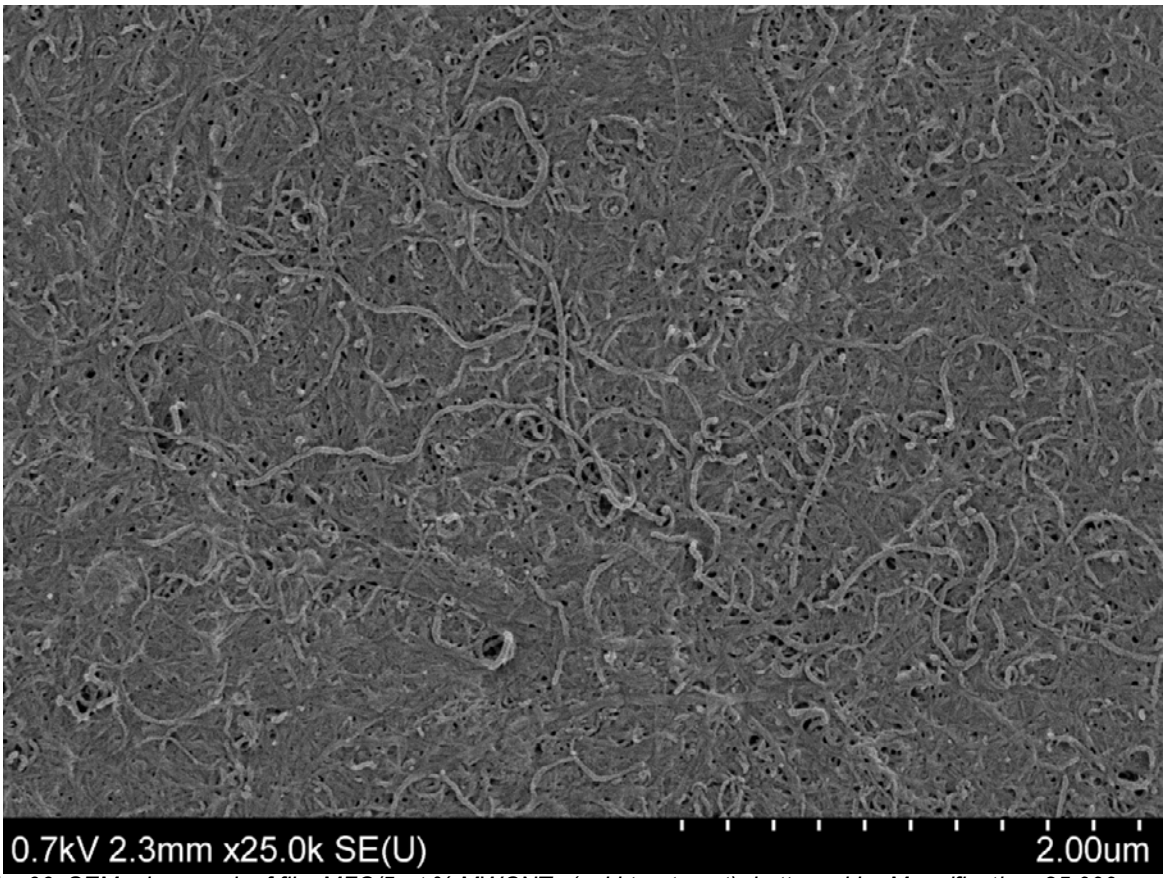

Fig. 66: SEM micrograph of film MFC/5 wt.% MWCNTs (acid treatment), bottom side. Magnification: 25 000x.

On the Fig. 67, there is SEM micrograph of top side of sample containing 5 wt.% of MWCNTs treated with basic oxidative treatment. There are obvious regions of MWCNTs that are not incorporated into cellulose nanofibres network. The size of these regions is around 1 – 2 μm.

The bottom side of the sample (Fig. 68) has similar structure to the top side. The areas of MWCNTs are larger (2 – 4 μm).

Structure of samples containing base treated MWCNTs explains why TGA data don´t follow the same trend like in case of composite films containing AT and ST MWCNTs. Sample just contains regions where is either more MFC or MWCNTs. The distribution is not homogenous through the area of the sample.

Morphology of the samples also suggests explanation for the higher MWCNTs concentration required for percolation than in case of surfactant treated MWCNTs. Because MWCNTs tend to agglomerate, more MWCNTs need to be added in order to achieve continuous network.

Concerning mechanical properties, slight increase is observed when 0.1 wt.% of BT MWCNTs was added. Such a small amount of MWCNTs was probably better dispersed in MFC. On the other hand, for higher MWCNTs content, separated regions might act as a defect in cellulose nanofibres network, that´s why there is decrease in mechanical properties in comparison to pure MFC film.

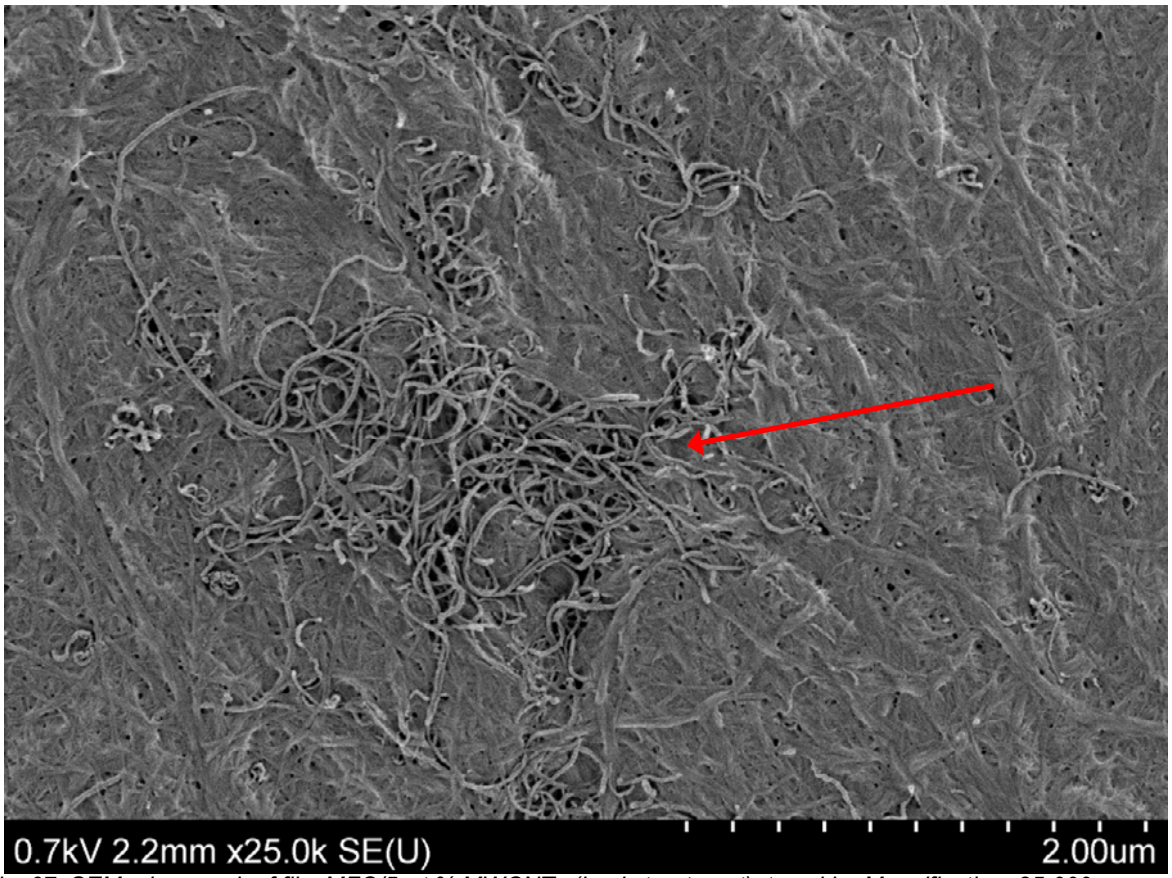

Fig. 67: SEM micrograph of film MFC/5 wt.% MWCNTs (basic treatment), top side. Magnification: 25 000x.

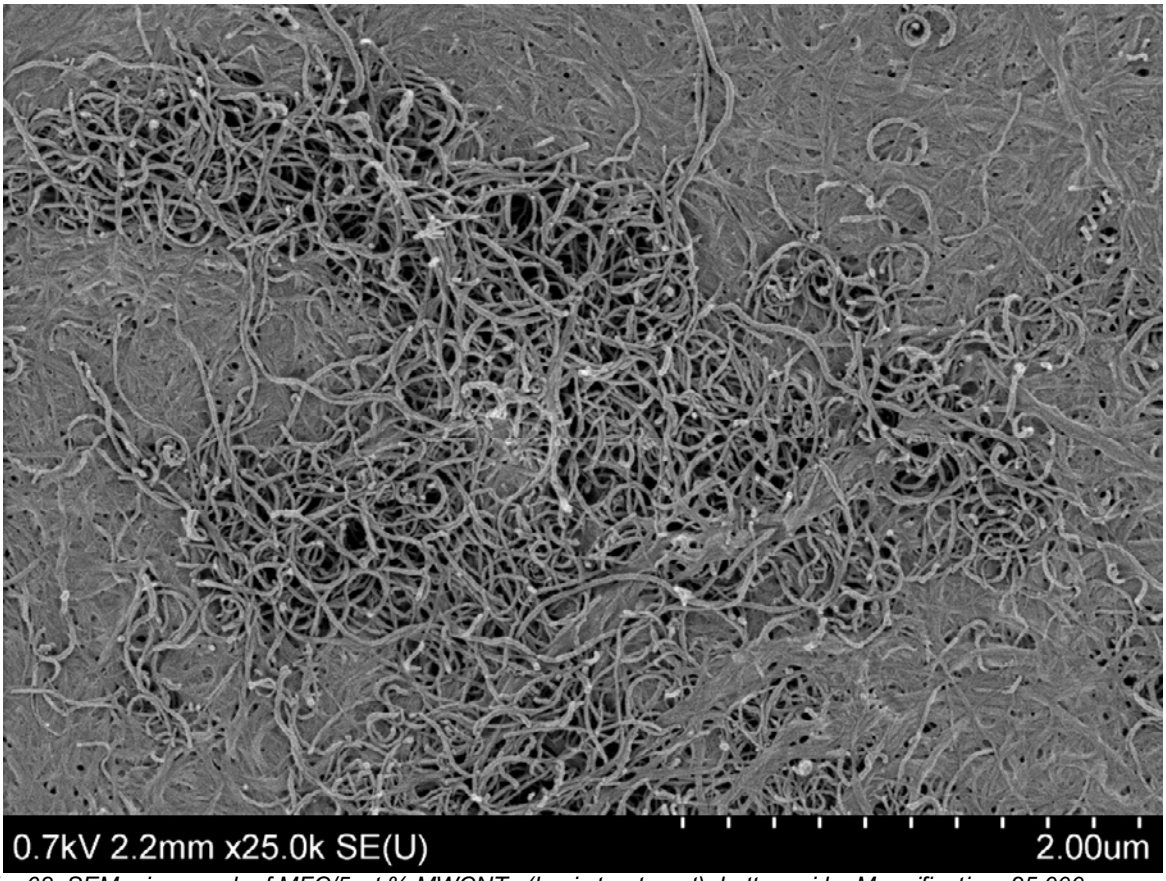

Fig. 68: SEM micrograph of MFC/5 wt.% MWCNTs (basic treatment), bottom side. Magnification: 25 000x.

In the Fig. 69, there is shown top side and on the Fig. 70, there is bottom side of the sample containing 5 wt.% of surfactant treated MWCNTs. In case of this sample, MWCNTs seems to have the best dispersion in MFC network in comparison to the previous treatments. There is only small difference in the amount of MWCNTs for the top and bottom side and MWCNTs are more incorporated into cellulose nanofibres than in case of BT MWCNTs.

The structure of composite films explains TGA data, where clear decrease in weigh loss at around 360°C is obvious with increasing amount of MWCNTs.

Despite quite good incorporation of MWCNTs into MFC, no improvement in mechanical properties is observed. There is probably poor interaction between MWCNTs and MFC. Another reason might be impurities and agglomerates present in the structure. These may act as defects.

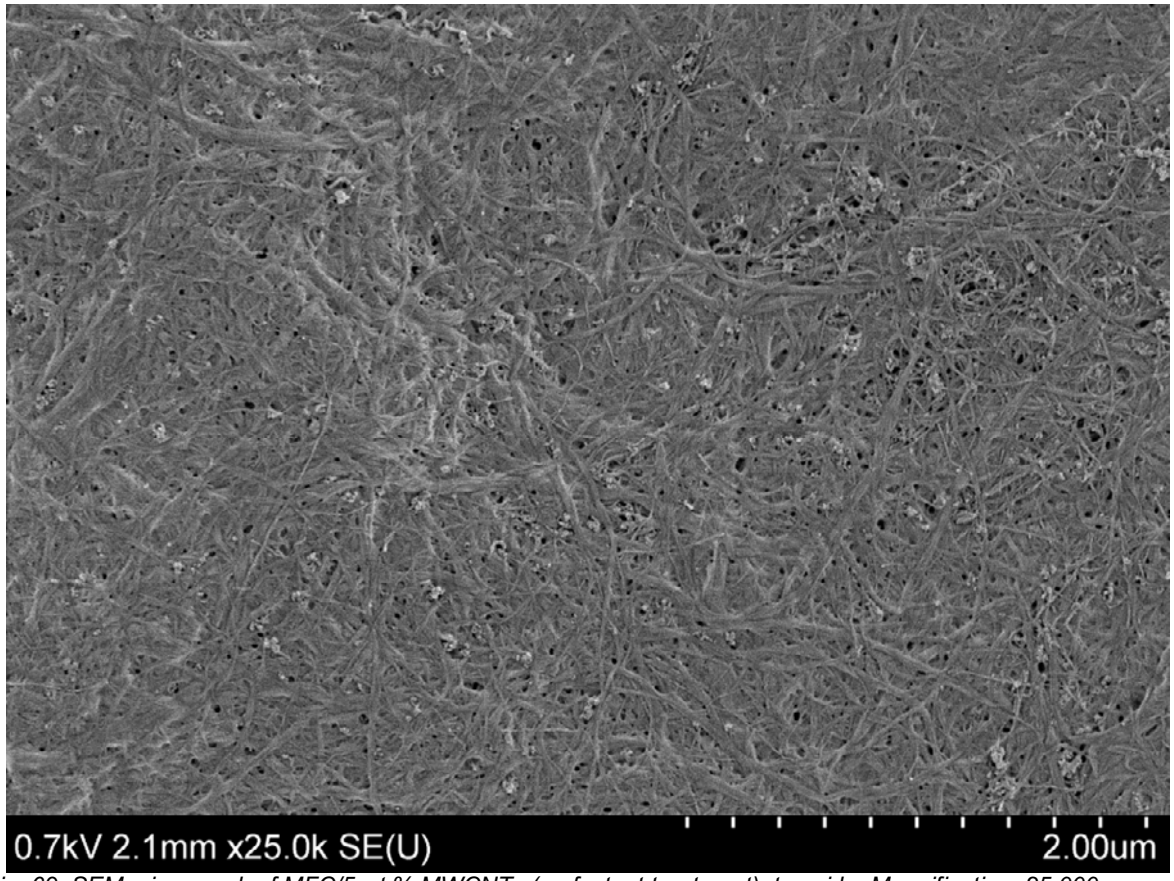

Fig. 69: SEM micrograph of MFC/5 wt.% MWCNTs (surfactant treatment). top side. Magnification: 25 000x.

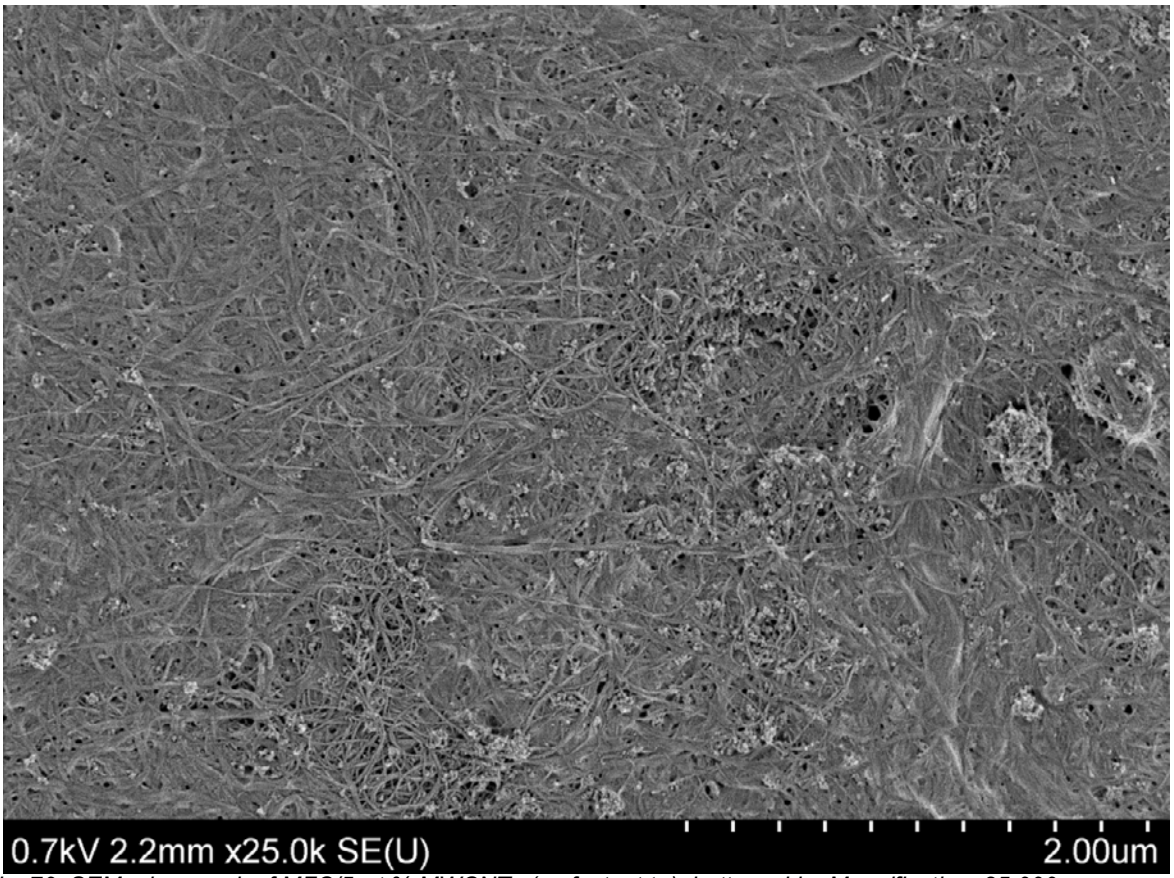

Fig. 70: SEM micrograph of MFC/5 wt.% MWCNTs (surfactant tr.), bottom side. Magnification: 25 000x.

Further investigations have to be done in order to gain better understanding of the structure-properties relation of the material. First, preparation of MWCNTs suspension can be improved. For example, purification step using less concentrated acid should be involved. Another improvement might be achieved by trying different surfactants like hexadecyltrimethylammonium bromide (CTAB), octyl phenol ethoxylate (Triton X-100) or Methocell^{TM} (cellulose based surfactant) and different surfactant concentration in order to get better stability of cellulose nanofibres-carbon nanotubes system.

Concerning the structure of composite films, it is not clear in which step the separation occurs. Both MFC and MWCNTs are in the form of stable water suspension and both components were mixed together. During the process of removing of water, cellulose nanofibres form network via hydrogen bonds. It was suggested that as the water is removing and cellulose network is formed, MWCNTs have tendency to agglomerate, because of higher affinity to each other than to MFC. Quality of system MFC/MWCNTs in water suspension can be studied for example by freeze-drying of the suspension, so the structure will be preserved.

The quality of incorporation of MWCNTs into MFC network can be further studied by SEM of cross-section of the samples.

Tensile test can be performed inside the SEM in order to obtain better understanding of mechanical properties and mechanism of deformation of the material.

6 CONCLUSION

New composite material based on microfibrillated cellulose matrix and multi-walled carbon nanotubes was prepared. Three different MWCNTs treatments were used and their effects on the properties and structure of resulting composite material were studied.

The morphology of composite films significantly differs when different MWCNTs treatments were used. The best distribution of MWCNTs in cellulose nanofibres matrix was found for MWCNTs dispersed using surfactant sodium dodecylsulphate. However, properties of the composite material might be affected by impurities present in the MWCNTs.

Using acid treatment, impurities were successfully removed and stable MWCNTs suspension in water was obtained. Nevertheless, separation of MWCNTs and MFC was observed with MWCNTs placed on one (bottom) side of the sample.

When basic oxidative treatment was used, impurities were removed as well. Suspension was not stable in water, that´s why surfactant was used. Dispersion of MWCNTs in MFC matrix was not homogenous, isolated regions of MWCNTs were found.

No significant effect of MWCNTs on mechanical properties was observed.

Concerning surface resistivity, typical percolation behaviour was observed and large decrease in surface resistivity was achieved. However, significant difference between the top and bottom side of the samples for all treatments was observed. This is caused by non-homogenous distribution of MWCNTs in the cellulose nanofibres network

The obtained results suggested that the most critical steps in MFC/MWCNTs composite preparation are the quality CNTs suspension and efficient surface treatment that would secure proper MFC/MWCNTs interaction. The CNTs treatment has to be chosen is such a way that will be able to make stable CNTs suspension and at the same time offers good compatibility with cellulose nanofibres. More investigation has to be done in order to gain better understanding of the structure-properties relation of the material, because both cellulose nanofibres and carbon nanotubes are materials with large potential in many different applications, such as electronic devices, biosensors, field emission displays, hydrogen storage, and composites, on account of their extraordinary physical, chemical, and structural properties, such as electrical, mechanical, and thermal characteristics [1]. Promising results have been produced on the use of carbon nanotubes in various electroanalytical nanotubes devices, and as electromechanical actuators for artificial muscles. The optical absorption of carbon nanotubes in the near-infrared has been used for the laser heating cancer therapy [46].

7 REFERENCES

[1] Kim H.S., pH-Sensitive Multiwalled Carbon Nanotube Dispersion with Silk Fibroins. *Biomacromolecules* 10, (2009), pp. 82–86.

[2] Poole A.J., Environmentally Sustainable Fibres from Regenerated Protein. *Biomacromolecules* 10, (2009), pp. 1-8.

[3] Siqueira G., Cellulose Whiskers versus Microfibrils: Influence of the Nature of the Nanoparticle and its Surface Functionalization on the Thermal and Mechanical Properties of Nanocomposites. *Biomacromolecules* 10, (2009), pp. 425–432.

[4] Pääkkö M., Enzymatic Hydrolysis Combined with Mechanical Shearing and High-Pressure Homogenization for Nanoscale Cellulose Fibrils and Strong Gels. *Biomacromolecules* 8, (2007), pp. 1934-1941.

[5] Teeri T.T., Biomimetic engineering of cellulose-based materials. *TRENDS in Biotechnology* 25, (2007), pp. 299 – 306.

[6] John M.J., Biofibres and biocomposites. *Carbohydrate Polymers* 71, (2008), pp. 343 – 364.

[7] Gindl W., All-cellulose nanocomposite. *Polymer* 46, (2005), pp. 10 221–10 225.

[8] Ahrenstedt L.N., Licentiate Thesis. Royal Institute of Technology, School of Biotechnology, Stockholm 2007.

[9] Fengel D., Wegener G., Ultrastructure Reactions, *Wood Chemistry,* Walter de Gruyter, Berlin, 1984.

[10] Berglund L. Cellulose based nanocomposites. Submitted as a chapter to *Natural fibres. biopolymers and their biocomposites.* Mohanty. Misra and Drzal (Eds), CRC Press LLC.

[11] Dufresne. A., Polysaccharide nanocrystals reinforced nanocomposite. *Can. J. Chem.* 86, (2008), 484–494.

[12] Henriksson. M., Doctoral Thesis. Royal Institute of Technology, School of Chemical Science and Engineering, Stockholm 2008.

[13] Simonsen. J., Biobased Nanocomposites: Chalenges and Oportunities [online]. Department of Wood Science & Engineering, Oregon State University, [11. 02. 2009]. Available from: www.swst.org/meetings/AM05/simonsen.pdf

[14] Battista. O. A., Microcrystal polymer science. New York: McGraw Hill Inc. 1975.

[15] Hasani M., Cationic surface functionalization of cellulose nanocrystals. *Soft Matter* 4, (2008), pp. 2238–2244.

[16] Goetz L., A novel nanocomposite film prepared from crosslinked cellulosic whiskers. *Carbohydrate Polymers* 75, (2009), pp. 85–89.

[17] Henriksson M., An environmentally friendly method for enzyme-assisted preparation of microfibrillated cellulose (MFC) nanofibres. *European Polymer Journal* 43, (2007), pp. 3434 – 3441.

[18] Saito T., Cellulose Nanofibres Prepared by TEMPO-Mediated Oxidation of Native Cellulose. *Biomacromolecules* 8, (2007), pp. 2485-2491.

[19] Syverud K., Strength and barrier properties of MFC films. *Cellulose* 16, (2009), pp. 75–85.

[20] Henriksson M., Cellulose Nanopaper Structures of High Toughness. *Biomacromolecules* 9, (2008), pp. 1579–1585.

[21] Siqueira G., Cellulose Whiskers versus Microfibrils: Influence of the Nature of the Nanoparticle and its Surface Functionalization on the Thermal and Mechanical Properties of Nanocomposites. *Biomacromolecules* 10, (2009), pp. 425–432.

[22] Chaplin M., Cellulose. Available at: http://www.lsbu.ac.uk/water/hycel.html [19. 02. 2009].
[23] Svagan A., Biomimetic Foams of High Mechanical Performance Based on Nanostructured Cell Walls Reinforced by Native Cellulose Nanofibrils. *Adv. Mater*. 20, (2008), pp. 1263–1269.
[24] Pääkkö M., Long and entangled native cellulose I nanofibers allow flexible aerogels and hierarchically porous templates for functionalities. *Soft Matter* 4, (2008), pp. 2492–2499.
[25] Yan Z., Cellulose synthesized by Acetobacter xylinum in the presence of multi-walled carbon nanotubes. *Carbohydrate Research* 343, (2008), pp. 73–80.
[26] Jung R., Electrically Conductive Transparent Papers Using Multiwalled Carbon Nanotubes. *Journal of Polymer Science: Part B: Polymer Physics* 46, (2008), pp. 1235–1242.
[27] Tasis D., Chemistry of carbon nanotubes. *Chemical Reviews* 106, (2006), pp. 1105 – 1136.
[28] Yehai.Y., Advances in Carbon-Nanotube Assembly. *Carbon Nanotubes* 1, (2007), pp. 24 - 42.
[29] Burchel T., Carbon Materials for Advanced Technologies. *Oxford: Elsevier Science*. 1999, pp. 18 - 19. ISBN 0-08-042683-2.
[30] Huang L., Orientated assembly of single-walled carbon nanotubes and applications. *Journal of Materials Chemistry* 37, (2007), pp. 3863-3874.
[31] AZoNanotechnology: Carbon Nanotubes - Overview of Properties, Classification, Fabrication and Synthesis [online], Polytechnic of Turin and the National Institute for Physics of Matter: *AZoM.com Pty.Ltd*. 2008, [19. 02. 2009]. Available at: http://www.azonano.com/details.asp?ArticleID=1199.
[32] Endo M., Development and Application of Carbon Nanotubes. *Japanese Journal of Applied Physics* 45 (2006), pp. 4883 – 4892.
[33] Harris P., Carbon nanotube science and technology [online], 2007, [19. 02. 2009]. Available at: http://www.personal.rdg.ac.uk/~scsharip/tubes.htm.
[34] Marsh D.H., Comparison of the stability of multiwalled carbon nanotube dispersions in water. *Phys. Chem.* 9, (2007), pp. 5490–5496.
[35] Grossiord N., Time-Dependent Study of the Exfoliation Process of Carbon Nanotubes in Aqueous Dispersions by Using UV-Visible Spectroscopy. *Anal. Chem*. 77, (2005), pp. 5135-5139.
[36] Salvetat J.P., Mechanical properties of carbon nanotubes. *Appl. Phys. A*. 69, (1999), pp. 255 – 260.
[37] Morinobu E., Development and Application of CNTs. *The Japan Society of Applied Physics* 45, (2006), pp. 4883 - 4892.
[38] Nogi M., Optically Transparent Nanofiber Paper. *Adv. Mater*. 20, (2009), pp. 1–4.
[39] Yano H., Optically Transparent Composites Reinforced with Networks of Bacterial Nanofibres. *Adv. Mater*. 17, (2005), pp. 153 – 155.
[40] Nogi M., Transparent Nanocomposites Based on Cellulose Produced by Bacteria Offer Potential Innovation in the Electronics Device Industry. *Adv. Mater.* 20, (2008), pp. 1849–1852.
[41] Baughman R.H., Carbon Nanotubes—the Route Toward Applications. *Science* 297, (2002), pp. 787 – 792.
[42] Haggenmueller R., Comparison of the Quality of Aqueous Dispersions of Single Wall Carbon Nanotubes Using Surfactants and Biomolecules. *Langmuir* 24, (2008), pp. 5070-5078.

[43] Rastogi R., Comparative study of carbon nanotube dispersion using surfactants. *Journal of Colloid and Interface Science* 328, (2008), pp.421 - 428.
[44] Datsyuk V., Chemical oxidation of multiwalled carbon nanotubes. *Carbon* 46, (2008), pp. 833 – 840.
[45] Hou P.X., Purification of carbon nanotubes. *Carbon* 46, (2008), pp. 2003 – 2025.
[46] Lu F., Advances in Bioapplications of Carbon Nanotubes. *Adv. Mater.* 21, (2009), pp. 139–152.
[47] Oya T., Production of electrically conductive paper by adding carbon nanotubes. *Carbon* 46, (2008), pp. 169 – 171.
[48] Jiang L., Production of aqueous colloidal dispersions of carbon nanotubes. *Journal of Colloid and Interface Science* 260, (2003), pp. 89–94.
[49] de Souza Lima M.M., Rodlike Cellulose Microcrystals: Structure, Properties, and Applications. Macromol. *Rapid Commun.* 25, (2004), pp. 771–787.
[50] Pieraccini S., Chiral Doping of Nematic Phases and Its Application to the Determination of Absolute Configuration. *Chirality* 20, (2008), pp. 749–759.
[51] Li L., Carbon nanotube induced polymer crystallization: The formation of nanohybrid shish–kebabs. *Polymer* 50, (2009), pp. 953–965.
[52] O'Connell M.J., Band gap fluorescence from individual single-walled carbon nanotubes. *Science* 297, (2002), pp. 593 – 596.
[53] Geng H.Z., Effect of Carbon Nanotube Types in Fabricating Flexible Transparent Conducting Films. *Journal of the Korean Physical Society* 53, (2008), pp. 979 – 985.
[54] Swapp S., Scanning Electron Microscopy [online]. University of Wyoming, [11. 03. 2009]. Available at: http://serc.carleton.edu/research_education/geochemsheets/techniques/SEM.html.
[55] Henry D., Electron-Sample Interaction [online], Louisiana State University, [11. 03. 2009]. Available at: http://serc.carleton.edu/research_education/geochemsheets/electroninteractions.html.
[56] Schweitzer J., Scanning Electron Microscope [online], Purdue University, [11. 03. 2009]. Available at: http://www.purdue.edu/REM/rs/sem.htm.
[57] Pendse D.R., Cathodoluminescence and Transmission Cathodoluminescence in Encyclopedia of Materials - Science and Technology. *Elsevier* 2001, pp. 1026.
[58] Mohomed K., Thermogravimetric Analysis: Theory, Operation, Calibration and Data Interpretation [online], [11. 03. 2009]. Available at: http://209.85.129.132/search?q=cache:pW7_O2bVHsgJ:membrane.ces.utexas.edu/Default.asp%3FCategory%3DHome%26Page%3DLabPractice%26Article%3DTGA+thermogravimetric+analysis&hl=en&ct=clnk&cd=6&client=safari.
[59] de Souza F.G., Electrical surface resistivity of conductive polymers – A non-Gaussian Approach for determination of confidence intervals. European Polymer Journal 44 (2008), pp. 3908 – 3914.
[60] Chaplin M., Cellulose [online], [07. 04. 2009]. Available at: http://www.lsbu.ac.uk/water/hycel.html.
[61] Docekalova H., Instrtumentální a strukturní analýza. Study handouts. Winter term 2007.
[62] Official webpage of Kutztown University: UV-Vis Absorbance Spectroscopy [online], [12. 03. 2009]. Available at: http://faculty.kutztown.edu/betts/html/UV_Vis_Absorbance.htm.
[63] Goldstein J., Scanning Electron Microscopy and X-Ray Microanalysis. Third Edition. Capter I: Itroduction. *Springer Science* 2007, pp. 1 – 3.

[64] Goldstein J., Scanning Electron Microscopy and X-Ray Microanalysis. Third Edition. Chapter II: The SEM and Its Modes of Operation. *Springer Science* 2007, pp. 29 - 47.
[65] Keithley: Model 8009 Resistivity Test Fixture. Instruction Manual [online], [05. 04. 2009]. Available at: http://www.keithley.com/products/instaccessories/testfixtures/?path=8009/Documents#2.
[66] Official webpage of Instron: Tensile testing. Available at: http://www.instron.us/wa/applications/test_types/tension/default.aspx [16. 03. 2009].
[67] Goyanes S., Carboxylation treatment of multiwalled carbon nanotubes monitored by infrared and ultraviolet spectroscopies and scanning probe microscopy. *Diamond & Related Materials* 16 (2007), pp. 412 – 417.
[68] Li Y., Purification of CVD synthesized single-wall carbon nanotubes by different acid oxidation treatments. *Nanotechnology* 15, (2004), pp. 1645 – 1649.
[69] Endo M., Development and Application of Carbon Nanotubes. *Japanese Journal of Applied Physics* 45, (2006), pp. 4883 – 4892.
[70] Collins P.C., Nanotubes for Electronics [online]. *Scientific American* (2000), pp. 62 – 69, [05. 04. 2009] Available at: www.research.ibm.com/nanoscience/NTs_SciAm_2000.pdf.
[71] Keithley: Model 8009 Resistivity Test Fixture. Data Sheet [online], [05. 04. 2009] Available at: http://www.keithley.com/products/instaccessories/testfixtures/?path=8009/Documents#1.
[72] Fugetsu B., Electrical conductivity and electromagnetic interference shielding efficiency of carbon nanotube/cellulose composite paper. *Carbon* 46 (2008), pp. 1253 – 1269.
[73] Yi J., Chiral-nematic self-ordering of rodlike cellulose nanocrystals grafted with poly(styrene) in both thermotropic and lyotropic states. *Polymer* 49, (2008), pp. 4406–4412.
[74] Dillon A.C., A Simple and Complete Purification of Single-Walled Carbon Nanotube Materials. *Advanced Materials* 11, (1999), pp. 1354 – 1358.
[75] Jha N., Synthesis and Thermal Conductivity of Copper Nanoparticle Decorated Multiwalled Carbon Nanotubes Based Nanofluids. *The Journal of Physical Chemistry C* 112, (2008), pp. 9315–9319.
[76] Kim S.T., Bulk polymerized polystyrene in the presence of multiwalled carbon nanotubes. *Colloid Polym Sci* 285, (2007), pp. 593–598.
[77] Grossiord N., Toolbox for Dispersing Carbon Nanotubes into Polymers To Get Conductive Nanocomposites. Chem. Mater. 18, (2006), pp. 1089-1099.

8 LIST OF ABBREVIATIONS

MFC	microfibrillated cellulose
CNTs	carbon nanotubes
MWCNTs	mutli-walled nanotubes
SWCNTs	single-walled nanotubes
CS_2	carbon disulphide
DP	degree of polymerization
CNC	cellulose nanocrystals
EPTMAC	epoxy-propyltrimethylammonium chloride
PMVENA	poly(methyl vinyl ether-co-maleic acid)
PEG	poly(ethylene glycol)
TEMPO	2,2,6,6-tetramethylpiperidine-1-oxyl
PCL	poly(caprolactone)
wt. %	percentage by weight
BC	bacterial cellulose
AFM	atomic force microscopy
SEM	scanning electron microscopy
CTE	thermal expansion coefficient
HiPCO	high pressure carbon monoxide
CVVD	catalytic chemical vapor deposition
SDS	sodium dodecyl sulfate
SDBS	sodium dodecyl benzenesulfonate
DTAB	dodecyltrimethylammonium bromide
CTAB	hexadecyltrimethylammonium bromide octyl phenol ethoxylate
HNO_3	nitric acid
H_2SO_4	sulphuric acid
H_2O_2	hydrogen peroxide
HCl	hydrochloric acid
$KMnO_4$	potassium permanganate
NaOH	sodium hydroxide
NH_4OH	ammonium hydroxide
K_2HPO_4	potassium hydrogen phosphate
KH_2PO_4	potassium dihydrogen phosphate
AT	HNO_3/H_2SO_4 treatment
BT	H_2O_2/NH_4OH treatment
ST	SDS treatment
TGA	thermogravimetric analysis
ρ_S	surface resistivity
V	voltage
I	current
R	surface resistance
g	distance between the guarded electrode and the ring electrode
P	effective perimeter of the guarded electrode
D_0	effective diameter of the guarded electrode
E	Young´s Modulus
σ	stress
ε	strain